Processing and Characterization of Nanocrystalline Materials

By

Gözde GENÇ

A Dissertion Submitted to the
Graduate School in Partial Fulfillment of the
Requirements for the Degree of

MASTER OF SCIENCE

Department: Chemical Engineering
Major: Chemical Engineering

Izmir Institute of Technology
Izmir,Turkey

February, 2004

ACKNOWLEDGEMENT

Thanks to Evrim Yakut for sacrificing so much for the neverending X-RD runs. Thanks to Hasan Demir for his creative practical solutions and expertise on xls. Thanks to Sedat Akkurt for his exactingness and understanding. Thanks to Muhsin Çiftçioğlu for his trust. Very special thanks to Devrim Balköse for the mental support in a hard day's morning.

ABSTRACT

Nanocrystalline materials with grain sizes under 100 nm have been counted as a very promising class of ceramic materials. The decrease in grain size imparts superior structural properties to the ceramic materials like increased fracture toughness, wear resistance and superplastic deformation at high temperatures. So, nanocrystalline ceramics can be used as structural materials in a wide range of uses covering advanced engineering applications such as aircraft and automotive technologies as well as electronics, computation and material sciences.

Nanocrystalline alumina has been a popular research subject for the last decade because of the superior structural properties of alumina besides lower cost compared to other nanocrystalline materials like zirconia and titania. The raw materials are generally transitional aluminas or aluminum hydroxides such as boehmite and gibbsite all of which are widely used in industry.

The main problem in nanocrystalline alumina production is to cope with agglomeration of fine powders or nano-particles in solutions due to interaction forces. Agglomeration cause nonhomogeneous microstructure with respectively larger pores which are very hard to eliminate during sintering. In this study a nanocrystalline commercial boehmite powder is used as the starting material and a homogeneous microstructure with respectively high density is aimed. Ultrasonic treatment is applied in order to reduce particle size and the stable dispersions of boehmite powder with a solid content of 30wt% was dried by spray drying. The effect of ultrasonic treatment, spray drying and compaction conditions were investigated and compared with bodies compacted from untreated powders. To see the effect of seeding on phase transformation behavior of boehmite, alpha alumina particles produced by combustion synthesis and broken into crystallites by ultrasonic treatment were used with a seed content less than 0.5%. Even that low amount of α-alumina reduced the transformation temperature by 100ºC but did not improve densification of alumina compacts.

The homogeneity of microstructure obtained by ultrasonic treatment and granulation by spray drying yielded the highest relative densities of 65.5 % of the theoretical density. The treatment has also led more uniform microstructures compared to untreated and seeded samples during the α-phase transition which is the most important stage for densification.

ÖZ

Nano-kristal malzemeler, 100 nm'den küçük kristal boyutları sayesinde sergiledikleri üstün özellikler nedeniyle son yılların en popüler araştırma konularından biri olmuştur. Kristal boyutlarının küçülmesiyle seramik malzemelerin mekanik özelliklerindeki gelişmeler şaşırtıcı boyutlardadır. Bu sayede seramik malzemelerin tokluğunun yanısıra aşınma dayanımı da artmaktadır. Nano boyutta seramik malzemelerin yüksek sıcaklıklarda gösterdiği süperplastik deformasyon, yeniden şekillendirilebilir seramik parçaların üretimine imkan veren bir özelliktir. Bu da nanokristal seramik malzemeleri otomotiv ve havacılık sanayilerinde olduğu gibi uzay teknolojisi ve özel mühendislik uygulamaları gibi üstün mekanik özellikler gerektiren alanlarda umut vadeden malzemeler haline getirmiştir.

Üstün mekanik özellikler sergileyen nano TiO_2 ve ZrO_2'nın yanısıra son on yıldır Al_2O_3 da pek çok araştırmaya konu olmuştur. Yaygın olarak kullanılan aluminanın bilinen mekanik üstünlüklerinin yanısıra nispeten ekonomik bir malzeme olması nano-boyutlarda üretiminin gerçekleştirilmesi için teşvik edici olmuştur. Bu çalışmada yoğun ve homojen nano-kristal alumina üretimi için boehmite hammade olarak kullanılmıştır. İnce boehmite tozunun ultrason uygulamasıyla suda disperse edilmesiyle elde edilen 30%'luk dispersiyonlar püskürtme kurutucuyla kurutularak küçük partiküllü toz haline getirilmiştir. Hazır tozdan elde edilen pelletlerle karşılaştırılarak uygulamanın mikroyapı ve faz değişim sıcaklıkları üzerindeki etkileri araştırılmıştır. Aynı yöntemle hazırlanan toza en fazla 0.5 % oranında α-alumina eklenmesiyle α-fazına geçiş sıcaklığında 100ºC düşüş gözlenmiştir.

Çalışma sonucunda ultrason uygulamasının ve püskürtme kurutmanın sinterlenen seramik parçaların yoğunluğu artırdığı tespit edilmiştir. Ultrason uygulamasıyla 20 nm büyüklüğünde kristallerine ayrılan ve püskürtme kurutucuyla 5µ civarında küresel partiküller haline getirilen boehmite tozunun işlem görmemiş toza kıyasla olduğu gibi aşılanmış ve işlem görmüş toza nazaran daha homojen bir mikro yapı sağladığı, faz değişimi sıcaklıklarının farkedilir derecede düştüğü ve alfa fazına geçiş sırasında yoğunlaşma hızının arttığı gözlenmiştir.

TABLE OF CONTENTS

LIST OF FIGURES vii

LIST OF TABLES xii

Chapter 1. INTRODUCTION 1

Chapter 2. NANOCRYSTALLINE CERAMIC MATERIALS 3

2.1. Synthesis of Nanocrystalline Materials 5
2.2. Compaction of Ultrafine Particles 9
2.3. Sintering 10
2.4. Mechanical Properties of Nanocrystalline Materials 16
2.5. Issues in Densification and Enhanced Mechanical Properties 18

Chapter 3. CONSOLIDATION 21

3.1. Slurry Preparation 22
3.2. Spray Drying 24
3.3. Compaction 31
3.4. Subsequent Phase Transformation and Densification of Alumina 35
3.5. Thermal Cycle 41

Chapter 4. BOEHMITE 46

4.1. Phase Transformation of Boehmite 47
4.2. Growth Characteristics of Boehmite 50
4.3. Seeding 54

Chapter 5. EXPERIMENTAL 56

Chapter 6. RESULTS AND DISCUSSION 59

6.1. Optimization of Slurries 59
6.2. Preparation and Characterization of the Seed 63
6.3. Characterization of the Slurries 59
6.4. Characterization of the Spray Dried Powders 66
6.5. Characterization of the Compacted Bodies 74

Chapter 7. CONCLUSIONS AND RECOMMENDATIONS 87

REFERENCES 89

APPENDIX Product Information Data Sheet of DISPERAL/Condea....A

Product Information....A1
Data Sheet....A2
Particle Size....A3
IR Spectrum and DTA/TG....A4
XRD Diagram and Pore Radii Distribution....A5
Preparation of a DISPERAL Dispersion....A6
Dispersibility, pH, Particle Size and Transmission....A7

APPENDIX Crystallite Sizes by Scherrer Formula....B

APPENDIX X-Ray Powder Diffraction Patterns....C

APPENDIX X-Ray Diffraction Patterns of Sintered Compacts....D

LIST OF FIGURES

Figure 2.1. Density of nanocrystalline versus commercial ZrO_2-3mol% Y_2O_3 3

Figure 2.2. Schematic illustration of an agglomerate..... 9

Figure 2.3. SEM micrographs of γ alumina (a) before transformation and (b) just after transformation into α phase 11

Figure 2.4. Schematic diagram illustrating the three stages of sintering. 12

Figure 2.5. Pressure-temperature phase diagram of α and γ phases of n-alumina. 14

Figure 3.1. Morphology of particle preparing by spray method. 24

Figure 3.2. Zeta potentials of alumina aqueous slurries without organic additives as a function of pH. 25

Figure 3.3. Relative Sedimentation Height versus pH for alumina suspensions in water without organic additives. 26

Figure 3.4. Zeta potentials versus amount of PAA for 30 vol.% alumina slurries as a function of pH. 26

Figure 3.5. Variation of the viscosity, η, with PAA concentration for 30 vol.% alumina slurries at pH 4 and 9 27

Figure 3.6. SEM images of spray dried granules of alumina from stable dispersions prepared by addition of 0.08% deflocculant and 15% binder at (a) pH 9 and (b) pH 4. 27

Figure 3.7. Schematics of the evolution of a spherical droplet of dispersed slurry during drying 29

Figure 3.8. A qualitative description of compaction showing the change in density of the powder in response to an applied stress 31

Figure 3.9. Effect of moisture on the variation of the Young's modulus with forming pressure for samples prepared with 3wt% PVA, moist and dry .. 32

Figure 3.10. The polymeric bridge surface, between two particles, increases by crashing progressively the binder layer until the grains come in contact. . 33

Figure 3.11. Effect of the mean size of spray-dried granules on the evolution of Young's modulus of pressed samples from powders containing 3 wt% PVA and the same residual moisture..... 34

Figure 3.12. SEM micrograph of fracture surface of alumina sample pressed at 80 MPa containing 3 wt% of dried PVA on dry basis of alumina powder 34

Figure 3.13 Typical densification curves of transitional alumina powder compact with an initial α-alumina content of 6%, cold isostatic compaction applied at 250 MPa, and heated at a rate of 1°C/min. 36

Figure 3.14. Variations of relative sintered density with sintering temperature for the respective compacts of ultrafine γ-alumina compacts..... 37

Figure 3.15. Relative density changes for gamma alumina to alpha alumina phase transition measured from dilatometry experiments as a function of green density for three powders and two different heating rates..... 37

Figure 3.16. Schematic transformation induced microstructure modifications (a) transformation and grain growth in green compact close packing, (b) nucleation, transformation and grain growth in low density green body. 38

Figure 3.17. Influence of the cold isostatic compaction pressure on the densification curves of γ-alumina with α-alumina content less than 0.5 %, for two different heating rates: 1ºC/min and 10ºC/min 39

Figure 3.18. The densities of green bodies pressed uniaxially at 440 MPa from ball-milled and unmodified powder..... 40

Figure 3.19. SEM micrographs of alumina bodies sintered at 1300°C and 80 MPa; without ball-milling and with the milling step. 40

Figure 3.20. Relative density changes for gamma alumina to alpha alumina phase transition measured from dilatometry experiments as a function of heating rate for a gamma alumina with 0.5% alpha phase. 41

Figure 3.21. Densification curves of γ-alumina with α-alumina content of less than 0.5% and 6.0%, compacted at 250 MPa and shrinked at two different heating rates: 1ºC/min and 10ºC/min. 42

Figure 3.22. Microstructures of sintered samples up to 1450ºC in constant heating rate conditions..... 43

Figure 3.23. Comparison of densification behaviors of powder with different α-alumina contents heated at a rate of 1ºC/min. 44

Figure 3.24. Schematic transformation induced microstructure modifications during nucleation, transformation, rearrangement and grain growth in low density green body with particle reaarangement α-alumina particles..... 45

Figure 4.1. (a)Dehydration sequence of various alumina hydroxides patterns of alumina. (b) Powder XRD phases derived from boehmite presursor.... 47

Figure 4.2. TG curves of boehmite samples prepared at different temperatures between 100ºC and 240ºC..... 48

Figure 4.3. Boehmite's crystalline structure.. 49

Figure 4.4. XRD patterns of alumina powder calcined at 900ºC for 1 h. 51

Figure 4.5. Relationship between the crystallite sizes of θ - and α -Al_2O_3 and the fraction of α -Al_2O_3 during θ to α -Al_2O_3 phase transformation with heating rates & DTA profiles of the θ→α-Al_2O_3 phase transformation and the fraction of α-Al_2O_3 with heating rates of (a) 10°C/min, (b) 5°C/min, and (c) 2°C/min 52

Figure 4.6. Schematic drawing of a typical exothermic peak of θ→α-Al_2O_3 phase transformationin DTA measurement 53

Figure 4.7. TEM micrographs showing the morphology of α-alumina derived from (a) pure boehmite (Route 1), (b) γ-alumina, (c) γ-alumina wiyh 3 wt% α-alumina, and (d) γ-alumina wiyh 3 wt% alumina-sol..... 55

Figure 5.1. SEM migrographs of boehmite powder used as starting material showing (a) agglomerates and (b) agglomerated crystallites..... 56

Figure 6.1. Zeta potential curve of boehmite. 59

Figure 6.2. Dynamic viscosity measurements of slurries prepared by (a) mechanical mixing, (b) ultrasonic treatment& milling and (c)ultrasonic treatment& milling and 2.5% PVA addition on dry basis.... 62

Figure 6.3. X-Ray Diffraction graph of Al_2O_3 seeds synthesized by combustion synthesis and used as seed..... 63

Figure 6.4. SEM micrographs of α-alumina seeds as synthesized.. 64

Figure 6.5. SEM micrographs of seed particles after ultrasonic treatment with milling**.**..... 64

Figure 6.6. SEM images of spray dried powders of boehmite slurries (a) 30 % and (b) 2 % with no binder.. 66

Figure 6.7. SEM images of spray dried powders of boehmite slurries (a) SL1 (b) SL2 with 2.5 % PVA binder addition on dry basis.. 66

Figure 6.8. SEM micrographs of spray dried powder A1 showing (a) granulation of fine powder with the aid of PVA and (b) microstructure of the surface of a granule at nanoscale... 67

Figure 6.9. TGA analysis for the powders of B(boehmite as received), A1 (spray dried boehmite powder from slurry SL1) and A2 (spray dried boehmite powder slurry SL2). 68

Figure 6.10. X-Ray Diffraction patterns for the powders of (a)B (b)A1 and (c)A2 71

Figure 6.11. SEM migrographs of the green bodies of (a)A1, (b) A2, (c) B powders compacted at 120 MPa.. 74

Figure 6.12. Density curves of sintered compacts of (a)B, (b) A1, (c) A2 powders at a temperature range of 1050-1300ºC. 76

Figure 6.13. SEM micrographs of B, A1, A2 compacts sintered at 1100ºC (a,b) untreated boehmite completely at θ-phase, (c,d) pretreated boehmite with local conversion to α-phase, (e,f) seeded boehmite transformed into α-phase 78

Figure 6.14. SEM micrographs of B, A1, A2 compacts sintered at 1150ºC (a,b) appearance of α-alumina crystallites surrounded by θ-phase which is still dominating in B samples, (c,d) coalescence behavior of α-alumina crystallites as the uniform microstructure of A1 samples, (e,f) two types of microstructures; vermicular and faceted α-alumina crystallites, caused by seeding in A2 samples.. 79

Figure 6.15. SEM micrographs of A1 and A2 compacts sintered at 1200ºC (a,b) A1 compacted at 120 MPa and 600MPa and (c,d) A2 compacted at 120 MPa and 600MPa respectively. 80

Figure 6.16. SEM micrographs illustrating phase transformation behavior of seeded boehmite samples (A2) sintered at (a) 1100ºC, (b) 1150ºC, (c) 1200ºC (d) 1300ºC..... 81

Figure 6.17. SEM micrographs of (a)B and (b)A2 sintered at 1150ºC. 82

Figure 6.18. SEM micrographs illustrating phase transformation behavior of untreated boehmite samples 'B' sintered at (a) 1100ºC, (b) 1150ºC, (c) 1200ºC (d) 1250ºC..... 83

Figure 6.19. SEM micrographs illustrating phase transformation behavior of ultrasonically treated and spray-dried boehmite samples 'A1' sintered at (a) 1100ºC, (b) 1150ºC, (c) 1200ºC (d) 1250ºC 83

Figure 6.20. SEM micrographs of untreated and treated boehmite samples; (a)B and (b)A1 sintered at 1200ºC 84

Figure 6.21. SEM micrographs of (a) B with a magnification of 15000x, (b,c) details from '(a)' with 50000x magnification and (d) A1 samples, sintered at 1250ºC 84

Figure 6.22. Comparison of X-RD diagrams of sintered pellets A1 and B at (a) 1110ºC and (b) 1130ºC. 86

Figure C1. XRD Diagram of Alumina Powders Calcined at 350ºC C1

Figure C2. XRD Diagram of Alumina Powders Calcined at 400ºC C2

Figure C3. XRD Diagram of Alumina Powders Calcined at 500ºC C3

Figure C4. XRD Diagram of Alumina Powders Calcined at 600ºC C4

Figure C5. XRD Diagram of Alumina Powders Calcined at 700ºC C5

Figure C6. XRD Diagram of Alumina Powders Calcined at 800ºC C6

Figure C7. XRD Diagram of Alumina Powders Calcined at 900ºC C7

Figure C8. XRD Diagram of Alumina Powders Calcined at 1000ºC C8

Figure C9. XRD Diagram of Alumina Powders Calcined at 1050ºC C9

Figure C10.XRD Diagram of Alumina Powders Calcined at 1100ºC C10

Figure C11.XRD Diagram of Alumina Powders Calcined at 1150ºC C11

Figure C12.XRD Diagram of Alumina Powders Calcined at 1200ºC C12

Figure D1. XRD Diagram of Alumina Pellets Sintered at 1100º C D1

Figure D2. XRD Diagram of Alumina Pellets Sintered at 1110º C D1

Figure D3. XRD Diagram of Alumina Pellets Sintered at 1120º C D2

Figure D4. XRD Diagram of Alumina Pellets Sintered at 1130º C D2

Figure C1. XRD Diagram of Alumina Pellets Sintered at 1140º C D3

Figure C1. XRD Diagram of Alumina Pellets Sintered at 1150º C D3

Figure C1. XRD Diagram of Alumina Pellets Sintered at 1160º C D4

Figure C1. XRD Diagram of Alumina Pellets Sintered at 1170º C D4

Figure C1. XRD Diagram of Alumina Pellets Sintered at 1180º C D5

Figure C1. XRD Diagram of Alumina Pellets Sintered at 1200º C D5

LIST OF TABLES

Table 2.1. Densification characteristics of gamma alumina powder with crystallite size of 15-20 nm. 42

Table 4.1. Boehmite transition temperatures into γ-Al_2O_3 and α-Al_2O_3 as a function of boehmite crystalline size 50

Table 6.1. Effect of ultrasonic treatment without and with the aid of ball milling. 60

Table 6.2. Particle size and solid content of fully dispersed boehmite slurries prepared by ultrasonic treatment and ball milling for 90 min at pH=3.5 as a function of decantation time 61

Table 6.3. Effect of temperature on particle size and efficiency of dispersion prepared by ultrasonic treatment and milling at pH=4.0. Initial solid loads are 20 wt%. 61

Table 6.4. Efficiency of treatment for dispersions from slurries with 30% solid content 62

Table 6.5. Properties of slurries (SL1 and SL2) which are dispersed by ultrasonic treatment for dispersions from slurries with 30% solid content 65

Table 6.6. Properties of powders named as B, A1 and A2 67

Table 6.7. Phase transition ranges of B, A1 and A2 boehmite powders 70

Table 6.8. (a) Densities of sintered compacts by Archimedes method,
(b) Relative densities with respect to theoretical density of alumina 75

Chapter 1

INTRODUCTION

Alumina is one of the most important materials in the ceramic industry because of its excellent properties. However applications of alumina as a structural ceramic are limited. Recently "nanocrystalline alumina ceramics" have attracted significant attention in a great extent in order to improve the mechanical properties.

Nanocrystalline materials are an exciting class of materials with grain sizes less than 100 nm. Nanocrystalline ceramics having submicron grain sizes have been stated as promising materials since 1980's and widely investigated for their unique structural properties. As grain size decreases to nanometric levels, the behavior of ceramic material changes showing extraordinary structural and mechanical properties such as conserved grain boundaries after sintering and ability to deform plastically under proper conditions. Nanocrystalline zirconia has been proved to have superficial mechanical properties and nanocrystalline titania is another superior material with the advantage of lower processing temperatures. But both are accounted to be special purpose ceramics with expensive raw materials and specific processing techniques. So nanometer size alpha alumina powder processing has been an attractive research area for the last decade.

Conventional methods for synthesizing alpha alumina powder involve solid state thermally driven transformations from the hydrates of aluminum oxide and the extent of conversion to the corundum structure depends on the temperature and the time of thermal treatment. Generally, the total conversion occurs above 1250ºC on heating and the grains can grow fast at higher phase transformation temperatures. Thus lowering the phase transformation temperatures is the target for preparing nano alpha alumina. The difficulty in low temperature sintering of nanocrystalline materials is poor density leaded by agglomeration. Small particles are extremely effected by Van der Waals forces and produce agglomerates and interaglomerate pores are hardly closed at even high temperatures. In order to overcome this problem specific processing techniques are employed which are pressure aided sintering, seeding and doping.

The aim of this study is to produce nano-size particles and uniform microstructures of unsintered compacts from boehmite powder to yield nanocrystalline alpha alumina and characterize the samples in order to investigate the effect of consolidation parameters on microstructure and structural properties of the product.

Boehmite slurries are stabilized by ultrasonic treatment without addition of a dispersing agent and spray-dried to fine-powder form with mean particle size of 5μ. The powder is compacted by uniaxial dry pressing and transformed to alpha phase by conventional pressureless sintering.

Chapter 2

NANOCRYSTALLINE CERAMIC MATERIALS

Nanocrystalline materials are an exciting class of materials with grain sizes less than 100 nm. Nanocrystalline ceramics having submicron grain sizes have been counted as very promising materials since 1980's and have been the subject of extensive research via their unique structural properties. As grain size decreases to nanometric levels, the behavior of ceramic material changes showing extraordinary structural and mechanical properties such as conserved grain boundaries after sintering and ability to deform plastically under proper conditions.

Nanostructured ceramic materials show a number of superior properties besides their deformability without fracture up to high stresses. Deformation at elevated temperatures brings reshapability within as well as use of nanocrystalline ceramics as joints in order to combine two ceramic parts for. The concept give the pave for designing ceramics and special composite materials for specific purposes. The significant grain boundary area surface offers applications as fuel cells and oxygen sensors where accelerated diffusion is a particular requirement. Low temperature processing is an important aspect particularly for nanocrystalline ceramics (Fig.1).

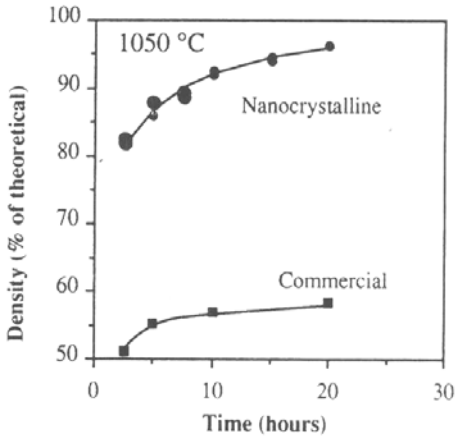

Fig.2.1. Density of nanocrystalline versus commercial (Tosoh TZ-3Y) ZrO_2-3mol% Y_2O_3 as a function of holding time when isothermally sintered at 1050ºC [2].

When compared to their conventional constitutes sintering temperatures of nanocrystalline ceramics are reduced up to 500ºC and more than that with pressure

aided heat treatments. Low temperature sinterability ensures outstanding microstructures providing grain boundary sliding and enhanced mechanical properties like increased toughness and wear resistance. [1-4]

Superplasticity is a major concept inspired by nanocrystalline grain size of ceramic materials. Superplasticity is the ability of a crystalline material to undergo large elongations prior to failure and strongly depends on the grain boundary characteristics. Ceramic materials exhibit superplasticity when their grain size is reduced to less than 1 micron in diameter. Work has been done with the aim of improving tensile elongation in ceramics, mainly zirconia-based materials. The phenomenon results from individual grains slide past each other during deformation which may somehow be called creep.

A primary feature of superplastic ceramic materials is that they are all fine grained. For 3 mol % yttria-stabilized tetragonal zirconia polycrystal (3Y-TZP) 800 % elongations have been reported. Although the mechanism of high-strain rate superplasticity is related to grain boundary sliding behavior of nanocrystalline ceramics, characteristics of microstructure depending on grain diffusion and effect of cavity formations require a complete understanding for further developments. Preliminary studies of fine-grained ZrO_2 and Al_2O_3 and their composites have shown that certain requirements must be met to achieve superplasticity: fine grain size, homogeneous microstructure and the inhibition of grain growth during high-temperature deformation. One useful method of controlling grain boundary characteristics is to dope the ceramics with impurities. Examples of this for superplastic tetragonal zirconia polycrystal and alumina ceramics have been a primary research area for the last decades and high-strain rate superplasticity of more than 1000 % elongations are reported up to date. [5-7]

These characteristics make nanocrystalline materials a promising candidate for high technology applications like space technologies and motorcrafts constituting a good alternative to metallic materials. Nanocristalline materials are promising various superlative applications mainly in space sciences, engineering sciences, electronic and optical sciences, materials sciences, and information and computing sciences.

2.1. Synthesis of Nanocrystalline Materials

Chemical precipitation of nanocrystalline oxide powders from cheaper salt solutions compared to alkoxide precursors at basic conditions (at pH values around 7-10) is among the simplest techniques for rapid synthesis of large amounts of material in a controlled fashion. By this method very small particle size (3-4 nanometer) is obtained yielding high surface areas of the final product. But the main disadvantage of this method is aggregation of the ultrafine precipitated particles in the solution. In addition, during drying, water, hydroxyl groups and other residual ions tend to form interparticle bonds and cause particle agglomeration. The type of these bonds determines the strength of the agglomerates and effects the compaction behavior of the material. Washing the powder with different alcohols or dehydration by azeotropic distillation were found to form soft agglomerates which are beneficial for high green densities in the compacted powders.

Different solvent systems and agitation methods result in different particle sizes. Ultrasonic treatment of precipitates results in finer particle size compared to that of magnetic stirring. Ultrasonic energy increases the nucleation density during the chemical precipitation by providing high localized energy increases via the acoustic cavitation. This, in turn, limits the growth of the precipitated particles compared to the growth of a limited number of nuclei formed during magnetic stirring. Use of convenient organic dispersants might also work well for inhibition of particle agglomeration. [3,8-9]

Sol-gel technology is a well established method for the preparation of catalytic active layers and thin films. Clear solutions that are termed as sols are generally formed by hydrolysis of alkoxides in dilute medias. One advantage of the method is the opportunity to obtain complex materials by incorporation of various additives in preparation of the solution. Another advantage of the sol-gel method is the variability in the netshape of the products. Xerogels, powders, layers and thin films are readily produced by this method. But it is not an appropriate way of producing bulk materials. The technique is a combined process of gel formation, aging, drying and heat treatment. Gelation chemistry is a main concept of sol-gel method. Consequently the initial gel structure impacts structural evolution in all subsequent processing steps. For a gel is not static during aging and drying, its properties can be designed by appropriate treatments.

Modification of precursor characteristics by involving different solvents and by introducing gel modifiers is a known attempt. Even the variations in the conditions of precipitation reaction like pH affects phase transition behavior and final properties of the synthesized materials. In this manner sol-gel technique has the ease of controlling properties of the product in preparing catalytic materials and membranes. [10-12]

Microemulsion which may be called as miscelle synthesis is a promising method to prepare nanometer sized particles. A microemulsion system which consists of an oil phase, a surfactant phase and an aqueous phase. The system is a thermodynamically stable isotropic dispersion of the aqueous phase within a continuous oil phase. The size of the droplets range in an interval of 5-20 nanometers in diameter. Chemical reaction takes place when the droplets containing reactants collide with each other and nanosized product particles form. Microemulsion processing techniques have been employed to synthesize nano-particles of ZrO_2, $BaTiO_3$, TiO_2 and the technique is successfully used for the production of spinel ($MgAl_2O_4$) and various spinel ferrite nanoparticles. One advantage of this versatile method is that nanoparticle size can be adjusted by small conditional changes -like concentration- during synthesis. This aqueous method uses readily available, inexpensive and easily handles precursors of metal nitrates. This eliminates the extra handling requirements that usually come across when moisture sensitive materials like alkoxides are used as precursor. [13,14]

Solution combustion technique is another versatile process leading to syntheses of single phase, solid solutions and composites as well as complex compound oxide phases in homogeneous form. The method utilizes metal nitrates as oxidizers and the fuel which is generally urea to induce highly exothermic redox reactions. Combustion reaction starts at 400ºC and simultaneously propogates. Since the reaction time is very short the final crystalline phases nucleate without further growth yielding ultrafine powders.

The process has the advantage of choice of a wide variety of fuels, rapid cooling leading to nucleation of crystallites without any growth and also has the potential to scale up. Because of the gas evolution, large particles or agglomerates can be disintegrated during the process and the products formed are of high purity. The resulting product is very fine particulates of friable agglomerates that can be easily ground to obtain a much finer particle size.

Urea has been proven to be a good fuel for the preparation of alumina and alumina related compounds and glycine for zirconia and zirconia related compounds by solution combustion technique. An appropriate mixture of different fuels like urea, glycine and ammonium acetate is reported to reduce nanoparticle size with combustion synthesis. Hydrazides are another class of fuels that are used for combustion synthesis. The fuel to precursor ratio is another parameter affecting particle size of the single phase or composite materials synthesized by combustion. The method is easy, quick and suitable for preparing nanomaterials without coming across to disadvantages associated by other wet chemistry methods. [15-16]

Mechanical milling is generally used as an additional function during synthesis because only mechanical treatment is not capable of creating ultrafine particles. However it is possible to produce larger particles which contain ultrafine grains by the aid of milling. This results from in situ localized phase transformations which occur because of localized damage. Anyhow milling is a common process in fabrication of nanocrystalline-grained macroparticles; one or more ductile precursors are fractured repeatedly during milling and reweld to form a fine-scale structure[1]. Then the precursors are led to react which may be called annealing. When the reaction is achieved in situ during milling the process is called a mechanochemical reaction. By virtue of the soluble matrix, the nanometer scale of the chemical reaction can be translated into nanometric particles. In other words nanosize precursors yield nanocrystalline materials by being exposed to a mechanical treatment before or during reaction. Anyway, the role of the milling is simply mixing the chemical reactants. Generally -exceptions are quite few- the milling treatment does not produce nanoparticles by reducing the particle size with direct fracture even at very high speeds and elongated milling time. A similar method is sonochemical reaction where the reaction medium is exposed to ultrasonic waves instead of application of milling.

An alternative to chemical and mechanochemical processing techniques is thermophysical methods which use large grained solid raw materials and then apply thermal energy, sometimes in the presence of mechanical stress, to reduce the solid to a powder form. The main category of thermoplastic synthesis is gas phase condensations. In this technique the solid is evaporated by heating to form a supersaturated vapor out of which small scale particles are condensed to obtain a nanoscale material.

Gas phase formation can be achieved by various alternative techniques, other than conventional heating, like electron beam evaporation, laser ablation, magnetron sputtering, arc discharge synthesis, etc. By applying these techniques a wide range of particle sizes, shapes and compositions may be obtained.

Thermophysical approaches are the cleanest ones of all the nanoceramic synthesis routes. For example, electron beam evaporation, sputtering, and ablation operations are typically performed in a well controlled atmosphere within a vacuum chamber. On the other hand, the need to evaporate in a low vapor pressure environment requires handling an expensive vacuum setup. This condition brings the problem of low production rates. Another disadvantage is the difficulty of multicomponent nanomaterial productions, which comes out of the differences of vapor pressures of components. The different volatilization rates require different energy inputs to compensate various sources during synthesis.

So, thermophysical approaches have been used to produce a wide variety of nanocrystalline materials, particularly serving to special purposes, but in small quantities. So the use of subsequent techniques have been restricted to researches mostly up to date. Commercialization of gas phase condensed nanomaterials can only be achieved by the construction of multiple parallel reactors and semicontinuous processing systems [1].

2.2. Compaction of Ultrafine Particles

The first step in the consolidation of a nanocrystalline powder to form a fully dense ceramic is the compaction of the powder particles. The powder compact is termed as a “green body”. Uniformity of particle packing in the green body is enormously effective on densification of the green body during sintering.

Nanometer sized ceramic powders are often heavily agglomerated. The Van der Waals attraction causes fine powder particles to bond together into agglomerates during synthesis, handling and especially drying. Agglomeration leads to green body microstructures with two types of pores as shown in Fig 2; inter-agglomerate pores and smaller intercrystallite pores within the agglomerate. During sintering, the elimination of the interagglomerate pores need high temperatures that also encourages grain growth which handicaps keeping the sintered grain size in nanometer regime.

The main issue in consolidation of nanoparticles is the elimination of agglomeration to yield fully dense ceramic bodies. Various packing techniques are employed for obtaining green compacts from ultra-fine powders or dispersions of nanoparticles [1].

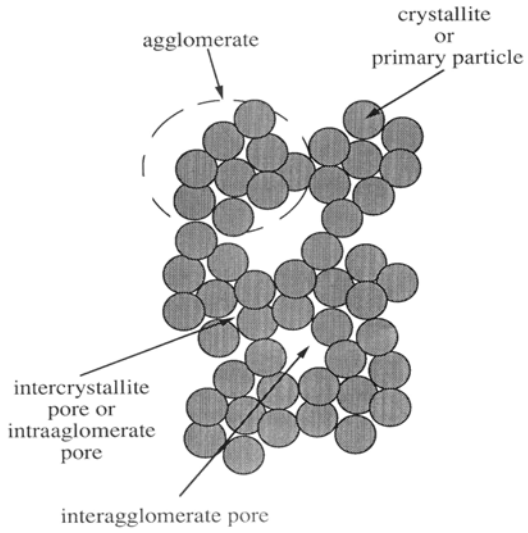

Fig.2.2. Schematic illustration of an agglomerate [2].

The simplest and most commonly used compaction method is uniaxial pressing of a powder in a die at room temperature. But this is the poorest method in terms of packing homogeneity. Examples of the relationships between increased compaction, increased green density and increased sintered density are available.

In cold isostatic pressing process, a powder is likely compacted by uniaxial pressing, then encapsulated in a deformable, leakproof membrane and immersed in a pressurized liquid. Applied stress is evenly distributed along all the surfaces. Severe density gradients and residual stresses are prevented and a more homogeneous particle packing is obtained compared to uniaxial pressing for the same level of applied stress.

Wet processing techniques such as tape casting, slip casting, pressure filtration and centrifugation typically produce much more homogeneously packed green bodies than samples consolidated in the dry state. The greater homogeneity of wet processed ceramic bodies results from particles sliding over one another and rearrange in the wet state, in orderly, packing efficient configurations. Thus, wet processing offers superior green bodies without pressure limitations encountered by dry pressing.

Osmotic consolidation is an effective technique for concentrating suspensions of nanometer scale ceramic particles. A suspension containing the particles is contained within a semipermeable membrane which allows the liquid but not the ceramic particles to pass through. The membrane bag is placed within a concentrated polymer solution. Chemical potential of the liquid is much higher inside the membrane, therefore the solvent from the particle suspension passes through the membrane. The osmotic potential has units of stress thus, can be compared to a mechanical stress pushing the particles inside the membrane yielding relatively dense green bodies. The method provides equivalent densities compared to pressure filtration.

2.3. Sintering

Compacts are further densified by heat treatment which is called sintering. Shrinkage due to phase transformation leads densification during sintering. Grain growth due to phase change which is called dynamic grain growth which is the main parameter to be controlled during heat treatment of the nanocrystalline green bodies. Thus, the prospects for producing fully dense compacts than retain nanocrystalline grain size are of minor use unless grain growth during sintering can be controlled. The problem of enhancing densification while simultaneously limiting grain growth is a central theme in the processing of these materials.

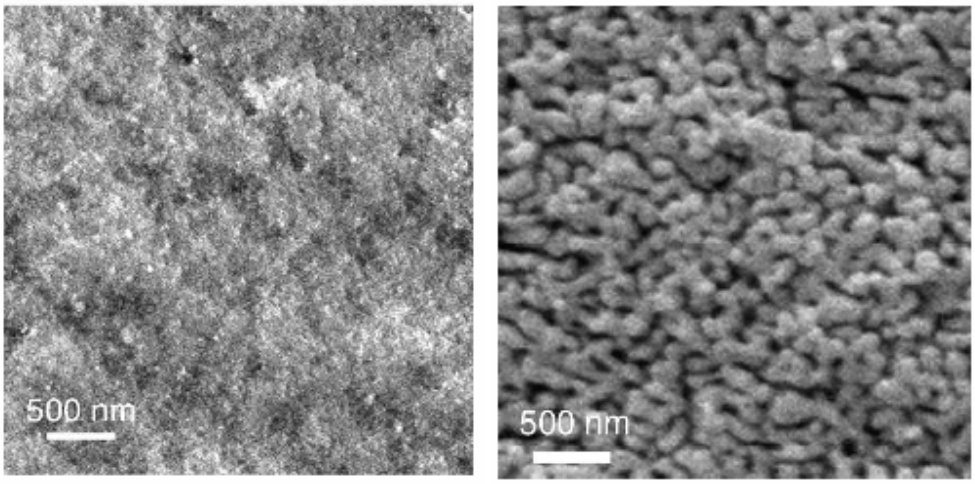

(a) (b)

Fig.2.3. SEM micrographs of γ alumina (a) before transformation and (b) just after transformation into α-phase (sintered at 1180ºC with 10 ºC/min heating rate in air) [17].

The most common method of densifying a ceramic green body is by pressureless sintering. The stages of pressureless sintering may be called as neck formation, network formation of open pores and closure of pores (Fig. 4.) The densification of a ceramic, or shrinkage of pores during pressureless sintering occurs by diffusion and the driving force for such diffusion is the reduction of the internal surface area associated with pores. Then densification occurs more quickly for pores with tighter curvature which explains the disadvantage caused by interagglomerate pores. The small pore samples

show superior densification behavior not only because their starting pore sizes are small, but because those pores remain small throughout sintering. That's why pressureless sintering is poor in densification process of nanocrystalline ceramics that tends to agglomerate drastically due to small particle sizes unless an additional treatment like doping or seeding is employed.

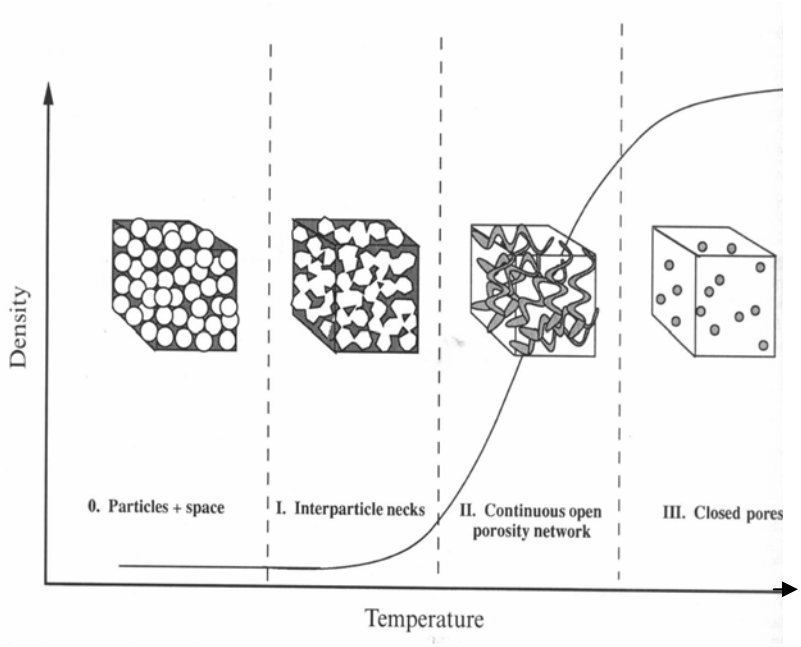

Fig.2.4. Schematic diagram illustrating the three stages of sintering [1].

Grain growth inhibitors have little effect on grain growth in the intermediate stage of sintering which may be related to open pore pinnings. The dopants' effect on grain growth appears once final stage sintering is reached and when the pores become closed. This requires high sintering temperatures and effect of dopants versus effect of temperature on grain growth has to be investigated in terms of interactions for each system.

Sinter forging is the simultaneous densification and deformation of a powder compact at elevated temperatures under a compressive stress. Usually the stress state is simple uniaxial compression but without a die. This technique allows larger shear strains to develop which are vital to the closure of pores in the sintering body.

Sinter-forging has been a preferred technique because of the severe grain growth problem during pressureless sintering. Presence of large pores which is the common problem in densification of agglomerated nanocreamic compacts prevent body from reaching theoretical densities under constant loads as well. But the densification rates increase with increasing strain and loading rates.

The rapid removal of large pores and the resulting fast densification rates for sinter-forged ceramics are explained on the basis of a strain controlled pore closure model. When the green body is compressed in a sinter-forging operation, the matrix deforms plastically and large pores are pressed flat. . The technique yields high densities at lower temperatures in shorter sintering times . [18-19]

Hot uniaxial pressing has also been used to consolidate nanocrystalline ceramics. Sintering is achieved under pressure by the aid of a die. The pressures are often high, like those in cold uniaxial pressure but results are quite good for small samples. For instance, hot pressing at 0.5-1.3 GPa and temperatures between 500 and 650ºC yield titania samples with 15 nm grain size and densities more than 95% of theoretical density. Hot pressing of chemically derived ZrO_2-3mol% Y_2O_3 under small stresses (23 MPa) led to full density with grain sizes of 80-90 nm.

It is reported that nucleation is the rate-limiting step of phase transformation. Since the transformation to the stable phases occur by means of nucleation and growth both of which are pressure and temperature dependent, density of the sintered bodies by means of nucleation and growth rates can be controlled by choice of processing conditions. For alumina, transformation to stable α-phase is achieved at low temperatures under high pressure which increases the nucleation rate of α-phase while its growth rate is slowed. The reduction of sintering temperature depending on high pressure is shown in Fig.2.5. for transition of alumina from γ to α phase. [1,20]

The use of fast heating rate in a ramp-and-hold sintering protocol can produce better densities at the same temperatures with slower heating rates.

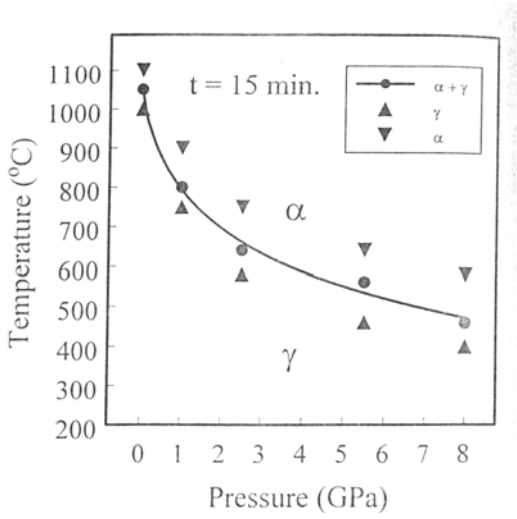

Fig.2.5. Pressure-temperature phase diagram of α and γ phases of n-alumina. The sintering time is given as 15 minutes [19].

In theory, nanocrystalline ceramics should be ideal for the rapid rate sintering. Fast firing of nanocrystalline thin films show reasonable results with densifications comparable to or better than conventional sintering of similar materials. Bulk samples, however, do not always fare as well. Studies on zirconia shows that effect of heating rate on the grain growth of the nanocrystalline powder compacts are negligible while it is one of the parameters of densification behavior under certain circumstances [20].

Microwave sintering is advantageous for several occasions due to rapid volumetric heating. Absorption of microwave energy by precursors results in the formation of many ceramic materials and varied microstructures. A unique characteristics of microwave heating is that microwaves penetrate the whole mass instantaneously so that change starts in every point simultaneously avoiding thermal gradients from conduction. But this statement is valid only for homogeneous bodies. Except this property, the phase, grain size and density achieved after microwave sintering are comparable to pressureless sintering. And sometimes microwave sintering yields warped and cracked specimens, particularly under fast heating rates and high sintering temperatures. This result is also encountered in the rapid rate heating of nanocrystalline materials using conventional radiation sources [21].

One other technique is plasma activated sintering in which a powder compact is subjected to one or more arc discharges before or during pressure assisted sintering. This method significantly reduce sintering temperatures and times. With respect to

nanocrystalline ceramics, the main benefit of using plasma activated sintering appears to be enhanced densification rates. The technique results fully dense ceramic materials after phase transformation is completed, but grain growth cannot be prevented. In this manner, the structures obtained are comparable to products of pressureless sintering and microwave sintering.

Shock compaction, which uses high velocity compressive waves to compact and sinter ceramic powders simultaneously is also being used to consolidate nanocrystalline materials. The shock wave induces high pressures besides causing localized heating of the particle surfaces due to friction between adjacent particles. In nanocrystalline particles this surface heating is quickly transported to the core of the particle and many ceramics have some degree of plasticity at this elevated temperatures. So, the ability of nanocrystalline ceramics to deform plastically makes it easier to achieve uncracked compacts than for the large grained ceramics. However, successful shock compaction of nanocrystalline ceramics requires a delicate balance between the shock wave rise time, the thermal conductivity of the material, preheat temperature and the ceramic particle size to coordinate heating and stress applications. So it is not a feasible method from a commercial standpoint. [1]

2.4. Mechanical Properties of Nanocrystalline Materials

The most obvious advantage of nanocrystalline ceramics with homogeneous and dense microstructure is improved mechanical properties compared to conventional ceramics.

Hardness of nanocrystalline ceramics appears to be less than the reported hardness values for large grained ceramics. This requires elimination of agglomeration during consolidation in the first place. Hence, reduction of hardness is mainly related to the density of the material.

Transformation toughened ceramics are reported to have improved fracture toughness related to prevention of grain growth by addition of stabilizing dopants. In this class of materials, a phase transformation occurs round a propagation crack due to grain boundary characteristics. The phase transformation creates an additional volume resulting accomodation by pushing the crack shot. The forcable closure of the cracks leads to fracture toughness values up to four times greater values compared to nontransformation toughened ceramics.

Improving fracture toughness to even greater values requires a complete understanding of grain boundary properties for multiphase nanoceramic materials. Grain boundary diffusion and grain boundary cavities are as important as grain size for toughened ceramic materials.

Nanocrystalline ceramics show a small amount of ductility at room temperature beyond that shown by large-grained ceramics. But they are superplastic at elevated temperatures. They show significant compressive ductility as well as strain rate sensitivities via superplastic deformations.

Superplasticity of ceramics has first been demonstrated in 1986 by Wakai et al. who obtained a tensile elongation of 170% at 1450ºC with yttria-stabilized tetragonal zirconia polycrystals. Currently elongations up to 1038 % have been reported for this material. Such large tensile ductility offers exciting opportunities to use superplastic forming techniques.

The phenomena has not been commercially accepted but has an obvious potential. The disadvantages of high forming temperatures and slow forming rates suppress their use but improvements are promising. Strain rates are dependent of various material properties which are still under investigation.

Grain size is known to be the main requirement for superplastic behavior. The nanocrystalline ceramics can deform at faster rates or lower temperatures for the same applied stress on the basis of reduced grain sizes. Relationship between grain size and forming rate and temperature is given as:

$$\dot{\varepsilon} = A\sigma^{n} d^{-p} D_o \exp(-Q/RT) \qquad [22]$$

In this equation, $\dot{\varepsilon}$ is the strain rate (forming rate), A is the material constant, σ is the applied stress, d is the grain size, and $D_o \exp(-Q/RT)$ is the diffusivity, which depends on Q, the activation energy for diffusion, R, the gas constant, and T, the temperature. p is the grain size exponent which has a value between 1 and 3. According to this equation a ten-fold reduction in grain size should accelerate forming rates by a factor of 100 to 1000 and decrease the forming temperatures by about 300ºC assuming a reference sintering temperature of about 1400ºC.

Porosity appears to play only a small role in the deformation of nanocrystalline materials while grain growth obviously reduces the ceramics deformation rates. The problem of grain growth, both during processing of the ceramic and during subsequent deformation is adressed as the primary approach.

During superplastic deformation of the dense ceramic, the grain size can be kept small if second phases are available to pin the grain boundaries. Otherwise grain growth is significant, but even in this case, the final grain size of a heavily deformed nanocrystalline ceramic is often less than the starting grain size of a commercial ceramic.

2.5. Issues in Densification and Enhanced Mechanical Properties

There have been three main approaches to counter the grain growth associated with densification to provide final microstructures in the nanometer regime. The first is the application of hot-pressing or sinterforging techniques. So applied pressures during sintering increase relative density besides limiting grain growth at reduced temperatures [19]. But this approach is not very favorable for industrial uses. Because it is almost impossible to apply homogeneous stress distributions by high pressures on large pieces.

The second, particularly for powders in a metastable crystallographic phase, is to use seeds of the final phase. The disadvantage of this treatment is the difficulty to find or produce the appropriate type, size and quality of seeds necessary to control the final microstructure. Recent researches are on the use of very fine (<20nm), very pure powders, linked with modifications of sintering cycles and sintering atmospheres to limit grain growth.

The third is the addition of dopants to modify diffusion processes, grain boundary migration and hence grain growth. Understanding the effect of dopants along with the processing of such fine powders is the approach which has been the main focus of authors over last decade.

The effect of doping elements on the phase transformation of metastable phases such as the transition aluminas has been investigated for many years. For alumina, dopants such as Ti or Mg do not significantly modify the phase transition temperature while elements such as Y or Zr delay the transformation by more than 50 °C at even very low addition ratios [17,23]. Nitrate salts of Ba, Pr as dopants are reported to delay α-transition of alumina obtaining remarkably high specific surface areas [24]. Alloying with SrO increased the sintering temperatures but also resulted in denser specimens with finer submicron grain sizes [25]. Sathiyakumar investigated influence of various ceramic oxide additives and wollastonite on density and reported fully dense aluminas by introducing a multiphase of CuO, TiO_2, MgO, B_2O_3 [26,27]. When effect of doping is investigated for anatase-rutile transformation of nanostructured titania it is observed that Cu and Ni enhanced transformation as well as sintering while La retarded both transformation and densification [28]. The approach of retarding phase transformation is to achieve higher surface areas which offers uses in using ceramic materials as catalyst supports. Densification by dopants is provided by increasing transition temperatures of

stable phases which is a contradiction to concept of low temperature sintering. In that way even full densities are achieved, superior mechanical properties like extraordinary toughness are not expected.

Improvement of high temperature mechanical properties by dopants in structural ceramics are also studied. Excellent superplastic properties were observed for Y-TZ, Al_2O_3-doped TZ, SiO_2-doped TZ and ZrO_2-dispersed Al_2O_3 systems as a result of dense, fine-grained, and homogeneous microstructures [7]. The homogeneous, dense and fine grained sintered bodies of Al_2O_3 and/or Mn_3O_4 dispersed 3YTZ were obtained by colloidal processing and show a high-strain rate superplasticity with more than 600% strain values [29]. It is also known that creep resistance of Al_2O_3 is enhanced by addition of ZrO_2, Y_2O_3 and Lu_2O_3 in small amounts. Nanocrystalline zirconia powders alloyed with oxides of trivalent (Y, La, Bi) and tetravalent (Ce, Th) cations were investigated at sintering temperatures corresponding to their maximum shrinkage rates [30]. Effects of additives on phase transformations of nanocrystalline ceramic materials are also widely investigated. For alumina, from gamma to alpha transformation mechanism is strongly affected by a number of cation additives. Transition metals such as Fe^{2+}, Cr^{3+} and Ti^{4+} has been reported to accelerate the phase transformation while Cs^{+}, Ba^{2+}, La^{3+} and Si^{4+} additives retard it as mentioned previously. ZnF_2 and AlF_3 additives reduce the transformation temperatures of γ to α alumina and nano α-alumina particles with less than 100 nm as well. [31]

Effect of CuO on strain rates and the mechanism of superplasticity at CuO-doped Y-TZP ceramics were investigated and found that strain rates are doubled with addition of CuO, independent of the quantity, because of formation of an amorphous phase at the grain boundaries. [32,33]. A recent approach is silica doping of zirconia which yielded high ductilities at 1250 ºC with extended superplastic elongations up to 1100 % and high fracture resistance under compression, shear and tensile stresses [34,35].

Recently, toughening by introduction of a ductile metal to ceramic matrix has gained importance in production of nanocrystalline composite materials with superior mechanical properties. Especially nickel is proposed to be a good additive for nanocrystalline alumina to increase both strength and toughness and economical for it yields dense composite materials by pressureless sintering. [36-37]

The mechanical properties in terms of toughness as well as superplasticity at elevated temperatures are approved to be enhanced in composite nanocrystalline materials. Zirconia toughened alumina seems to be a favorite material for research studies related to nanoceramics. It is reported than grain boundary sliding is easier in Al_2O_3-ZrO_2 nano-composites causing a higher ductility compared to pure alumina and zirconia materials. That is related to conservation of grain boundary cavities during superplastic deformation due to multiphase interactions at the boundaries. On the other hand, dispersion of zirconia into alumina hinders grain growth of alumina. Moreover, the grain boundary cohesion is increased by addition of zirconia since the energy of Al_2O_3-ZrO_2 grain boundaries is smaller than Al_2O_3- Al_2O_3 grain boundaries. Such a microstructure makes Al_2O_3-ZrO_2 nano-composites an interesting candidate for superplastic forming processes. [38-39]

In this study, nanocrystalline boehmite powder is used as the precursor to obtain nanocrystallite alumina. Effect of mechanical pretreatment, sintering conditions and changes in microstructure and phase transformation behaviors are investigated in cases of seeded and unseeded boehmite powders.

Chapter 3

CONSOLIDATION

Alumina is a widely used ceramic in a variety of engineering fields with excellent chemical stability and good mechanical properties besides relatively low cost in the manufacturing process. It is an advanced ceramic in the applications of metallurgy, electrical insulating, microelectronics and as a structural ceramics. Transitional aluminas are used as catalysts, catalyst supports, adsorbents, coatings, fine-ceramics and abrasives.

The optimization of the process parameters becomes relevant from the cost-effectiveness view for commercialization of the products. Applications of structural ceramics demand specific physico-chemical characteristics of the precursors which in turn directly depend on processing routes employed.

In the manufacture of sub-micron high purity alumina powder, preparation of starting materials is one of the important processing step to achieve the desired particle size distributions for specific applications. The precursor powder that influence the microstructure and structural properties of the final product are to be characterized by means of chemical composition, particle size distribution, flow ability, morphology and density. To achieve the ideal properties in a cost-effective way, it is essential to optimize the characteristics of the precursors and minimizing energy consumption during consolidation which includes drying the prepared slurry or synthesized sol, mechanical pretreatment and compaction of powders obtained by appropriate forming, drying and sintering of the green bodies. In all steps, grain size of the ceramic has to be kept in nanoscale and agglomeration has to be prevented in order to yield highly dense sintered compacts with uniform microstructure.

3.1. Slurry Preparation

In many ceramic shaping processes such as slip-casting, tape-casting or spray-drying, the dispersion of the ceramic powder in an aqueous medium is required. These aqueous suspensions have to fulfill several requirements. The particles should not settle fast and remain in suspension, because otherwise segregation occurs which causes density inhomogeneities in the cast objects. In addition, the slurries have to be easily reproduced and be insensitive to slight variations in solid content, chemical composition and storage time. They also have to be of high solids content to reduce energy consumption in the drying stage. Milling is one of the important processing steps to achieve small particle size with high solid content of the slurries.

The prevailing trend in ceramic processing is the development of very fine particles in order to enhance sintering rates as well as to reduce the size scale for uniformity in blends. However, the combination of high solids loading and small particles leads to a viscosity increase because of increased particle-particle interactions and consequently to difficulties in slurry handling.

Ceramic powders have the tendency to agglomerate due to the attractive intra-particle Van der Waals forces. This tendency can be eliminated with the addition of appropriate dispersants which alter the powder surface properties so that repulsive forces overcome attractive ones and the particles remain separated in suspension. They act either due to electrostatic repulsion resulting from the overlapping of electrical double layers or due to steric hindrance resulting from absorption of large molecules.

When the rheological properties of concentrated slurries of alumina powder prepared by milling is investigated, it is reported that it is possible to maximize the solid loading through the milling and maintain the slurry pumpable. The slurry was subjected to freeze-drying to obtain ready-to-press granules which could be sintered to higher density with improved microstructure compared with that obtained by spray drying[40].

Various dispersants are used for the stabilization of oxide powder slurries but poly-methyl-acrylate salts which are usually referred with their commercial names like Darvan and Dolapix, are most frequently employed. The kind of organic dispersant used affect the green density of the specimens as well as the grain size of the sintered bodies. The slurries with optimized rheological properties with the appropriate type and amount of dispersants are utilized for the preparation of slip cast specimens and it is reported

that an increase on slurry solids content increased the density in the green and fired state and yielded better mechanical properties for alumina suspensions [41].

When the method of granulation is spray-drying use of dispersants is a more complex phenomena. If the slurry is to be spray-dried use of binders are required in addition to dispersants to impart good mechanical properties to the green body. But addition of binder drastically increases the viscosity. It has to be pointed that, for every case, the effects of rheological behavior of the slurry on the product properties has to be investigated for determining the appropriate type and concentration of dispersants and binders.

3.2. Spray Drying

Among the industrial methods of powder manufacturing the probably most versatile powder processing method is spray drying. Spray drying is the process by which a water or organic-based suspension which is called slurry, is transformed into a dry powder by spraying the fluid feed material into a hot drying medium. This process is a widely used method of producing granulated feed material for compaction processes. Spray drying enables the fabrication of composite powder by aggregation of any kind of small particles using an appropriate organic binder. Atomizing and drying lead to a large variety of powder shapes, from uniform solid spheres which are regarded as ideal granules for most spraying systems to elongated, pancake, donut shaped, needlelike or hollow granules.

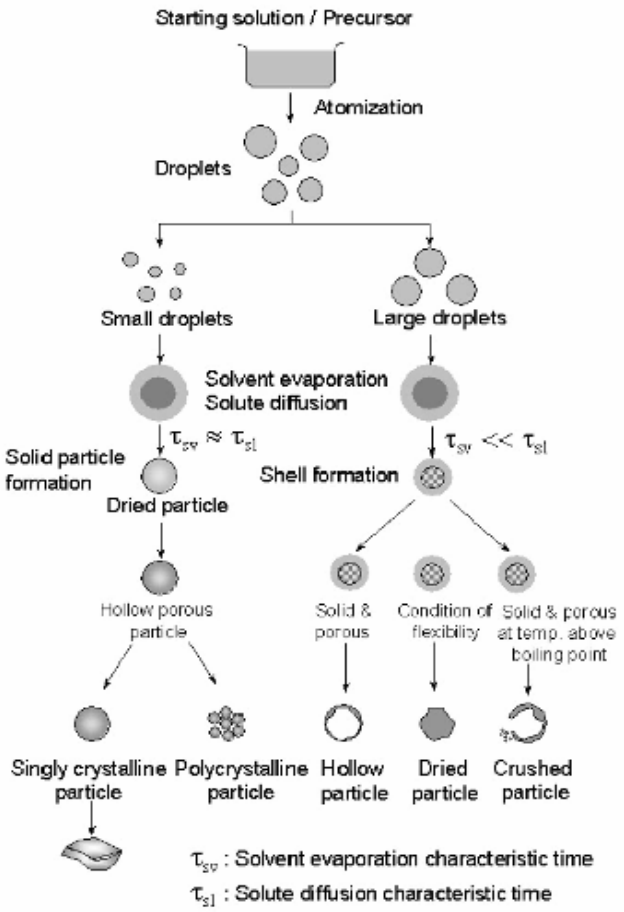

Fig.3.1. Morphology of particle prepared by spray method [43].

In previous studies effect of pH, binder and level of deflocculant in the slurries fed to spray dryer on size and shape of atomized particles are investigated and it is confirmed that suspension preparation is a controlling factor of the properties of spray dried powders.

Tsetsekou et al. reported poly(methacrylate) (Darvan C)/ PEG as the best pair they tried in order to have spray-dried granules with a diameter about 50 μm [42]. Bertrand et al. studied the slurry characteristics in terms of binder and dispersant contents at different pH versus zeta potential, dispersing efficiency and viscosity, yielding spray dried powders of about 35 μm mean particle size [44]. They used PAA as dispersant and styrene-acrylic acid ester copolymer as binder. The results of this study can be counted as a reference for comparison with the proceedings achieved in the present study including slurry preparation.

Zeta potential is expected to be higher than 40 mV for a successful dispersion. So, it is required to keep away from the isoelectric point where zeta potential is zero. Fig.3.2 shows change of surface charge of alumina particles with changing pH without introduction of any organic additives. The yield of dispersions at different pH is measured in terms of relative sediment height (Fig.3.3).

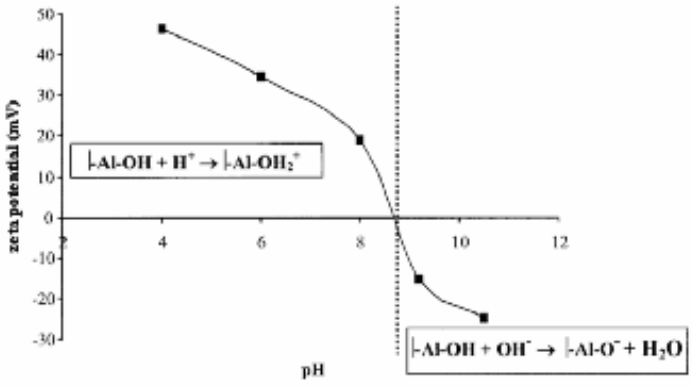

Fig.3.2. Zeta potentials of alumina aqueous slurries without organic additives as a function of pH. Isoelectric Point is reached at pH 8.7 [44].

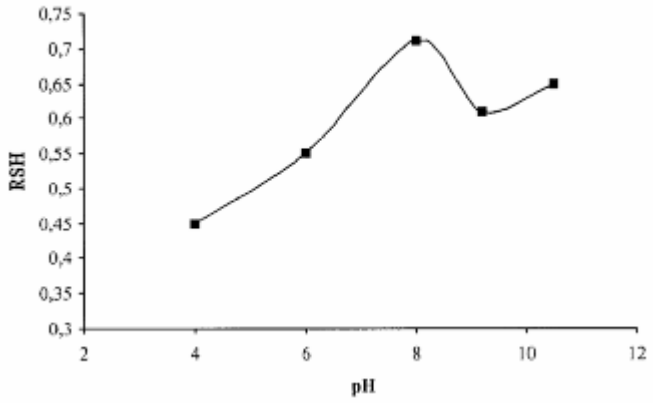

Fig.3.3. Relative Sedimentation Height (sediment cake height over suspension height, RSH) versus pH for alumina suspensions in water without organic additives [44].

Strong correlations are observed between dispersion efficiency in terms of sediment height, zeta potential and viscosity. When Fig.3.4 and Fig.3.5 are noticed, it is determined that the optimum conditions for a stable alumina slurry with maximum dispersed portion is obtained by 0.08 wt% PAA addition at pH=9. But the sediment height is no lower than alumina slurries containing no dispersant, the only advantage of the use of PAA additive is stability of the suspension which is an important parameter for the idealization of spray-drying process. The stabilization is electrosteric for this case and viscosity is at a relatively low level.

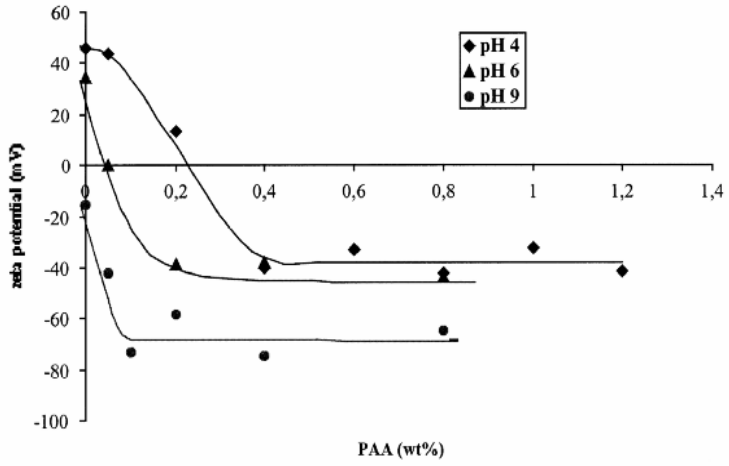

Fig.3.4. Zeta potentials versus amount of PAA for 30 vol.% alumina slurries as a function of pH [44].

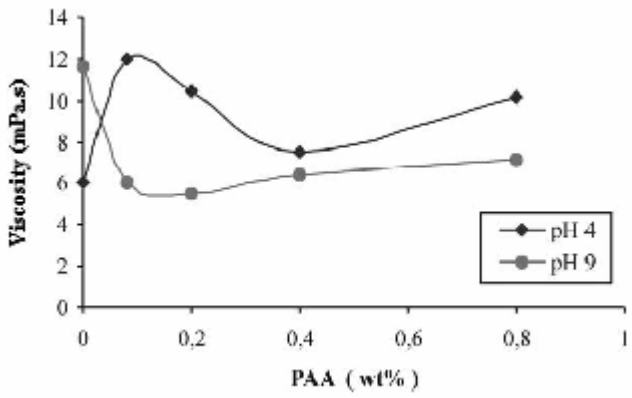

Fig.3.5. Variation of the viscosity, η, with PAA concentration for 30 vol.% alumina slurries at pH 4 and 9 [44].

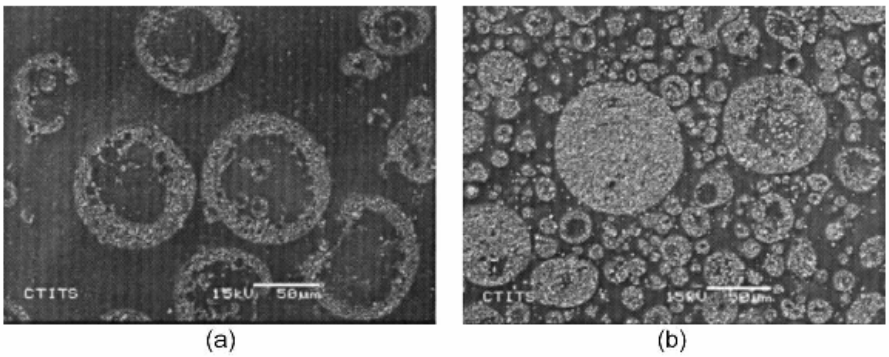

Fig.3.6. SEM images of spray dried granules of alumina from stable dispersions prepared by addition of 0.08% deflocculant and 15% binder at (a) pH 9 and (b) pH 4 [44].

As can be seen from Fig.3.6, dispersant (PAA) and binder addition yield high dispersion efficiencies besides stability only at basic medium, at pH=9, which ends up with hollow granules whereas the flocculated slurry prepared at pH=4 leads solid particles.

Effect of dispersant and binder interactions on slurry characteristics and in turn properties of powder, green bodies and eventual products are critical and requires a wide investigation. Dispersant-binder compatibility is necessary in order to ensure optimal slurry stability and rheology. Binder addition can cause destabilization of slurries already stabilized. A stable slurry with appropriate viscosity and high solid content is still a primary subject of research. In addition to polymeric dispersants, water soluble nonionic polymeric binders, are commonly added to obtain strong green parts

for ease of compaction. Most often, binders are nonionic polymers and the interaction with the oxide powder surfaces mainly proceeds via dispersive forces and hydrogen bonding. Such interactions are weak compared to the electrostatic interactions typically encountered for polyelectrolytes. The consequences of this difference in affinity between dispersant and binder for the powder surface is the increase of the viscosity of the suspension due to a large amount of binder remaining in solution and the nonhomogeneous distribution of the organic binder in the granule after spray-drying and in the green bodies. The competitive nature of polymer adsorption in systems involving two or more reagents are studied to predict coadsorbtion behavior of PAA and PVA, typical polymers used as a dispersant and binder, respectively, in the colloidal processing of alumina suspensions. It is concluded that the addition of PVA and PAA in binary systems has no bearing on their adsorption characteristics with respect to either pH or polymer concentration which makes the process very difficult to optimize [45].

To overcome the problems caused by multicomponent systems, use of a polyelectrolyte which acts as both dispersant and binding agent is offered. Sulfonic copolymers are one of the candidates. Besides sulfonic copolymers with two functional groups that are hydroxyls and sulfonic groups, synthesized copolymers are reported to be efficient dispersants for aqueous suspensions of alumina when the fraction of carboxyl groups is larger than 35% within the macromolecular chain. The amount of carboxyl groups controls the effective charge density of the particle surface and the copolymer is a successful dispersant with small quantities (<1%) added to the slurry yielding high solid contents. Hydroxyl groups in the copolymer are expected to act as a binder after forming of alumina by dry pressing.[46-48] The effect of these copolymers on the cohesion and mechanical properties of green products is under investigation.

Comparative studies among various binders on slurry viscosity for spray drying applications have shown that for the same binder concentration dramatic viscosity changes are observed from a binder to the other. Bush et al. evaluated commercial organic binders of PVA (poly vinyl alcohol), PEG (poly ethylene glycol) and CMC (carboxy methyl cellulose) with respect to slurry viscosity, granule diameter and green density of compacted specimens and concluded that PEG and PVA produces slurries with lowest viscosity whereas CMC produces the hardest grains. With respect to the properties of pressed bodies, PVA binders are reported to provide high green strength whereas PEG binders provide higher green density [42].

PVA is the most common binder in dry pressed ceramics. PVA, as a water soluble binder, is completely dissolved in slurries. But adsorption tests carried on high pH values indicated that adsorption density of PVA on alumina is much less compared to PAA. PVA is a nonionic molecule and the forces of interaction with alumina is attributed primarily to hydrogen bonding. The higher adsorption density in the alkaline pH range may be explained on the basis of increased hydroxilation of the alumina surface at highly basic pH values leading to increased hydrogen bonding capability.

It has also been reported that PVA tend to migrate and exhibit a nonhomogeneous distribution in ceramic powders after drying. Baklouti and Mandanas have investigated the segregation behavior of PVA during spray-drying and modelled the formation of spherical droplets with the aid of binder in presence of the organic dispersant PAA. As shown schematically in Fig.3.7, more than adsorbed quantity is proved to stay on the surface of droplets. So a barrier is formed at the surface of particles increasing green strength, causing good cohesion under pressing. An additional effect of this barrier is slowing the drying rate. An addition of 2-4% PVA decreases the evaporation rate by 12-20 % during constant rate drying period.

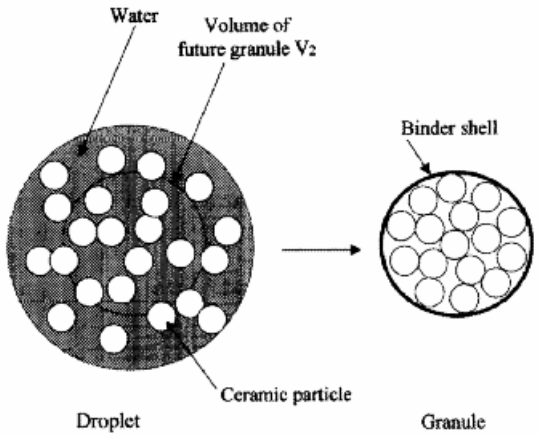

Fig.3.7. Schematics of the evolution of a spherical droplet of dispersed slurry during drying [50].

Evaluations of PVA behavior under heat treatments show that, its existence has influence on the strength and microstructure of sintered bodies as well as granules and green compacts. Baklouti et al. reports that degradation of PVA occurs at a wide temperature range due to loss of adsorbed water up to 200 ºC and gradual thermal decomposition up to 600ºC which is a wide interval during heat treatments. Therefore homogeneity of binder distribution is an important aspect on phase transformation processes of ultrafine ceramic powders. The nonuniform distribution of the organic binder in spray-dried granules can lead to microstructural defects during subsequent pressing. The voids occurred in that way are difficult to remove during sintering. Such processing voids create fracture centers and reduce the strength of the fired body [49-51].

3.3. Compaction

Compaction of spray-dried ceramic powders is a widely used forming process. Dry pressing involves the uniaxial compaction of spray dried granules consisting ceramic particles bound by an organic binder. A schematic compaction curve is shown in Fig.3.8, where the part density increases in two stages due to granule rearrangement and deformation, and particle rearrangement. Then upon releasing the compaction pressure, the part expands. The expansion occurs as both elastic springback due to energy stored in the structure and a viscoelastic relaxation that is time-dependent.

The two common problems that may come out of compaction are, failure due to expansion in form of end caps or delamination, or dimensional variability. Therefore the binder content and binder plasticity are extremely important on quality of the compacts. When the binder content is increased, the compaction stress has to increase due to the greater amount of binder which needs to be deformed and displaced. On the other hand, the Young's modulus increases when the binder content increases or when the porosity decreases.

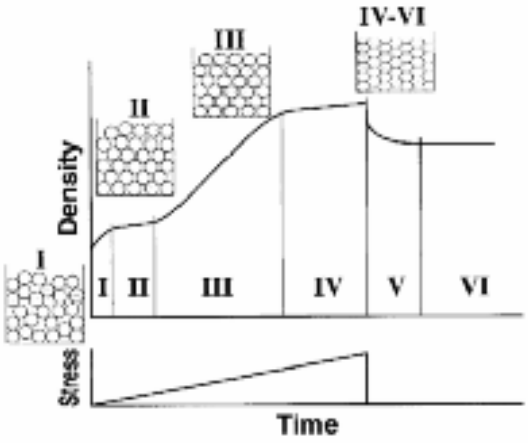

Fig.3.8. A qualitative description of compaction showing the change in density of the powder in response to an applied stress: Regions show (I) granule rearrangement, (II) initial granule yield, (III) massive granule deformation, (IV) compression of the dense compact, (IV-V) the part is ejected and undergoes instantaneous springback, (V) time dependent relaxation, and (VI) ultimate density [52].

Binder type is critical on shrinkage and springback behaviors of compacted bodies. The working temperature and glass transition temperature of the polymer are to

be considered in selection of binder for specific purposes. When pressing a powder with a binder whose T_g is much lower than working temperature the binder is easily deformed and high green densities are yielded at moderate stresses. As binder T_g increases it becomes stiffer and brittle which requires higher compaction stresses. T_g of PVA is 79ºC which can be reduced by plasticizers such as glycerol, ethylene glycol or water [52].

A water soluble binder readily absorbs water from the atmosphere to an equilibrium moisture level. The plasticizers stated above increase moisture capacity of the binder. The effect of moisture on the compaction behavior of the agglomerates prepared using PEG is not marked. But in the PVA system, the yield pressure of the wet agglomerates is lower than that of the dry agglomerates. At the same compaction pressure level, the green densities of wet agglomerates are significantly higher than that of dry ones. Dried PVA exhibit poor strength as shown in Fig.3.9. So, modifying the moisture content to obtain binder plasticity is important for a satisfactory compaction.

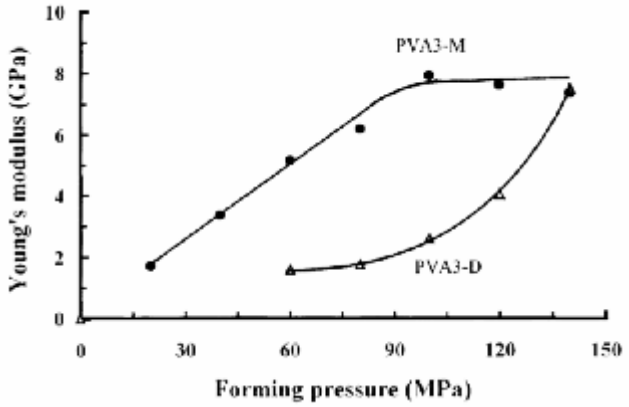

Fig.3.9. Effect of moisture on the variation of the Young's modulus with forming pressure for samples prepared with 3 wt% PVA, moist and dry [53].

During pressing, the total surface of the polymeric bridges increases by crushing progressively the binder layer between alumina particles (Fig.3.10). The pressure necessary to totally crush the layer of the binder between two spherical alumina particles and then to reach the contact between particles can be estimated on the basis of the hardness of the binder which is directly related to Young's modulus of the

polymer[53]. When the binder is ductile, Young's modulus increases rapidly and linearly with forming pressure until it reaches a plateau which is the maximum value.

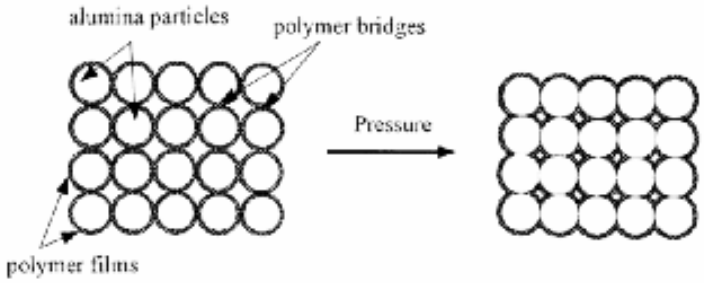

Fig.3.10. The polymeric bridge surface, between two particles, increases by crashing progressively the binder layer until the grains come in contact. Above this pressure, the Young's modulus remains constant [53].

In order to confirm the main contribution of the concentration of binder located within the granule, small spray-dried alumina granules of about 20 μm mean size containing 3wt% PVA are compared with the ones of 200 μm with the same amount of PVA with respect to alumina. A parallel evolution of the Young's modulus versus forming pressure is obtained of samples prepared from the two sizes of granules. Because the relative amount of binder segregated during drying are similar in both cases, even though the thickness of the external polymeric layer is greatly reduced in the case of 20 μm diameter granules as confirmed by Fig.3.11. Appearance of spray dried and compacted granules after addition of 3 % dry PVA are displayed in Fig.3.12.

Sample size is another parameter to have a significant effect on yield of the compaction. In larger samples, the surface area to volume ratio is smaller for the influence of die wall friction on the bulk compaction of the powder is reduced. The friction can be reduced by using an appropriate lubricant. But the residue of the lubricant may cause impurities by remaining on the bodies after sintering. [54-55]

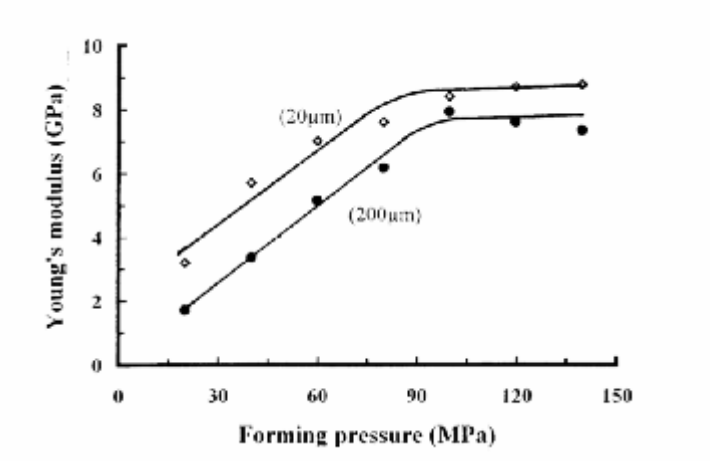

Fig.3.11. Effect of the mean size of spray-dried granules on the evolution of Young's modulus of pressed samples from powders containing 3 wt% PVA and the same residual moisture [53].

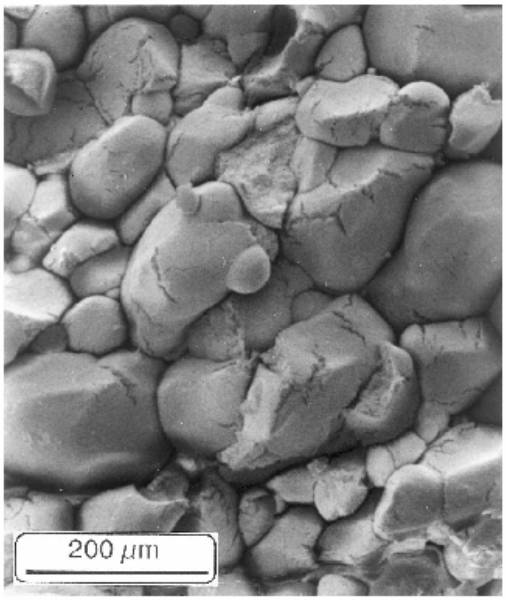

Fig.3.12. SEM micrograph of fracture surface of alumina sample pressed at 80 MPa containing 3 wt% of dried PVA on dry basis of alumina powder [53].

3.4. Subsequent Phase Transformation and Densification of Alumina

Phase transformation is the main phenomena to consider in order to enhance the densification of nanostructured alumina. To achieve full densities with final grain sizes <100 nm without grain growth in the final stages of densification, the relative kinetics of grain boundary movement and grain growth have to be controlled and tuned. By following the densification curves and the corresponding microstructural evolution the key mechanism of phase transformation assisted densification can be understood [56].

For systems where the starting powders exist in a stable crystallographic phase, very promising results have been achieved. But for nanosized powders which exist in a metastable crystallographic phase, the control of the transformation into the stable phase avoiding an explosive grain growth seems to be the most difficult step towards fully dense nanograined ceramics.

The densification of alumina during phase transformation from γ to α-phase occur in two stages (notated as R1 and R2 in Fig.3.13) in constant heating rate experiments. Densification rate curves are computed from shrinkage data of γ-alumina with particle size of 15-20 nm. The first is a rapid densification associated with the phase transition of γ-Al_2O_3 via transition aluminas (δ and θ) to the stable α-phase at around 1200º C. The second is a slower densification of α- Al_2O_3 at higher temperatures.

The studies on densification and microstructure of alumina via phase transformations under pressureless heat treatments show that resulting densities of the sintered products strongly depend on green density, conditions of thermal cycle and the content of α-phase.

Green densities of pellets pressed from alumina nanopowder higher than 60% of the theoretical density were not achieved at room temperature and at compacting pressures less than 1 GPa. This maximum density is still lower than the density attainable with coarse grained alumina powder where densities close to the theoretical fractional density of spherical non-agglomerated random dense packed particles of about 64% are achieved.

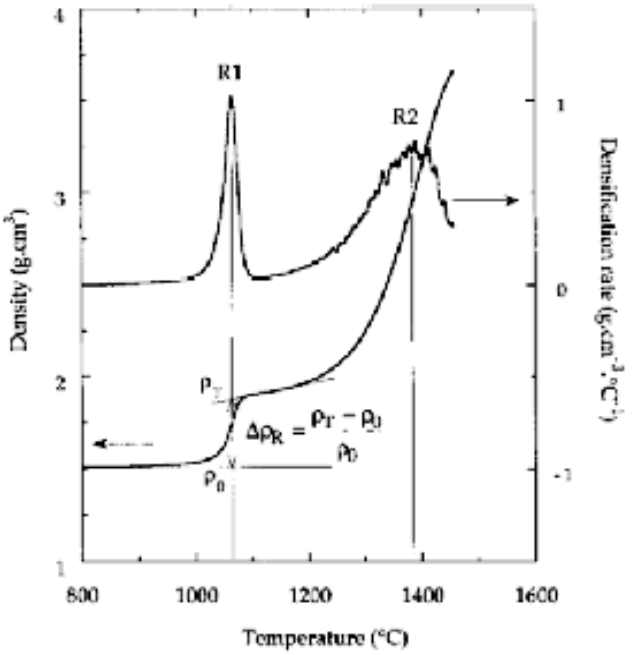

Fig.3.13. Typical densification curves of transitional alumina powder compact with an initial α-alumina content of 6%, cold isostatic compaction applied at 250 MPa, and heated at a rate of 1°C/min [56].

The effect of compact density and α-alumina seeding on densification and microstructure evolution during the sintering of ultrafine alumina samples compacted at mega and giga levels are illustrated as shown in Fig.3.14. by Ahn et al. [57]. The green density affects the sintered density and grain size as well as onset temperature of γ- α phase transition.

Recent studies on gamma alumina powder compacts have shown that the densification observed during the phase transition into alpha alumina increases as the green density decreases. The level of densification is much higher than what would be expected from the difference in density between the metastable and stable crystallographic phases and can be further enhanced by increasing the heating rate and α-alumina level of the precursor as shown in Fig.3.15 .

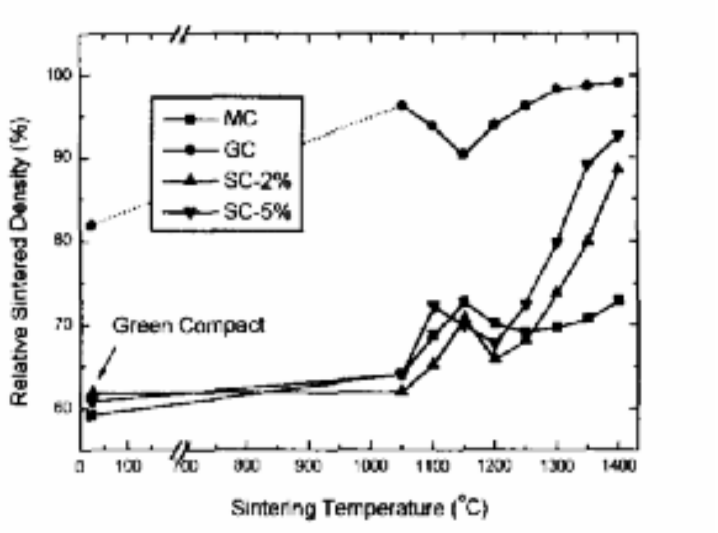

Fig.3.14. Variations of relative sintered density with sintering temperature for the respective compacts of ultrafine γ-alumina compacts: MC (green bodies with 58% of theoretical density), GC (green bodies with 83% of theoretical density, compacted under 4.5 GPa), SC-2% and SC-5% (seeded compact with α-alumina particles smaller than 115 nm, at contents of 2% and 5%) [57].

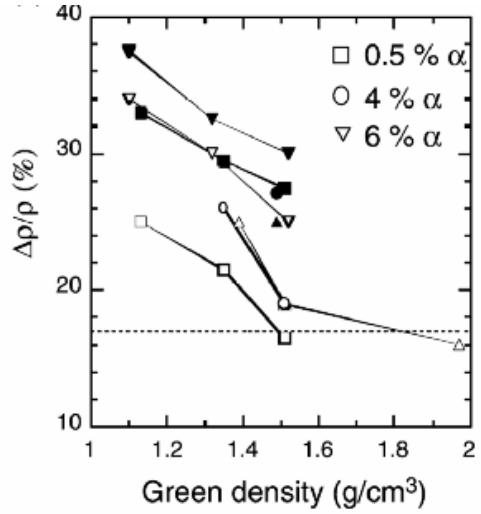

Fig.3.15. Relative density changes for gamma alumina to alpha alumina phase transition measured from dilatometry experiments as a function of green density for three powders and two different heating rates (open symbols 1Cº/min, filled symbols 10ºC/min) [17].

The packing of nanopowder is complicated by the fact that they are invariably made up of agglomerates 10-20 times larger than the primary nanoparticle. One major factor in the densification of nanopowder compacts is to stimulate interagglomerate densification and not to have a predominance of intra-agglomerate densification leaving large stable pores in the final piece (Fig.3.16).

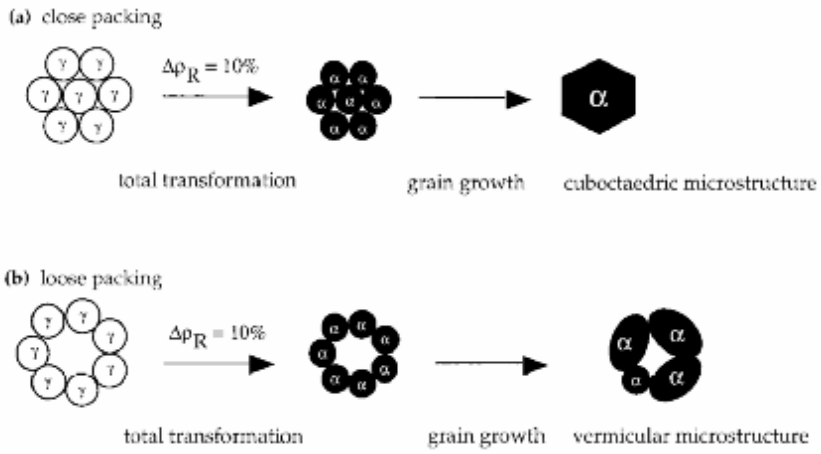

Fig.3.16. Schematic transformation induced microstructure modifications (a) transformation and grain growth in green compact close packing, (b) nucleation, transformation and grain growth in low density green body [56].

Fig.3.17 illustrates the effect of cold isostatic press (CIP) pressure on the densification behavior of the alumina powders. For the same heating rate, temperature of the the first densification peak decreases when the CIP pressure increases which agrees with the studies carried by green compacts prepared by extremely high compaction pressures at GPa level.

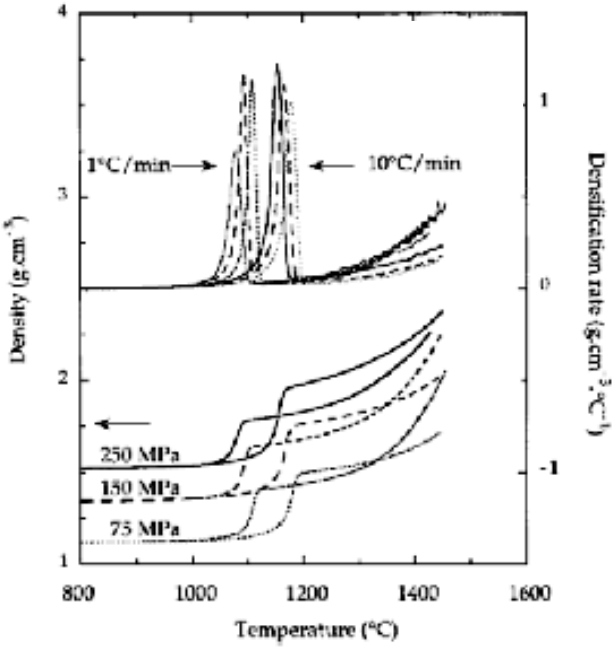

Fig. 3.17. Influence of the cold isostatic compaction pressure on the densification curves of γ-alumina with α-alumina content less than 0.5 %, for two different heating rates: 1ºC/min and 10ºC/min [56].

In the manufacture of sub-micron high purity alumina powder, "milling" is another important process applied during consolidation to increase the yield of dispersions and achieve desired particle sizes. Milling reduces energy consumption and prevents contamination from the grinding systems. In the case of agglomerated particles the packing density tends to decrease and can be correlated with increasing attraction between particles with decreasing particle size due to e.g. van-der-Waals interaction.

The bonding between the particles of strong agglomerates are expected to be much stronger than the bonding between particles which are only attracted by van-der-Waals interaction. Whereas particles which are only attracted by weak interaction can more easily slide into voids of the green body during compaction, the particles in strong agglomerates have to experience large shearing forces necessary for neck cleavage to occur before sliding of these particles can take place. Therefore a modification of the nanopowder by reducing the amount of necks between particles before compaction will be a key to obtain larger green densities at lower compacting pressures. The goal of this work is to demonstrate a simple ball milling method which can be applied to nanopowders in order to crack strong agglomerates.

Green bodies pressed from the powders produced by laser ablation method and treated by a short milling process exhibit up to 15% higher densities than bodies prepared from the unmodified material (Fig.3.18). It is also demonstrated that the sintering activity of the milled nanopowder significantly increases leading to almost dense material at simplified sintering conditions (Fig.3.19).

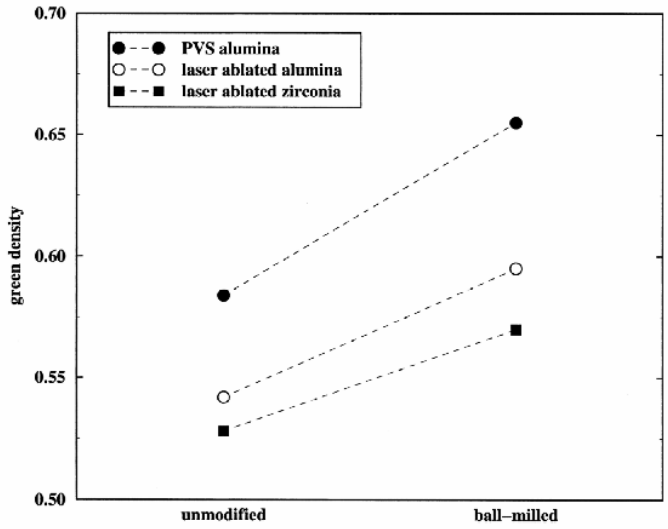

Fig.3.18. The densities of green bodies pressed uniaxially at 440 MPa from ball-milled and unmodified powder [58].

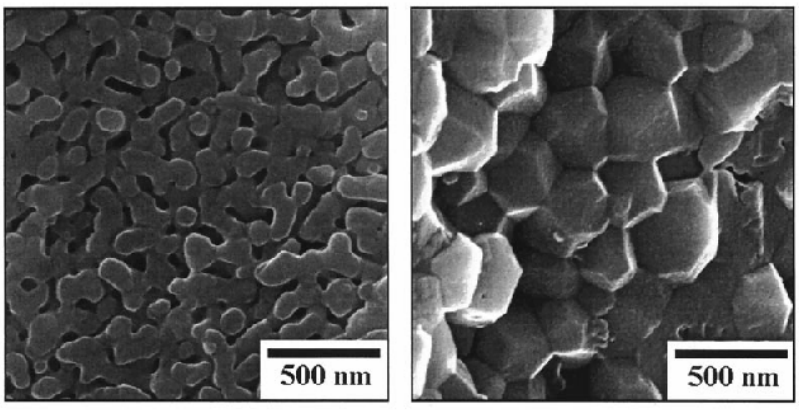

Fig.3.19. SEM micrographs of alumina bodies sintered at 1300°C and 80 MPa; without ball-milling (left) and with the milling step (right) [58].

3.5. Thermal Cycle and Content of α-Phase

Heating rate has to be considered as an important parameter on microstructure of sintered bodies as well as its effects on densification rate. The densification behavior of γ-alumina containing 0.5% of stable phase has been shown for various heating rates between 5ºC and 30ºC in Fig. 3.20.

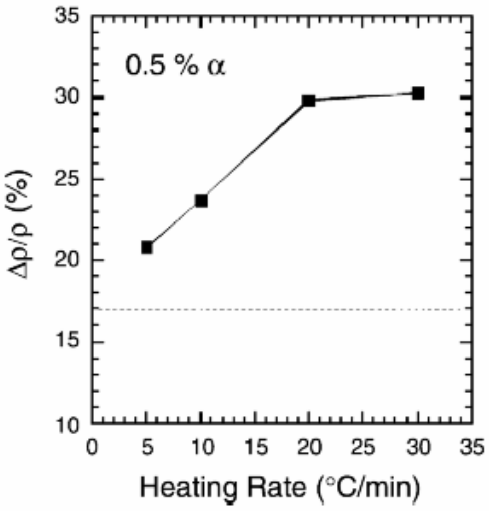

Fig.3.20. Relative density changes for gamma alumina to alpha alumina phase transition measured from dilatometry experiments as a function of heating rate for a gamma alumina with 0.5% alpha phase[17].

Legros et al. have shown the role of heating rate on each parameter that is effective in densification of sintered aluminas with various contents of alpha phase in their detailed study [56]. Effects of heating at 1ºC/min and 10ºC/min rates on densification rates and ranges are demonstrated in Fig 3.21. Typical microstructures of sintered samples with constant heating rates of 1ºC/min and 10ºC/min up to 1450ºC are also shown in Fig.3.22. It is possible to see that the sample with the lowest content of alpha phase exhibits vermicular microstructures; but this is less pronounced in case of 10ºC/min heating rate. It is obvious in the micrographs that grain size is higher for the lower heating rate and densities are rather low at about 2.35 g/cm^3. Sintered γ-alumina samples with α-content of 6% have cuboctahedral grains without marked vermicular microstructure and the density of the sample sintered with a heating rate of 1ºC/min (Fig.3.22-d) is nearly 90% of the theoretical density.

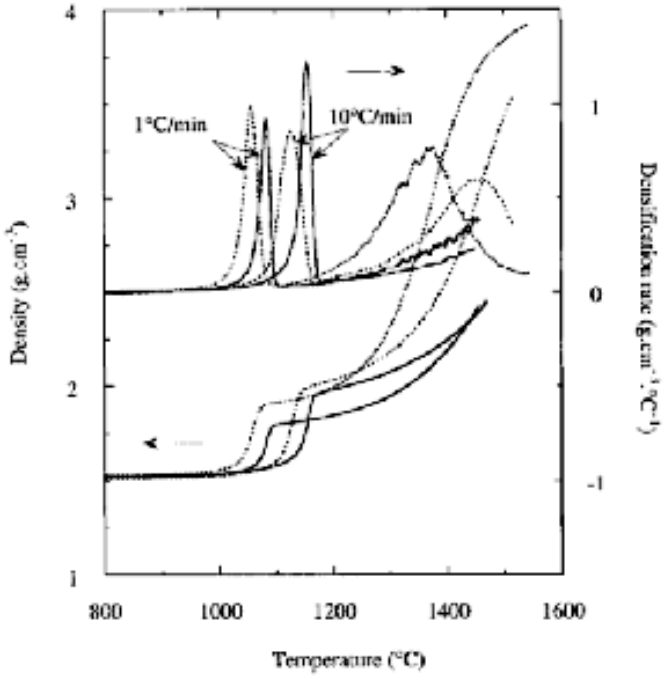

Fig.3.21. Densification curves of γ-alumina with α-alumina content of less than 0.5% and 6.0%, compacted at 250 MPa and shrinked at two different heating rates: 1ºC/min and 10ºC/min [56].

As well as heating rates, formation of fully dense nanograined ceramics using a two-step sintering treatment which limits grain growth in the final stages of densification is demonstrated. The study includes a densification to about 75% density in the first stage and then lowering the temperature by 100-150 ºC in the second step whereby densification is completed without further growth. It is explained that the final densification without grain growth by the reduction of the grain boundary migration kinetics with respect to grain boundary diffusion [59]. Successful preheating treatments are also reported for densification of alpha alumina with submicron particle size [60-62]. It is figured that most of the grain growth takes place in the first stage and gives grains between 5-10 times the original powder primary particle size.

Sintering conditions for densification of commercial aluminas dispersed or flocculated and slipcasted are also investigated and elongated sintering time is signified as the critical parameter on densification at low sintering temperatures [63].

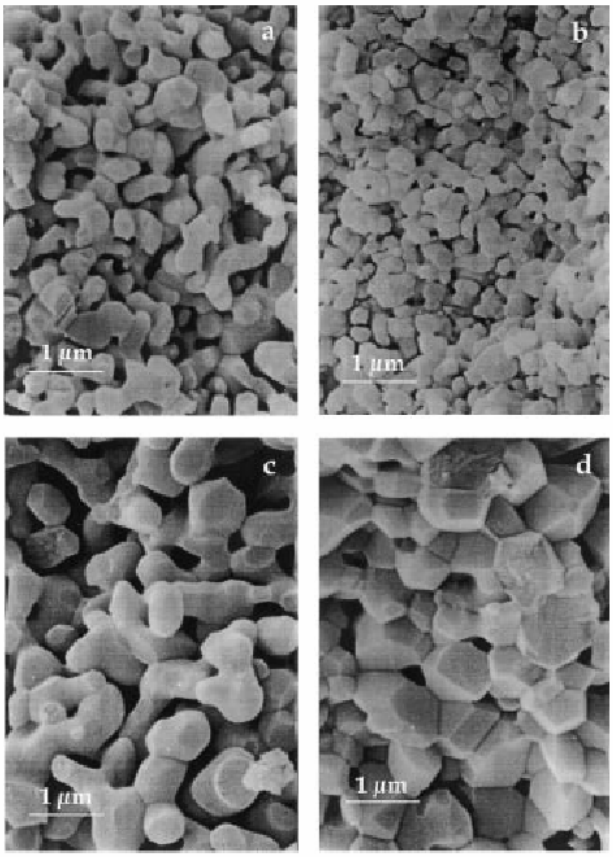

Fig.3.22. Microstructures of sintered samples up to 1450ºC in constant heating rate conditions: (a) with α content < 0.5, 10ºC/min heating rate, ρ =2.37 g/cm^3 ; (b) 6% α content, 10 ºC/min heating rate, ρ =2.98 g/cm^3; (c) with α content < 0.5, 1ºC/min heating rate, ρ =2.35 g/cm^3; (d) 6% α content, 1 ºC/min heating rate, ρ =3.61 g/cm^3. All green samples were cold isostatically pressed under 250 MPa [56].

Densification by rearrangement via phase transformation has been developed by using seeds of the stable phase. This controls the transformation and number of nuclei per unit volume, producing dense materials with grain sizes of a few hundred nanometers at temperatures as low as 1200ºC for alumina. In addition to given information in previous sections, Fig.3.23 summarizes how the densification is significantly enhanced in the alpha phase when up to 6% of the alpha phase is present in the gamma alumina compacts.

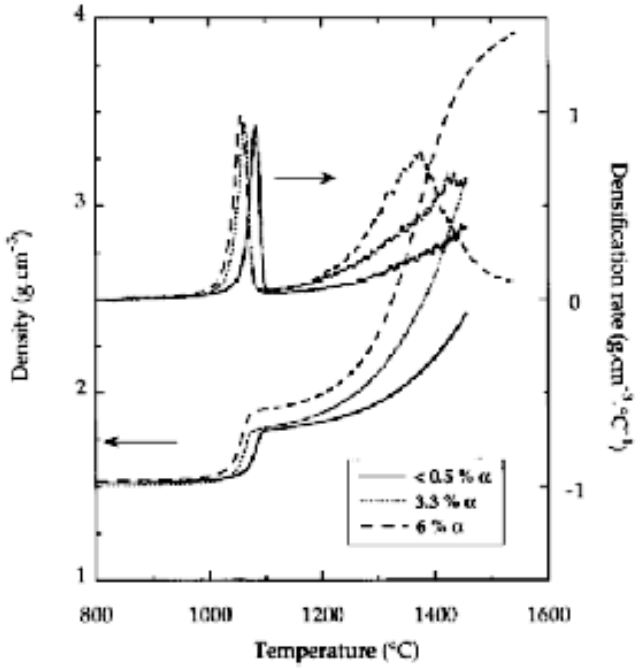

Fig.3.23. Comparison of densification behaviors of powder with different α-alumina contents heated at a rate of 1ºC/min [56].

The relative density change $\Delta\rho/\rho$ expected for the gamma (3.41 g/cm^3) to alpha (3.897 g/cm^3) transition is 17 %. In almost all cases this is enhanced and may be explained by mechanism of rearrangement and coalescence. The enhanced relative density change brought about particle rearrangement during transformation as shown in Fig.3.24.

Despite this success, the problem of producing small well-dispersed seeds at a reasonable cost, as well as the inherent problems of agglomeration linked to the drying of gel precursors often limits the use of the approach.

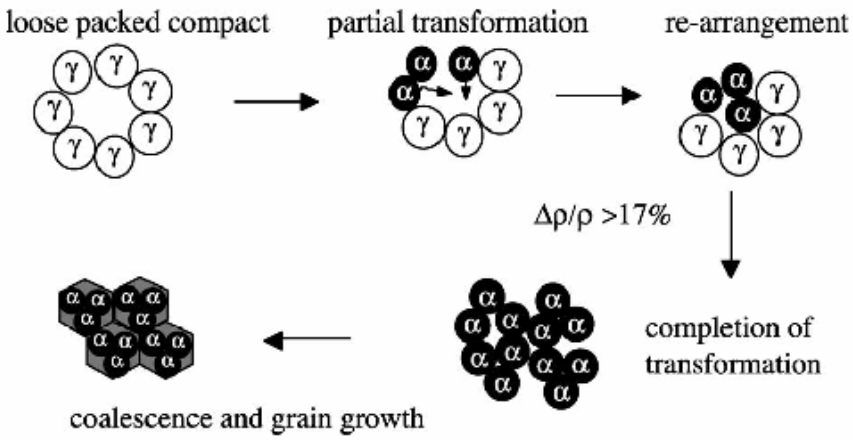

Fig.3.24 Schematic transformation induced microstructure modifications during nucleation, transformation, rearrangement and grain growth in low density green body with particle reaarangement α-alumina particles [17].

Chapter 4

BOEHMITE

When sintering nano-sized precursor powders densification is very often accompanied with an accelerated grain growth. In order to suppress grain growth during densification it is necessary to enhance the densification kinetics and to depress grain growth kinetics to handle the proccessing temperature that yields nano-structure ceramics. This critical temperature above which grain growth rate becomes appreciable is determined by the properties of the precursor powders, such as their particle size, reactivity, degree of agglomeration, etc. In this manner, the use of well de-agglomerated nano-sized precursors is crucial to suppress grain growth and obtain homogeneous microstructures. The two factors which seem essential to achieve fully dense nano-grained ceramics are very fine <20 nm non-agglomerated powders and the use of appropriate sintering cycles.

Alumina is generally obtained by heat treatments of aluminum hydroxides such as boehmite, gibbsite or other transitional aluminas. But it is shown that transitional aluminas, namely γ- or δ-Al_2O_3 with nanocrystalline structure are not suitable starting materials for the production of dense alumina bodies with grain size less than 100 nm. The transformation temperature of nanocrystalline alumina from γ to α phase is decreased from about 1400ºC at ambient pressure to 800ºC and nano-grain sizes are obtained with densities more than 95% of the theoretical density (3.98 g/cm^3) by Mayo et al. But the process requires very high pressures more than 5 GPa [19]. In order to apply an efficient pressureless sintering, transitional aluminas and stable α-alumina are rather obtained from the alumina hydroxide precursors like $Al(OH)_3$ (gibbsite and bayerite) or AlOOH (boehmite and diaspore) by hydroxilation. The phase transformation routes of those are shown in Fig.4.1.

Among various precursors whose thermal transformation behaviors have intensively been studied, boehmite has been the most studied starting material to produce alumina for it is a widely used commercial product available in both sol and powder forms, offerring a wide range of chemical and physical properties.

4.1. Phase Transformation of Boehmite

When boehmite is annealed, it undergoes a series of phase transformations: from boehmite into γ-alumina and then into δ and θ-alumina, which are the transitional aluminas. Phase transition routes are shown for alumina from various starting materials in Fig.4.1. Eventual phase is known as α-alumina (or corundum) which is thermodynamically the most stable alumina phase.

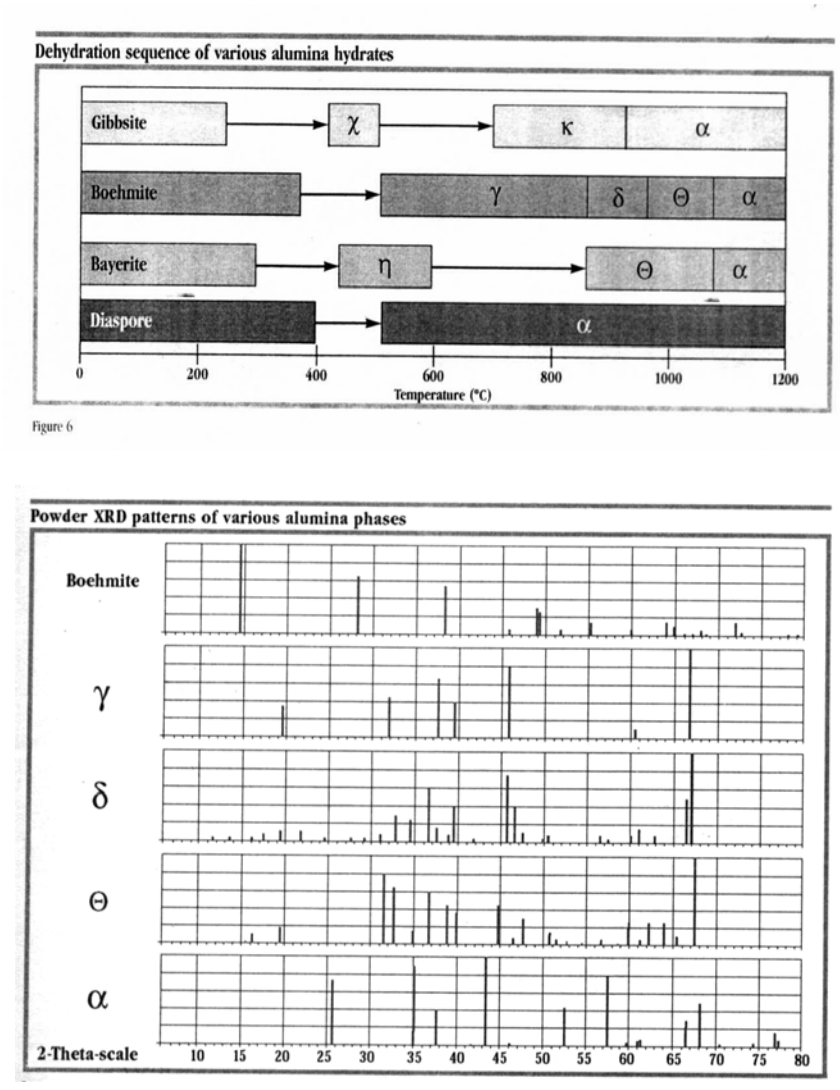

Fig.4.1. (a)Dehydration sequence of various alumina hydroxides patterns of alumina. (b) Powder XRD phases derived from boehmite presursor [App.A].

The transformations of γ-Al_2O_3 into δ and θ-Al_2O_3 proceeds pseudomorphically, requiring small amounts of energy that are hardly detected in DTA experiments. DTA and TG curves of boehmite alumina with a crystal size of 10 nm and particle size of 25 μm are given in Fig.4.2. where it is seen that the transformation of boehmite into γ-Al_2O_3 is endothermic and occurs after partial dehydroxilation between 300 and 550ºC while the transformation of transitional aluminas into α- Al_2O_3 is exothermic and requires complete dehydroxilation which occurs between 800 and 1300ºC.

The significant weight loss below 200ºC occurs from water desorption. The weight loss observed between 200 and 550ºC correspons to transformation to γ-phase and produced by removal of hydroxyls. This was quantified by using the following stichiometric equation for boehmite transformation:

$$2\gamma\text{-AlOOH} \rightarrow H_2O + Al_2O_3$$

But the amount of hydroxyls leaving the sample is larger than expected from stoichiometry for nanocrystalline boehmite as can be seen from TG analysis (Fig.4.2).

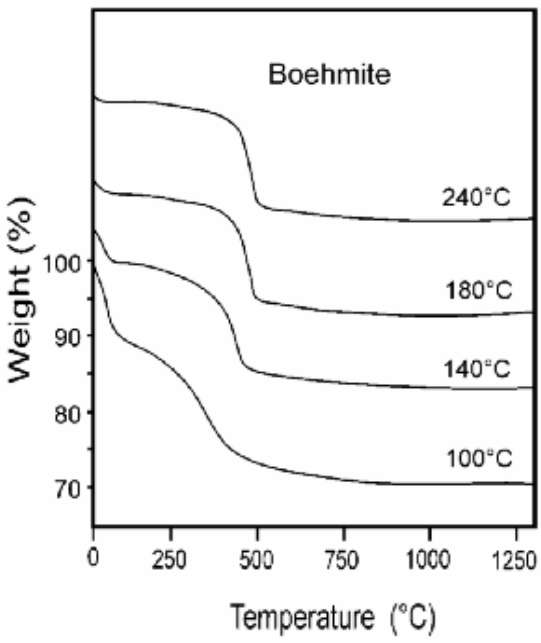

Fig.4.2. TGA curves of boehmite samples prepared at different temperatures between 100ºC and 240ºC [64] .

This behavior is put to depend on crystalline structure of boehmite; the weight loss via hydroxyl groups are observed to be relative to crystalline size of boehmite precursor. The dependence of γ-transformation on the crystallite size can be explained by crystalline structure of boehmite which is illustrated by Fig.4.3.

Boehmite crystallites are made of double layers of octahedra with an aluminum atom near their center and two hydroxyls and four oxygen atoms in their vertices (Fig.4.3). The octahedra in the double layers interact strongly with each other, but the interaction between double layers is via hydrogen bond and is weak. The transition temperature from boehmite into γ-alumina depends on the hydrogen bond strength between the octahedral double layers that sustain the crystalline structure.

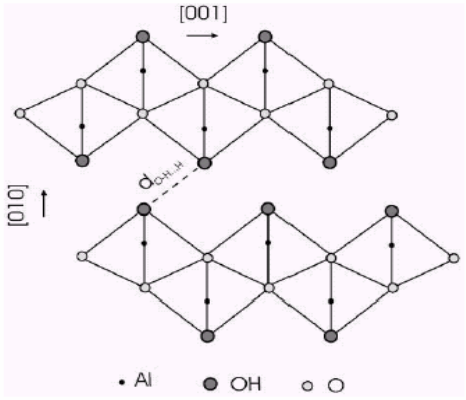

Fig.4.3. Boehmite's crystalline structure. Double octahedral layers are held together through hydrogen bonds [64].

So the exothermic transformation temperature from transitional aluminas into α-Al_2O_3 varies with boehmite's crystal size, too: it increases with larger crystal sizes. Dependence of transition temperatures and crystallite sizes of metastable γ and stable α phases are given in Table 4.1. Also the properties of γ-Al_2O_3 and α-Al_2O_3 derived from boehmite are strongly affected by its crystallinity in the means of atomic bond lengths and bond angles.

4.2. Growth characteristics of boehmite

During thermal treatment aluminum oxide hydroxide (AlO(OH)) undergoes the following series of polymorphic phase transformations before final conversion to the thermodynamically stable phase, α-Al_2O_3 polymorph called corundum.

Boehmite$\rightarrow \gamma \rightarrow \delta \rightarrow \theta \rightarrow \alpha$-$Al_2O_3$

Wen&Yen investigated the growth characteristics of the crystallites and agglomerates during the final phase transformation ($\theta \rightarrow \alpha$) of ultrafine alumina powders [65]. They calcined the dispersed and spray-dried boehmite powder at 900ºC for one hour and obtained a powder that is composed of δ- Al_2O_3 and θ-Al_2O_3 . The X-Ray powder diffraction pattern of the calcined powder is given in Fig. 4.4.

Table 4.1. Boehmite transition temperatures into γ-Al_2O_3 and α-Al_2O_3 as a function of boehmite crystalline size [64].

Boehmite crystal size $d_{(020)}$ nm	γ-Al_2O_3 crystal size $d\gamma$ nm	γ-Al_2O_3 transition temp. T ºC	α-Al_2O_3 transition temp. T ºC
1.13	2.65	380	1190
1.56	2.69	403	1198
2.04	3.0	413	1203
2.42	3.3	428	1206
6.90	4.5	471	1249
14.2	6.2	508	1289
26.3	6.6	528	1290

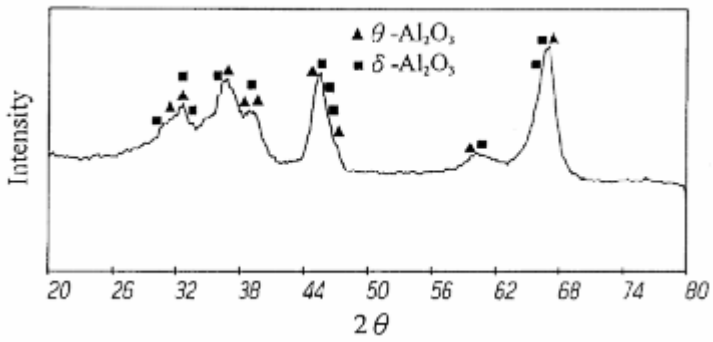

Fig.4.4. XRD patterns of alumina powder calcined at 900ºC for 1 h [65].

The calcined powder is taken as the starting material for α-Al_2O_3 and further heating is applied to observe phase transformation characteristics. It has been shown that heating rate is important on transition temperature to α-phase as well as crystallite size and degree of transformation in terms of α-Al_2O_3 content. Comparing the change in the crystallite size with the fraction variation of α-Al_2O_3 (Fig.4.5) it can be seen that the size suddenly increases from 17 nm to 45 nm in the period before the formation of a large amount of α-Al_2O_3, for various heating rates. Then the growth seizes and remains unchanged at 45-55 nm until the phase transformation from θ-phase to α-phase is completed.

In Fig.4.6 DTA profiles for the same heating rates are given. It is obvious that exothermic peaks of phase transformation to α-Al_2O_3 are corresponding to drastic increases in α-Al_2O_3 contents. The authors have resulted that nucleation of α-Al_2O_3 proceeds throughout the period of phase transformation. Thus the flat portion of the DTA profiles can represent the periods in which nucleation is predominant.

Growth mechanism of α-Al_2O_3 crystallite is proposed to occur in two distinct modes. One is a well known mechanism where the growth takes place through migration of the crystallite boundaries between individual α-Al_2O_3 crystallites and their surrounding θ-Al_2O_3 crystallites matrix. The other, which is a new approach peculiar to this study, is that the growth is achieved by the coalescence of the α-Al_2O_3 nuclei.

It is presumed that the exothermic peak is dominated by growth of α-crystallites following the nucleation as shown in Fig.4.6 and the crystallite growth starts from the nucleation stage. The crystallite growth by coalescence would be achieved before that if there existed a substantial amount of α-Al_2O_3 nuclei.

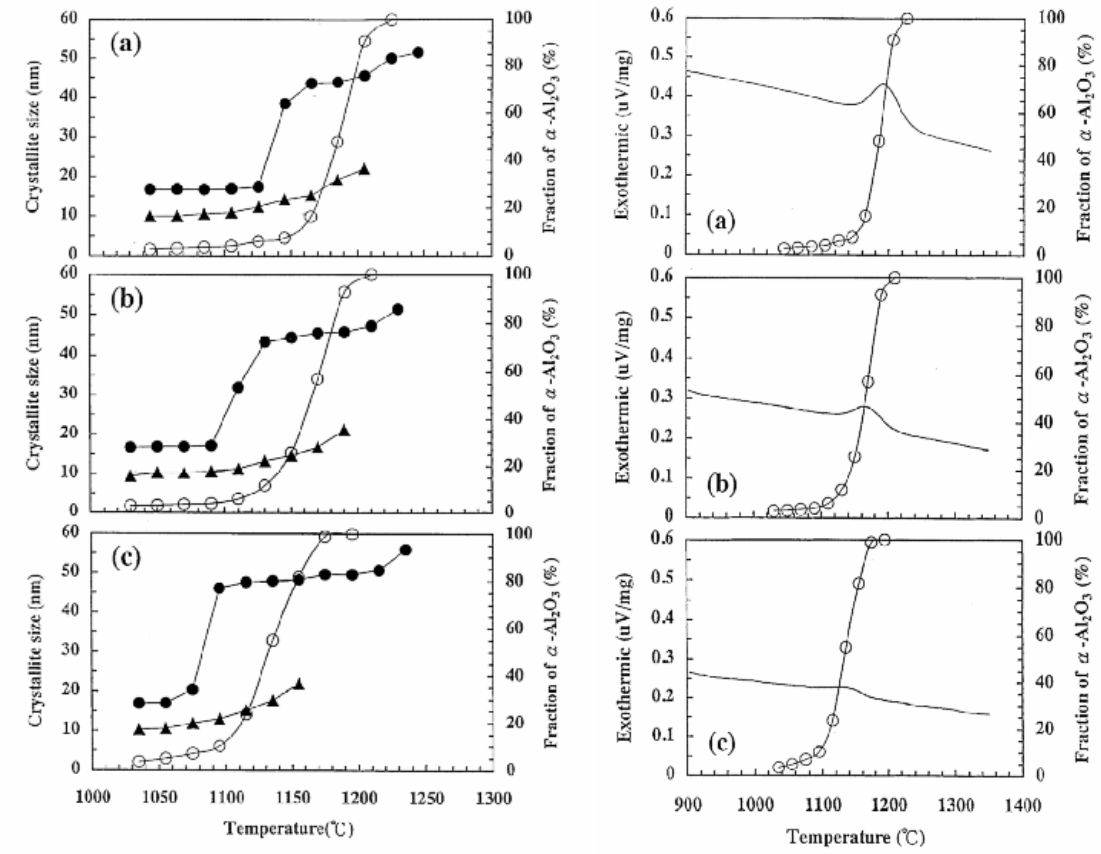

Fig.4.5. Relationship between the crystallite sizes of θ - and α -Al_2O_3 and the fraction of α -Al_2O_3 during θ to α -Al_2O_3 phase transformation with heating rates & DTA profiles of the θ→α-Al_2O_3 phase transformation and the fraction of α-Al_2O_3 with heating rates of (a) 10°C/min, (b) 5°C/min, and (c) 2°C/min (● crystallite sizes of α-Al_2O_3, ▲crystallite sizes of θ -Al2O3, ○ fraction of α -Al2O3) [65].

Heating rates lowers the onset temperature (T_n) of DTA Profiles because θ-Al_2O_3 crystallites attain critical size at lower temperatures. Therefore the area of crystallite growth decreases with the lowering of heating rates because lower heating rates create coarser θ-Al_2O_3 crystallites and cause relatively more amount of α-Al_2O_3 in the nucleation stage.

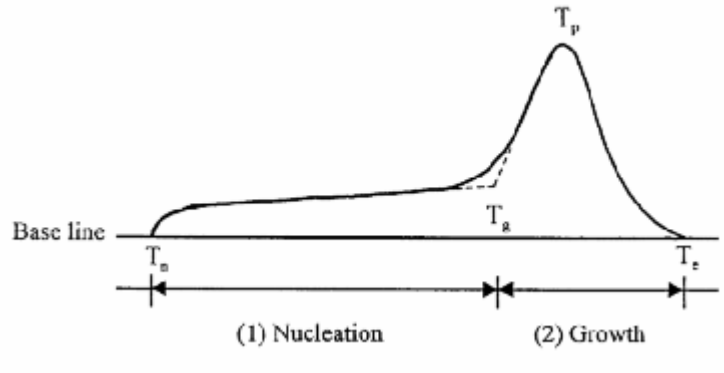

Fig.4.6. Schematic drawing of a typical exothermic peak of $\theta \rightarrow \alpha$-$Al_2O_3$ phase transformationin DTA measurement [65].

4.3. Seeding

The α-alumina seeding of precursor gels (mostly boehmite) was explored and developed by Messing et.al. Seeding reduces the transformation temperature and results in a refinement of the final microstructure especially by prevention of vermicular structures. Messing and Kumagai has shown that each α-alumina particle acts as a multiple nucleation site. So θ to α-Al_2O_3 transformation occurs in a controlled fashion leading fine, dense and homogeneous crystalline structures with reduced porosity [66,67].

The most difficult part of seeding is finding very fine particle sized seeds and introducing them homogeneously into precursor. Introduction of dopant or seed by wet milling is a brand new method. Milling alumina slurries by zirconia balls to distribute trace amounts of zirconia in order to prevent grain growth is a very recent approach as well as milling the precursor alumina slurries with high purity α-Al_2O_3 balls for seeding [68]. In this process amount of seed content depends on milling time.

Conventionally seeding is employed by the finest portion of ultrafine high purity alumina powder (AKP-30 or AKP-50 by Sumitomo). The particles which are in the nanoscale range are seperated by high speed centrifuging or sedimentation methods of prepared dispersions [69].

Youn et al. designated addition of an alumina sol into γ-alumina to reduce the α-phase transformation temperature down to 600ºC which they call sol effect. The transformation is reported to complete at 1100ºC. At higher temperatures a rapid increase of α-alumina is observed and this behavior is explained as self-seeding effect. The sol-effect is proposed to produced very fine α-Al_2O_3 powder with little agglomeration (Fig.4.7.)

Boccaccini and Kaya reports that the final sintered microstructure of alumina derived from pure boehmite sol is very porous even after sintering for a long time (>6 h) at 1600 ºC. In their study where they applied electrophoretic deposition to obtain alumina matrix, they used δ-alumina which contained small amount of α-alumina particles for seeding to yield better densification. It is proposed that δ-alumina might be a better seed than micrometric α-alumina particles for its nanoscale crystalline sizes [71].

	Precursor	Onset temp.	Finishing temp.
Route 1	Boehmite powder	1100°C	1200°C
Route 2	Alumina-sol dried	1000°C	1100°C
Route 3	γ-alumina + 3 wt% α-alumina	1000°C	1100°C
Route 4	γ-alumina + 3 wt% alumina-sol	600°C	1100°C

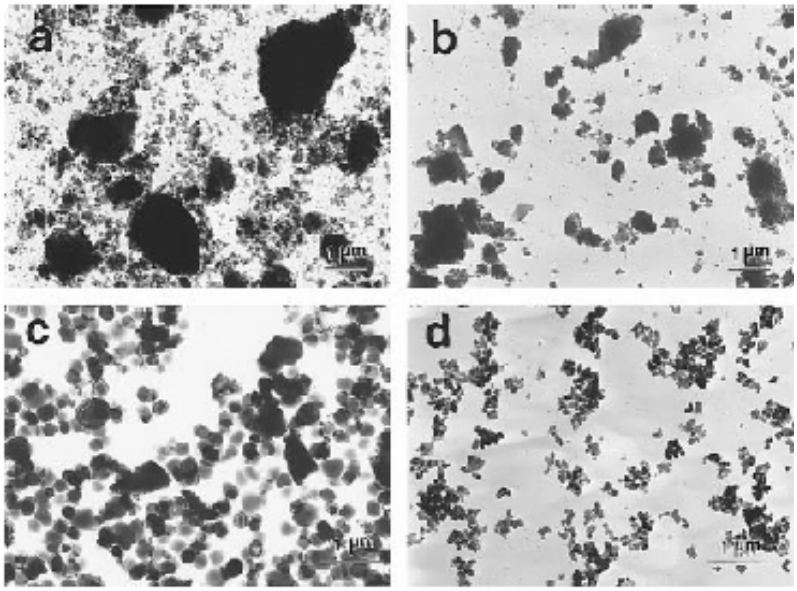

Fig.4.7. TEM micrographs showing the morphology of α-alumina derived from (a) pure boehmite (Route 1), (b) γ-alumina, (c) γ-alumina wiyh 3 wt% α-alumina (Route 3), and (d) γ-alumina wiyh 3 wt% alumina-sol (Route 4). All powders were heat treated at 1100 ºC [70].

α-Fe_2O_3 has also been used as seed for alumina sols. Tartaj and Messing reports about seeding boehmite sol with α-Fe_2O_3 sol to obtain full densities and homogeneous microstructures by conventional sintering at 1300ºC [72]. Wet ball milling by high purity alumina balls, centrifuging ultrafine α-Al_2O_3 powder (by Sumitomo) and using the finest particles as seed, seeding boehmite slurry directly with alumina sols or calcined alumina hydroxides and use of δ-alumina solutions containing a little α-Al_2O_3 are tried in the search of α-Al_2O_3 powders of less then 20 nm in order to use as seed.

Chapter 5

EXPERIMENTAL

Commercial boehmite (DISPERAL/Condea) with an average particle size of 10μm and crystallite size of 10 nm was used as starting material. SEM micrographs of the starting material is given in Fig.5.1. pH of boehmite slurry with a solid content of 30 wt.% was adjusted by dilute HNO_3 solution. Optimum pH for an ideally dispersed slurry was determined by zeta potential measurements at Zetasizer (3000 HSA Malvern, DTS 5301)

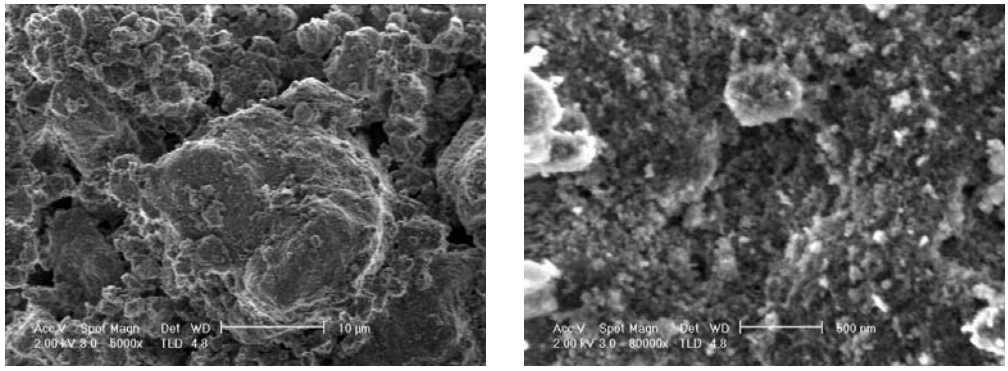

(a) (b)

Fig.5.1. SEM micrographs of boehmite powder used as starting material showing (a) agglomerates and (b) agglomerated crystallites.

The boehmite slurries prepared at an optimum pH range of 4.0-4.5 were dispersed by ultrasonic treatment at Transsonic Instrument (T780-TH-Elma HF-Freg) with the aid of light milling achieved by glass balls with a diameter of 3mm. Particle size measurements were also carried on Zetasizer instrument.

Optimum time for ultrasonic treatment for a stable dispersion was determined from ultrasonic treatment of boehmite slurries with a solid content of 2 % at pH =4.5, being agitated at 500 rpm. In order to prepare a high solid content slurry, 30 % aqueous boehmite was ultrasonicated for 2 hours at 35ºC and 55ºC. pH of the slurry was kept 4.0 during treatment, no mechanical agitation was applied. Milling was achieved by

vibration of balls within the sample during ultrasonic treatment. Volumetric ratio of the bulk glass balls to total was ¼ when added to slurry. No additives were used.

After certain intervals of ultrasonic treatment, samples were centrifuged at 2000 rpm for 10 min. Dispersed portions were removed and dried at 50°C for 36 hours for gravimetric analysis. Sediment heights of slurries were also measured in 15 ml test tubes after centrifugation at 2000 rpm for 10 min.

Stability of the dispersions were determined from particle size and solid content data of decanted samples. Optimum decantation time for a stable slurry was determined experimentally. Solid content and particle size of the samples were watched for eight days after the slurries are dispersed by ultrasonic treatment. The stable dispersions were taken by a peristaltic pump in order to prevent mixing of the sediment into stable slurry.

The alpha alumina crystals that were used for seeding were synthesized by combustion synthesis of $Al(NO_3)_3.9H_2O$ (Aldrich, 98.3%). Urea (Sigma, 99.99%) was used as fuel for combustion in stoichiometric ratio. The crystalline structure of the seed was determined by X-Ray Diffractometer (Philips X'Pert Pro CuK_α 1.54) and microstructure before and after ultrasonic treatment were observed from SEM micrographs. Seeding material was added to boehmite dispersion in 2wt.% on dry basis and ultrasonicated for 2 hours with the boehmite powder. The actual amount of seed that was introduced into the slurry was determined by ultrasonication of a blank solution and determination of dispersed portion by drying at 80ºC for 6 h after separation by centrifuging. The two slurries, seeded and unseeded, were decanted for one day. Solid content of the dispersions and particle size measurements were conducted in order to determine the efficiency of the ultrasonic treatment as described before.

2.5 wt.% PVA (Aldrich, MW 8000-10000) on dry basis was added to slurries as the binding agent. PVA solution was prepared before addition and stirred for 30 min by a magnetic stirrer after addition to provide a well mixing. Viscosities were determined by Brookfield DV-III Programmable Rheometer .

The slurries were spray dried in Buchi Mini Spray Dryer (B290) The drying parameters were set to feed rate of 7.5 ml/min (25%), aspiration rate of 35 m^3/h (90%) and inlet temperature of 160ºC. TGA measurement of the powders are employed by a Thermal Gravimetric Analyzer (Seteram, Labsys 1600ºC). Particle size and morphology of the powder was investigated by SEM (Philips XL 30S FEG) observations.

The obtained boehmite powder was calcined at various temperatures in a range of 350ºC -1200ºC for two hours with a heating rate of 10ºC/min at a Carbolite CWF 1300. Heat treated powders were analyzed by X-Ray Diffractometer in order to follow phase transformation behavior of the ceramic powder.

The powders were compacted at 120 MPa and 600 MPa by uniaxial pressing. Green bodies were sintered in a temperature range of 1050ºC -1300ºC for two hours with heating rate of 10ºC/min. Densities of sintered bodies were determined by Archimedes method. Phase transitions of compacts after sintering at 1050ºC -1300ºC were detected by X-Ray Diffractometer. Microstuctures of the samples sintered at given temperatures were observed from SEM images of the fracture surfaces. Crystallite sizes of commercial boehmite and synthesized α-alumina powder calculated by Sherrer formula were also confirmed by SEM micrographs.

Chapter 6

RESULTS AND DISCUSSION

6.1. Optimization of Slurries

Ideal pH for the boehmite dispersion was determined in terms of zeta potential. Boehmite powder was dispersed in deionized water at various pH values adjusted by dilute HNO_3 solution. Zeta potential of each dispersion was measured in order to check the isoelectric point which was at pH of 8.4 as can be seen on Fig. 3.

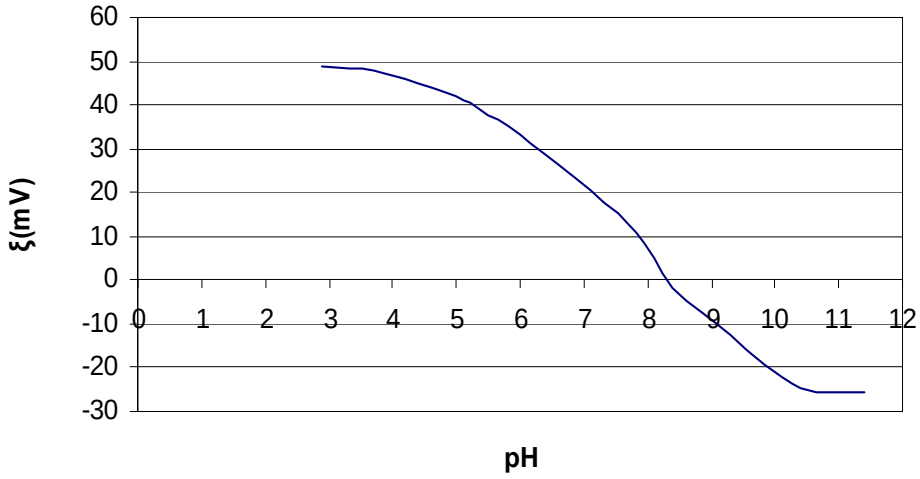

Fig. 6.1. Zeta potential curve of boehmite.

From the zeta potential data lower pH values promise better dispersing efficiencies with respect to higher surface charges yielding more intensive repulsive forces. A pH range of 3.5-4.5 appear to be the most beneficial working range in dispersing process of boehmite.

The best solid load of dispersion by ultrasonic treatment were determined in 90 minutes as shown in Table 6.1. Mechanical agitation in the presence of glass balls at a diameter of 3 mm. was applied to increase the efficiency of ultrasonic treatment. Medium pH was kept at 4.5 during the treatment.

Table 6.1. Effect of ultrasonic treatment without and with the aid of ball milling. (Slurries contain 2 wt% boehmite and pH was adjusted to 4.0.)

	Efficiency of Treatment (% dispersed powder)		
Ultrasonic Treatment Time (min)	Ultrasonic Treatment	Ultrasonic Treatment and Mechanical Mixing	Ultrasonic Treatment and Ball Milling
30	22	25	64
60	27	45	77
90	33	50	98
120	32	52	99

Centrifugation was not a practical method to handle stable dispersions. Decantation has been optimized for a stable dispersion having reduced particle size. Besides it was useful for the separation of dispersion from the sediment. Particle size and solid content measurements displayed in Table 6.2 have shown that leaving the slurry to settle for one day yielded an optimum slurry with the smallest particle size and was sufficient to obtain a stable suspension. After eight days the slurry still kept stable althought an increase in particle size has been observed.

Temperature of ultrasonic treatment affected the slurry viscosity as seen in Table 6.3. The viscosity measurements of the stabilized dispersions were carried after a day of decantation. The results showed that higher temperature caused increased viscosity and reduced the efficiency of the treatment yielding dispersions with lower contents. So the temperature of ultrasonic treatment bath was kept under 35ºC for all experiments.

Viscosity of the slurry is a very critical parameter for it effects the properties of dry powders and in turn compact bodies. Ultrasonic treatment was approved to yield quite low viscosities even after two days of decantation.

Table 6.2. Particle size and solid content of fully dispersed boehmite slurries prepared by ultrasonic treatment and ballmilling for 90 min. at pH=3.5 as a function of decantation time.

Decantation time (day)	pH	Solid content (%)	Av. Particle Size -by intensity- (nm)	Particle size -by number- (nm)
1	3.74	2.01	145 167 153	17 21 19
2	3.74	2.06	134 139 135	46 17 63
3	3.76	2.04	128 133 133	27 18 30
8	3.76	2.05	107 112 112	35 30 26

Table.6.3. Effect of temperature on particle size and efficiency of dispersion prepared by ultrasonic treatment and milling at pH=4.0. Initial solid loads were 20 wt%.

T ºC	Ultrasonic treatment (min.)	Solid content (%)	Particle size -by number- (nm)	Viscosity Shear Rate=100/s (mPas)
35	120	19	14 15 15	8.1
55	90	15	11 13 28	12.2

Table 6.4. shows the dispersion efficiency of ultrasonication treatment in terms of solid content of dispersion and viscosity for a slurry with 30wt% solid content and pH=4.0 treated at 35º C. Effect of PVA addition has also been investigated and shown that viscosity value was still much lower than the one obtained by conventional mixing process.

Table.6.4. Efficiency of treatment for dispersions from slurries with 30% solid content.

Treatment:	Solid (%)	Efficiency (%)	Viscosity Shear Rate=50/s (mPas)
Mechanical mixing	24.6	82.0	106
Ultrasonic treatment	23.4	78.0	14
Ultrasonic treatment & milling and 2.5 % PVA addition	28.1	93.6	23

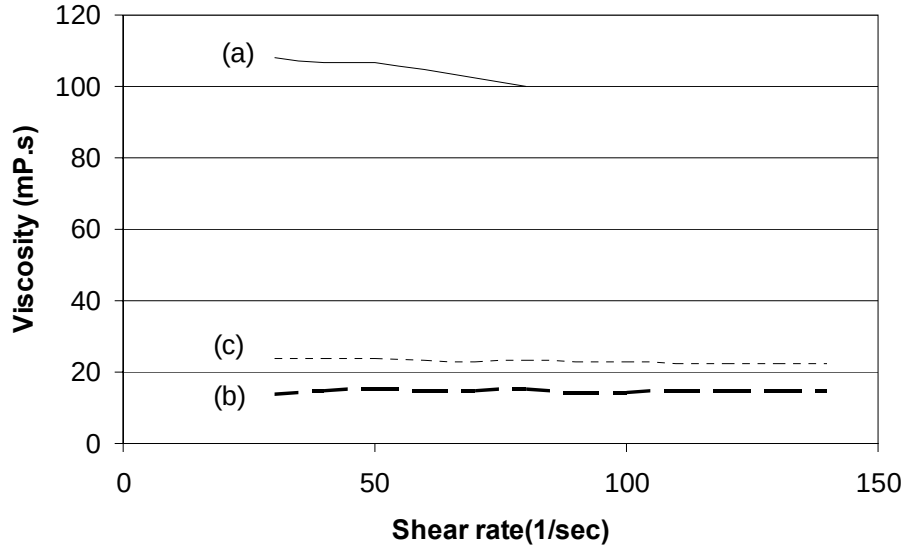

Fig.6.2. Dynamic viscosity measurements of slurries prepared by (a) mechanical mixing (b) ultrasonic treatment& milling and (c)ultrasonic treatment& milling and 2.5% PVA addition on dry basis. All samples were decanted for one day to handle the stable dispersions.

6.2. Preparation and Characterization of the Seed

In this study a new material was obtained by combustion synthesis of $Al(NO_3)_3$ in order to use as seeding material. Aluminum nitrate octa-hydrate was used as the source material to synthesize α-Al_2O_3 by combustion with the use of urea as fuel in stoichiometric ratio. The reaction is:

$$2[Al(NO_3)_3.9H_2O] + 5\ CO(NH_2)_2 \rightarrow Al_2O_3 + 5\ CO_2 + 19\ H_2O + 14\ N_2$$

The X-Ray Diffraction pattern of synthesized powder confirmed that it was α-alumina (Fig.6.3). Crystallite size of the seed as synthesized was shown to be much less than 100 nm by application of Scherrer Equation. (App.B2)

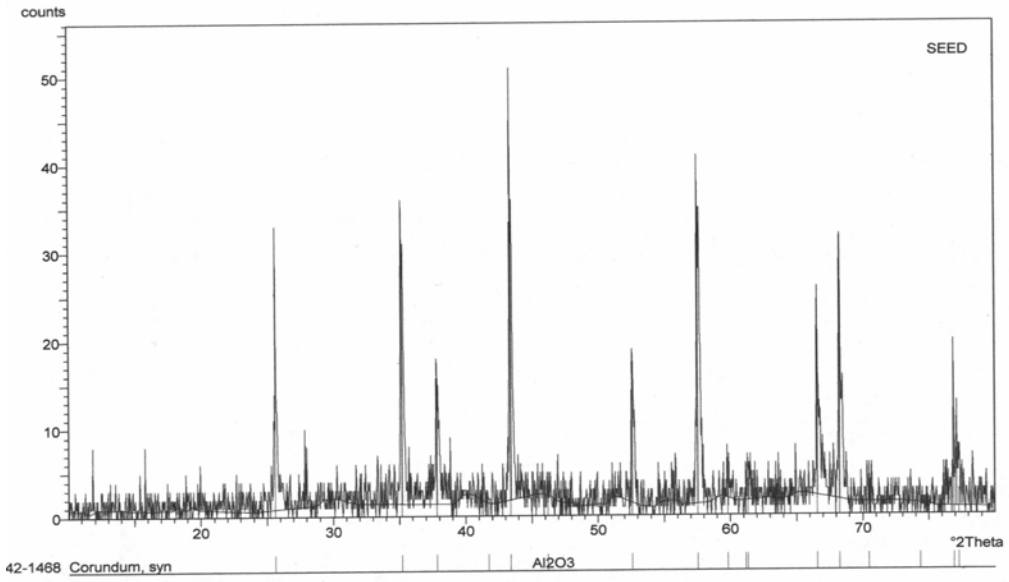

Fig.6.3. X-Ray Diffraction graph of Al_2O_3 seeds synthesized by combustion synthesis and used as seed.

SEM micrographs of the synthesized α-Al_2O_3 shows the microstructure. α-Al_2O_3 produced by combustion synthesis appeared to be in flakes having a submicron thickness. Grain size of the material was in micrometers while the crystallites appear to be less than 50 nm (Fig.6.4).

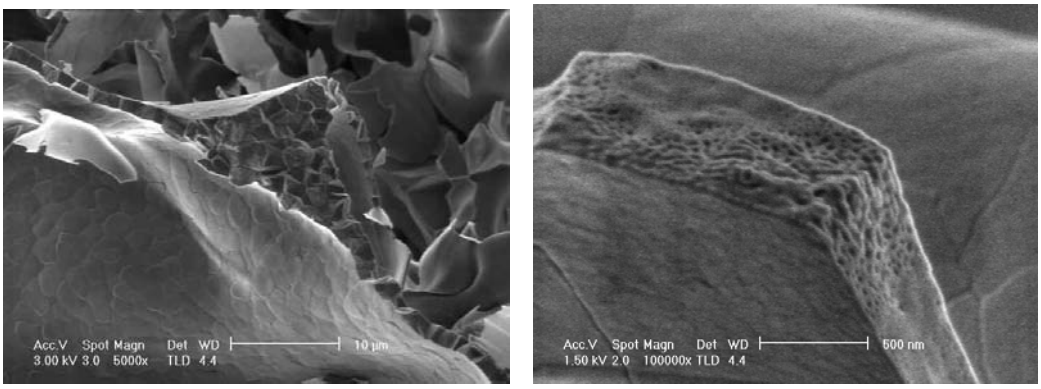

Fig.6.4. SEM micrographs of α-alumina seeds as synthesized. It was noticed that crystallites were in nanometric scale while the width of the grains were about 1 µm.

In experimental study it was observed that grains were easily separated by ultrasonic treatment. After ultrasonic treatment with the aid of milling for 6 hours, a fraction of seed grains was detected to be broken into crystallites. Some grains were broken while some looked like they were reduced in size by the effect of abrasion (Fig.6.5).

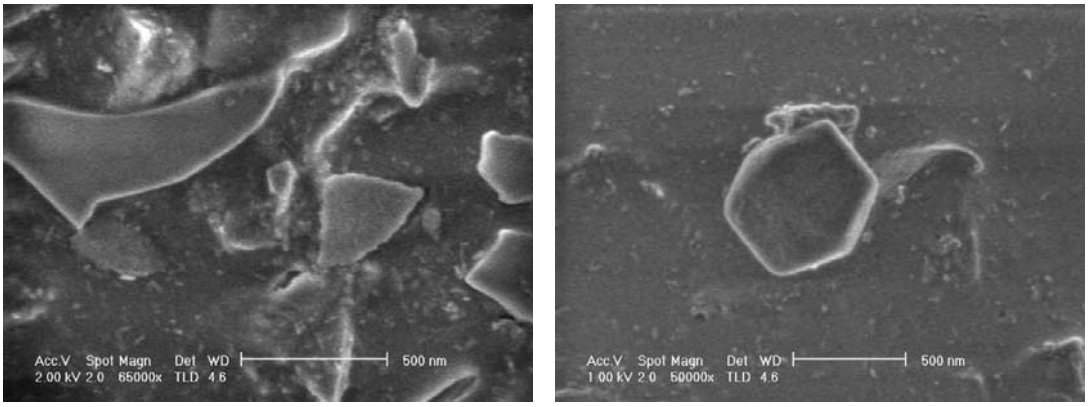

Fig.6.5. SEM micrographs of seed particles after ultrasonic treatment with milling.

The disintegrated and dispersed part of seed addition (2% on dry basis) to prepared boehmite dispersion was determined by a blank experiment during ultrasonic treatment . The yield of blank seed dispersion was only 7 %, which in fact corresponded to a seed content of 0.14 %. That means a trace amount of seed crystallites with particle size less than 50 nm. was introduced into slurry. The α-alumina content of seeded slurries has been assumed as <0.5% referring to the blank experiment and considering the possible variations in dispersion efficiency.

6.3. Characterization of Slurries

Boehmite dispersions used in this study were prepared in order to have 30% solid contents. Table 6.5 is given to tabulate the physical and rheological properties of slurries used as starting materials for treated boehmite powders and then compacts.

Table 6.5. Properties of slurries (SL1 and SL2) which are dispersed by ultrasonic treatment.

SLURRY	pH	Solid (%)	Viscosity Shear Rate=100 /s (mPa.s)	Particle size -by number- (nm)
SL1	4.1	28.1	10.3	24
Boehmite 30 wt%		(94 % yield)		21
(2.5 wt% PVA)*				16
SL2	4.1	29.2	10.3	27
Boehmite 30 wt%		(98 % yield)		27
(2.5 wt% PVA + α-Al_2O_3< 0.5 %)				14

* PVA amount was determined on dry basis.

The results showed that ultrasonic treatment was quite succesful in dispersing the commercial boehmite. No mechanical agitation was required for the preparation of almost fully dispersed slurries. pH value that was employed is the upper limit suggested in product sheet of the boehmite (App. A6). Therefore the added nitric acid amount was much lower than suggested ratio.

The major advantage of the treatment was the decrease in viscosity of the slurry from expected value of 500 mPa.s that is given for a dispersion with 30% solid load (App.A6). The measured particle sizes were much lower than the given values for dispersions prepared by intensive mechanical mixing at the same solid contents (App.A7) and also the values determined experimentally which varied between 25 and 220 nm measured by number.

6.4. Characterization of Spray Dried Powders

Spray drying of stable slurries with low solid content yielded spherical granules with a particle size in the submicron range. The slurries with low viscosity and increased solid content up to 30% increased the particle size up to 10μm with a wider size distribution range (Fig.6.6). But the fine powders could not be compacted without the aid of an appropriate binder. In our boehmite slurries PVA (MW:8000-10000) was used as binder in 2.5 % content on dry basis.

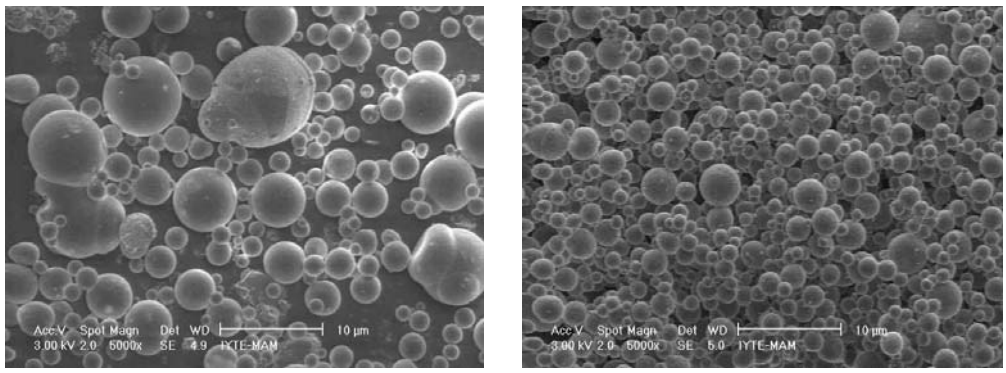

(a) (b)

Fig. 6.6. SEM images of spray dried powders of boehmite slurries (a) 30 % and (b) 2 % with no binder.

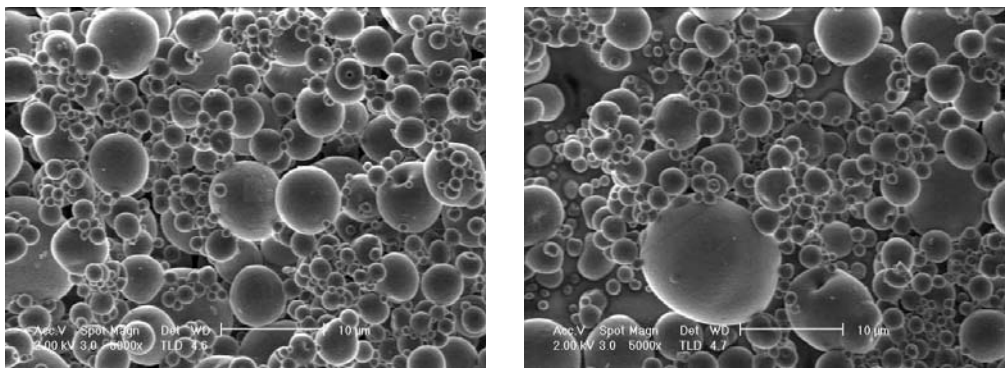

(a) (b)

Fig. 6.7. SEM images of spray dried powders of boehmite slurries (a) SL1 (b) SL2 with 2.5 % PVA binder addition on dry basis.

Slurries called as SL1 and SL2 were spray dried under the same drying conditions. (Feed rate 25%, Aspiration rate 90 % and Drying Temperature was 160ºC). Water content of the spray-dried powders were 3.0-3.5 %. The powders produced by spray drying were notated as A1 and A2 referring to the powders shown in Fig.6.7.a&b respectively. The nomenclature for the powders mentioned in this study are summarized as follows.

Table.6.6. Properties of powders named as B, A1 and A2.

Powder:	Source	Treatment	PVA (wt%)	α-Al_2O_3 (wt%)
B	Commercial (Disperal)	Untreated	0.0	0.0
A1	Slurry SL1	Spray-dried	2.5	0.0
A2	Slurry SL2	Spray-dried	2.5	< 0.5 %

Spray dried particles were solid spheres at a size range between 0.1-10 microns. The surface of the particles were smooth and denser compared to ingredients of the granules, probably due to PVA segregation which is shown in Fig.6.8. PVA was predicted to form an envelope covering the particles (See Fig.3.6). Therefore better adhesion during compaction and increased green strength were expected via PVA addition.

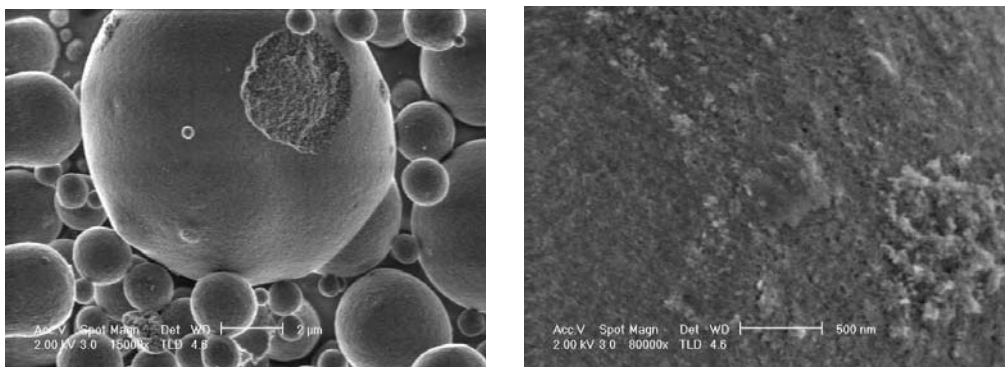

(a) (b)

Fig.6.8. SEM micrographs of spray dried powder A1 showing (a) granulation of fine powder with the aid of PVA and (b) microstructure of the surface of a granule at nanoscale.

Powders named as A1 and A2, obtained by spray drying of the prepared slurries were compared with B, commercial boehmite powder as received. TG curves of the powders show the characteristics of powders in terms of water relaese, dehydroxilation and PVA degredation (Fig.6.9)

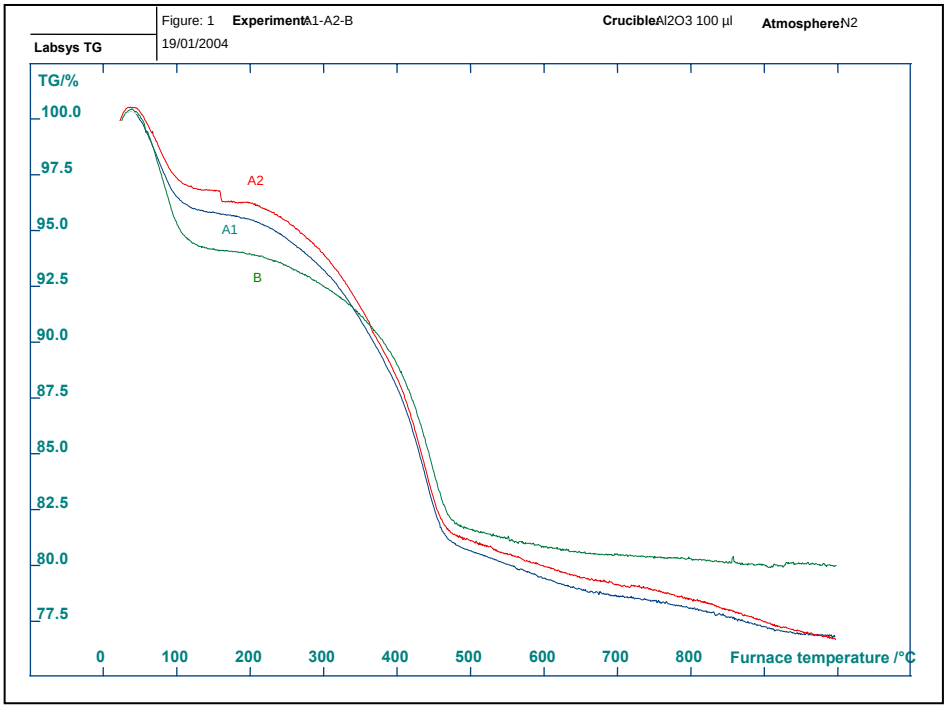

Fig.6.9. TGA analysis for the powders of B(boehmite as received), A1 (spray dried boehmite powder from slurry SL1) and A2 (spray dried boehmite powder from slurry SL2).

The first weight loss under 100ºC in TGA diagram was leaded by water evaporation. Water contents of the powders are 3.5 % for A1, 2.7 % for A2 and 5.7 % for B. It is reported that PVA starts to degrade at 180ºC and completely disappears at about 600ºC [49-51]. Most of the PVA content disappeared at about 400ºC and the remaining amount can be assumed negligible. Then TGA curves of the three powders showed almost identical characters until 450ºC where gamma transformation of boehmite started (See App-A.4.2). The gamma transformation of the spray dried powders seemed to start slightly earlier than untreated boehmite powder. The reduction

in gamma transition temperature was also confirmed by X-Ray Diffraction analysis of the calcined powders. (App.C)

During phase transformation of boehmite to γ-alumina the rate of hydroxyl group release was increased in spray-dried powders. That was related to effect of pretreatment on crystallite size and, in turn, phase transition behavior as explained in Chapter 4 (See Fig.4.2).

The XRD data and crystallite size information of B is given in App.B.1. The comparison of the thermal analysis and XRD investigations with Table 4.1. shows that the transition behaviors of spray-dried boehmite powders were much better than can be expected. It is proposed that a boehmite powder that transforms to gamma phase at 430ºC have a crystallite size of 2.5 nm. [64] The boehmite powder used in this study showed almost identical phase transformation behavior although the crystallite size calculated from the corresponded peak (020) by Scherrer formula was 12.7 nm.

X-Ray Diffraction diagrams of the three powders calcined at various temperatures between 350ºC and 1200ºC state the phase transformation path of each powder (Fig.6.10).

Phase transformation temperatures were noticably reduced by ultrasonic treatment and spray-drying of boehmite slurries which was related to reduction of crystallite and particle sizes which produce a controlled microstructure in green compacts. That show that regulation of microstructure in terms of homogeneity and particle size can reduce the sintering temperature causing a difference of 50ºC. The effect of seeding on phase transformation behaviour of boehmite powders are illustrated showing the reduction of α-phase transition temperature down to 1100ºC which corresponds to a drop of 100ºC in sintering temperature.

Table 6.7 displays the phase transition ranges of each sample which exhibits the effect of treatments on phase transformations of boehmite to γ-, δ-, θ- and α-phases respectively.

Table. 6.7. Phase transition ranges of B, A1 and A2 boehmite powders.

	B	**A1**	**A2**
γ-phase	500-700 ºC	400-700 ºC	400-700 ºC
δ-phase	800-1150 ºC	800-1150 ºC	800-900 ºC
θ-phase	1000-1150 ºC	900-1150 ºC	900-1100 ºC
α-phase	1200ºC →	1150ºC →	1100ºC →

Referring to App.C which contains XRD diagrams of A1, A2 and B at each temperature value carried in this study the main differences in phase transformation behaviors appear at temperatures; 400ºC, 900ºC and 1100ºC. γ-phase appeared at 400ºC for A1 and A2 samples while B was still totally boehmite (App.C2). There was not a significant difference in the beginning of δ-transformation for all samples but the phase remained for a very short interval in seeded samples and converted to θ-phase very fast. θ-phase appeared at A1 samples at lower temperatures than untreated samples, but θ- and δ-phases coexisted until 1050ºC where α-phase came out.

Effect of seeding on phase transition temperature of each phase, even in very low α-alumina contents, was an expected behavior. But this study also reveals that particle size reduction by ultrasonic treatment and a tidy microstructure obtained by spray drying remarkably reduced the phase transformation temperatures. When X-Ray Diffraction diagrams were compared, another noticable effect of ultrasonic treatment and spray-drying appeared as a decrease in the number of peaks for the treated (A1) samples during phase transitions. Although the ranges were widened for treated samples the phase transitions occured sharply which was most probably another result of homogeneity in microstructure. The effect of a controlled microstructure of green bodies on densification behavior and microstructure of sintered bodies were also remarkable.

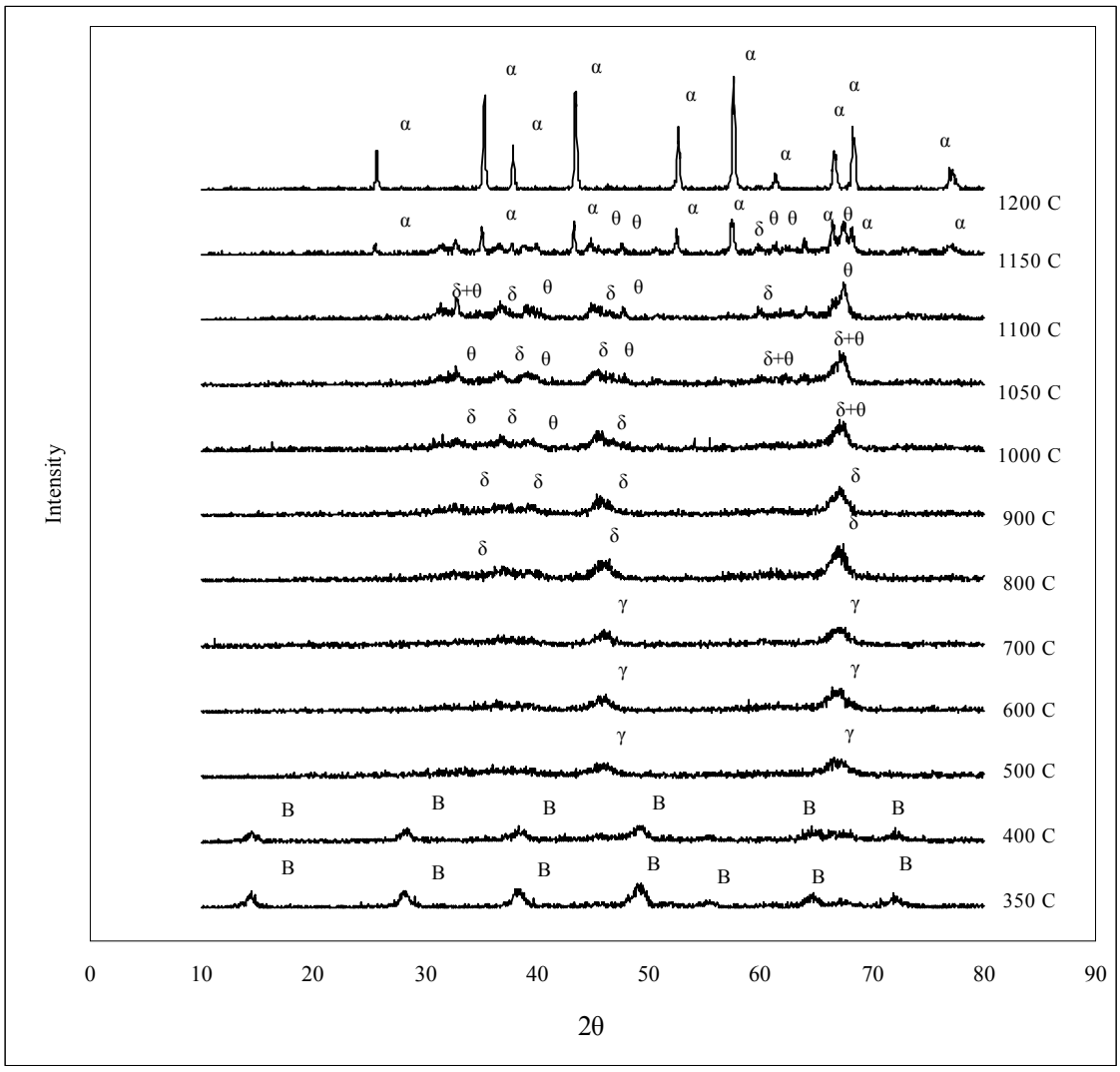

Fig.6.10.(a) X-Ray Diffraction patterns of B (Boehmite powder as received),

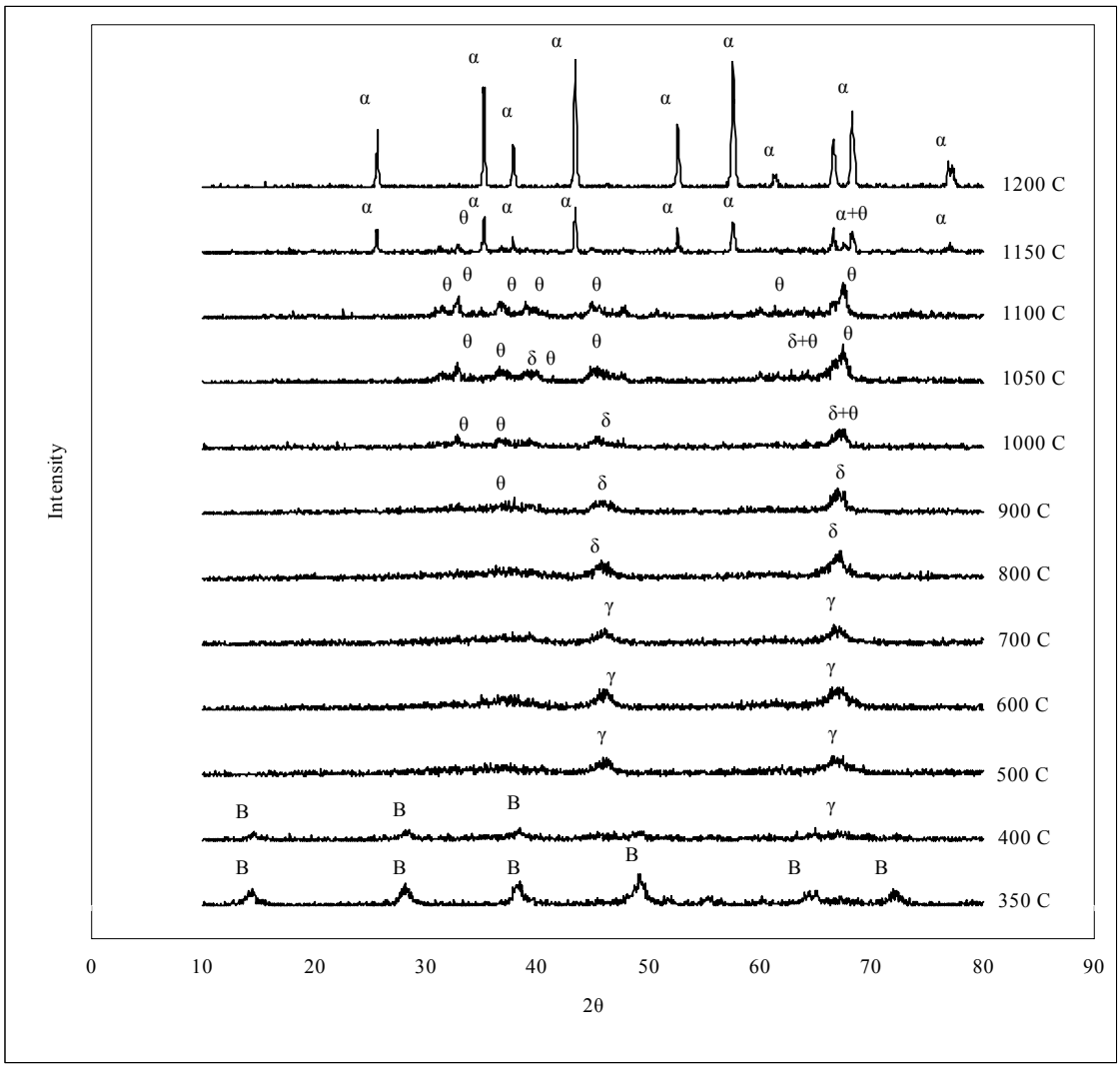

Fig.6.10. (b) X-Ray Diffraction patterns of A1 (boehmite powder ultrasonicated for 2 h at pH=4.5 and spray dryed with addition of 2.5 % PVA),

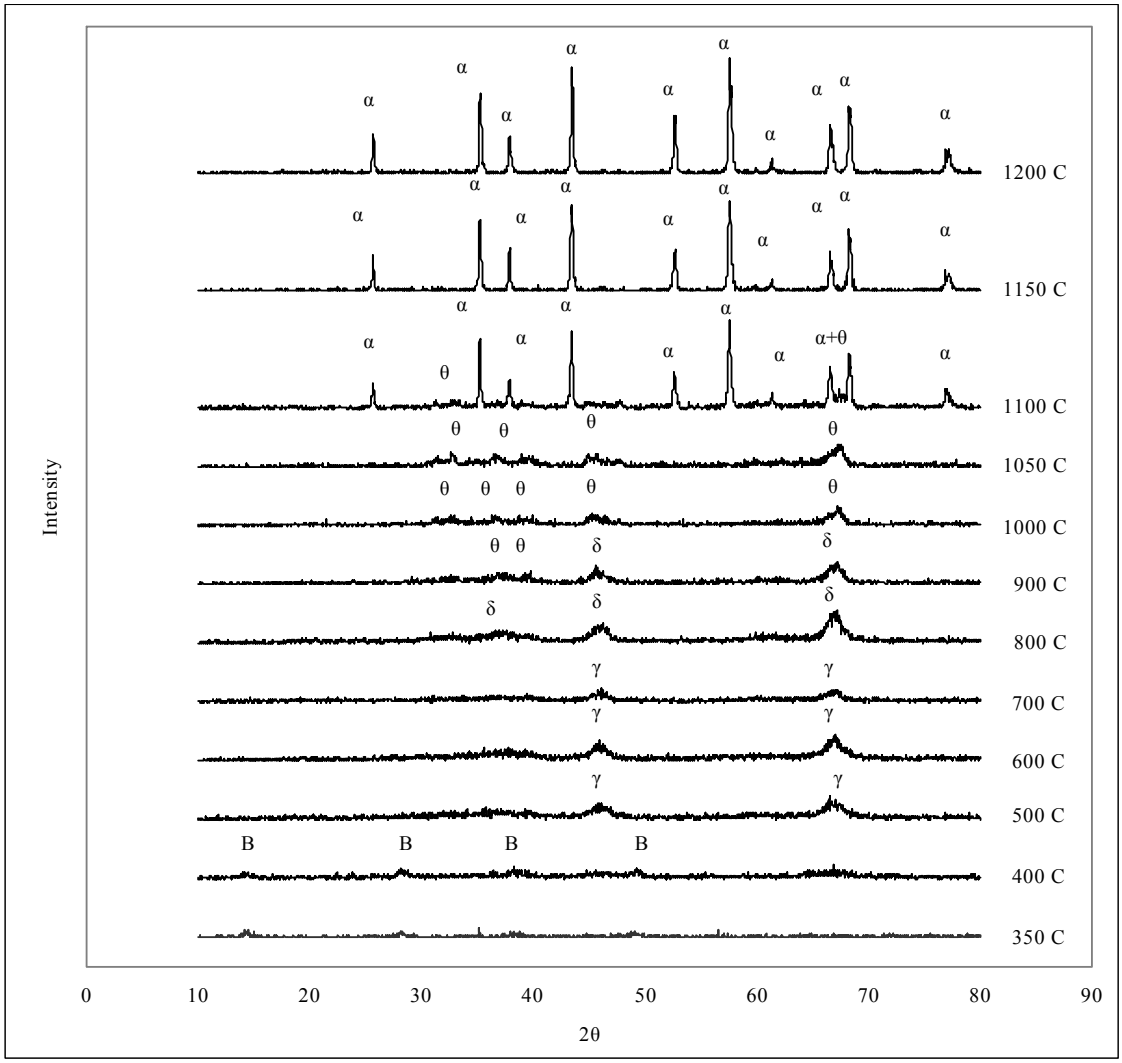

Fig.6.10. (c) X-Ray Diffraction patterns of A2, (boehmite powder seeded by 2% Al_2O_3, ultrasonicated for 2 h at pH=4.5 and spray dryed with addition of 2.5 % PVA).

6.5. Characterization of the Compacted Bodies

Green bodies with 40-42 % of theoretical density were obtained after compaction of powders B, A1 and A2 by uniaxial press at 120 MPa. All compacts have a density of 1.60-1.70 g/cm^3. SEM micrographs of the pellets are given in Fig.6.11.

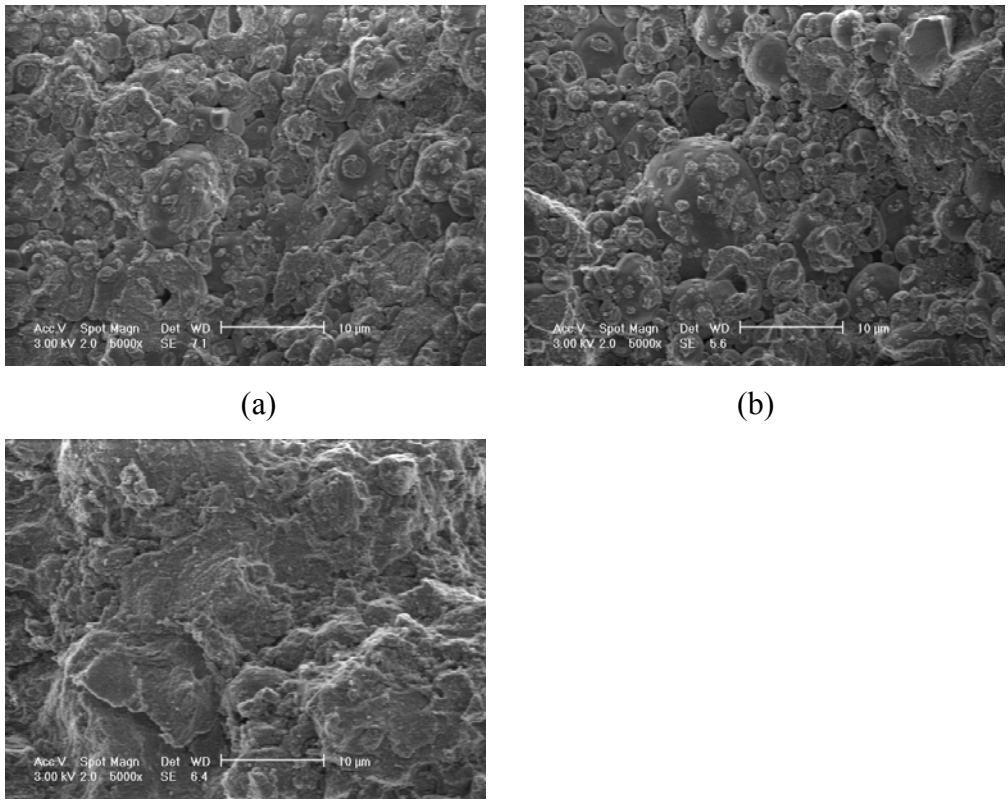

(a) (b)

(c)

Fig.6.11. SEM migrographs of the green bodies of (a)A1, (b) A2, (c) B powders compacted at 120 MPa.

It is obvious that spherical shape and particle size distribution of spray dried powders were much more advantegous to obtain a compact with a more uniform microstructure compared to boehmite powder pressed as received. Spray drying caused a more controlled particle distribution within green compacts preventing greater agglomerates and interagglomerate pores that occurred in B samples. It was also noticed that at a stress level of 120 MPa of uniaxial pressing, not all particles smashed. The image of smashed particles show that hollow granules existed but they were few in number. PVA envelopes were easily distinguished.

Densities of the sintered compacts displays that only the pretreatment of ultrasonication and spray drying yielded better densification than slightly seeded samples as well as untreated powder compacts. Table 6.8 shows the densities of sintered bodies and the corresponding percentage values of the theoretical density which is 3.989 g/cm^3 for pure alumina.

Table 6.8.a. Densities of sintered compacts by Archimedes Method,

Sample	1050ºC	1100ºC	1150ºC	1200ºC	1250ºC	1300ºC
B (g/cm^3)	1,65	1,90	2,24	2,40	2,54	2,52
A1(g/cm^3**)**	1,75	2,01	2,45	2,57	2,60	2,61
A2(g/cm^3)	1,71	2,09	2,30	2,35	2,48	2,54

b. Relative densities with respect to theoretical density of alumina.

Sample	1050ºC	1100ºC	1150ºC	1200ºC	1250ºC	1300ºC
B (%)	41.5	47.8	57.5	60.2	63.8	63.4
A1(%**)**	44.2	50.5	61.5	64.5	65.5	65.7
A2(%)	43.1	52.5	58.0	59.2	62.4	64.1

The densities of the compacts of A1 and A2 pressed at 600 MPa and sintered at 1200ºC were 2.64 g/cm^3 (66.4%) and 2.60 g/cm^3 (65.3%). This proves that compaction had very little effect on sintered densities with poor densification rates at higher green densities. 100% of the pores were open pores as determined by Archimedes.

On the other hand the homogeneity led by the pretreatment including ultrasonic treatment and spray-drying caused an improvement in density. Even the difference in densities is not high it is remarkable. Densification curve of A1 sample showed a steeper range at 1100-1150ºC interval than A2 and B as seen in Fig. 6.12.

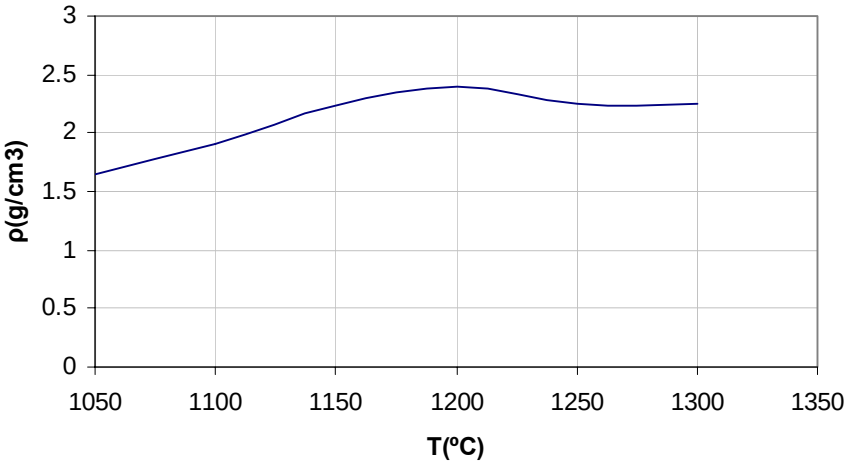

(a)

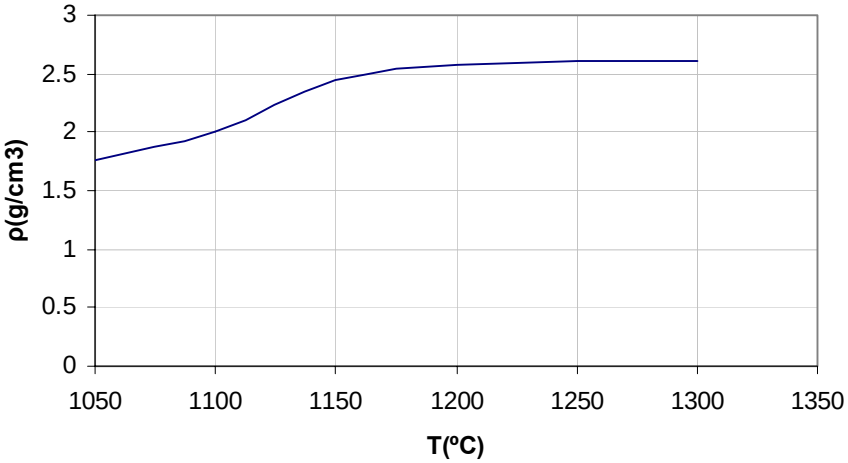

(b)

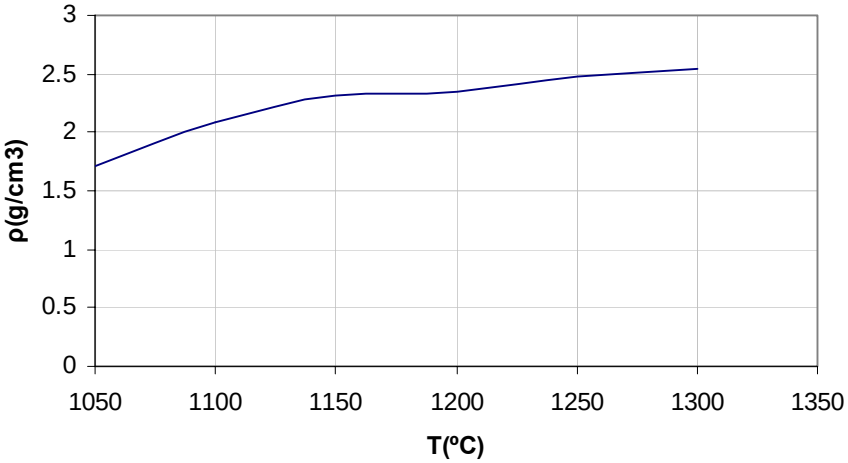

(c)

Fig. 6.12. Density curves of sintered compacts of (a)B, (b) A1, (c) A2 powders at a temperature range of 1050-1300ºC.

It was detected from XRD diagrams that untreated boehmite undergoes alpha transformation at 1150ºC. SEM micrographs confirmed that untreated boehmite compacts contained no α-Al_2O_3 at 1100 ºC. They also show that size reduction by ultrasonic treatment was effective on reduction of phase transition temperature. Alpha transition of A1 powder started at 1100ºC while A2 was completely turned to α-Al_2O_3.

SEM observations from the fracture surfaces of sintered pellets show that phase transition proceeded faster at the particle surfaces. The grain growth proceeded drastically at the surfaces when compared to inner parts of the spherical packs.

Growth mechanisms of α-nuclei were detected by SEM. The two growth mechanisms mentioned about growth characteristics of θ-alumina during transformation to α-phase were visible [65].

As can be seen from Fig.6.13 (b) and (d), nucleation started to occur locally within θ-phase in B samples at 1150ºC meanwhile the nuclei that already occurred were integrating in A1 samples. The alpha cristallites that just formed were less than 50 nm. (Fig.6.13.b) while the coalescents exceeded 500nm (Fig.6.13.d).

The micrographs show that phase transformation proceeded in a controlled fashion in A1 samples exhibiting uniform microstructure. The same coalesence behavior was visible in A2 samples, too. But the microstructure was not that homogeneous that was related to existence of seed particles. The merging of the alpha centers into an integrated body was also noticable on Fig.6.14 (e). The limiting effect of seeding on vermicular structure could be detected on Fig.6.14 (f), but this faceted structure didn't represent the general structure, it appeared at 1150ºC only and was not permanent.

The effect of compaction pressure on A1 and A2 samples sintered at 1200ºC are displayed in Fig.6.15. The voids due to loose compaction were eliminated but cracks occurred at the bodies compacted at 600 MPa. Therefore no improvement in final densities of the sintered bodies was recorded. Besides, a close compaction had no limiting effect on grain growth or vermicular structure.

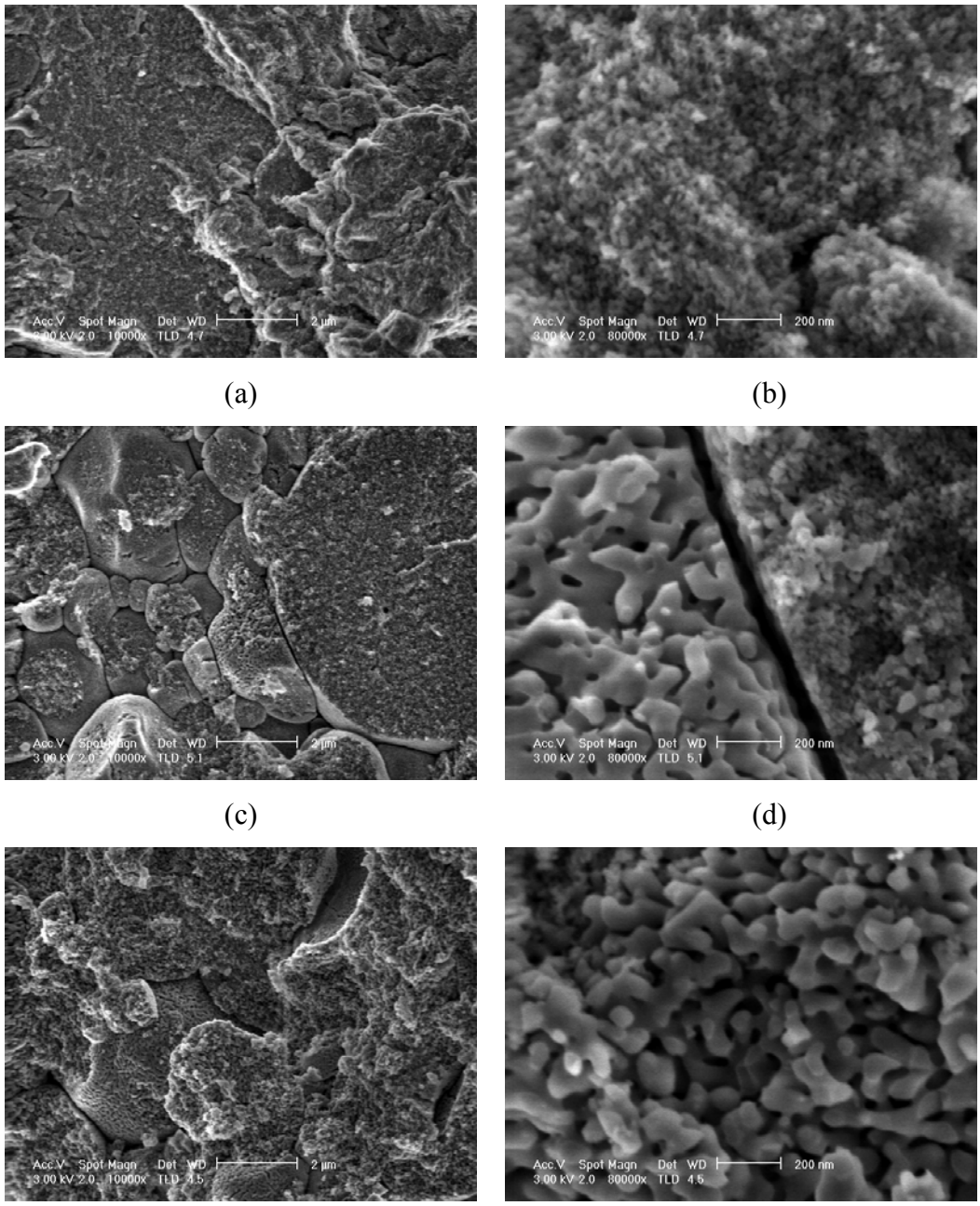

Fig.6.13. SEM micrographs of B, A1 and A2 compacts sintered at 1100ºC ; (a,b) untreated boehmite completely at θ-phase, (c,d) pretreated boehmite with local conversion to α-phase, (e,f) seeded boehmite transformed into α-phase.

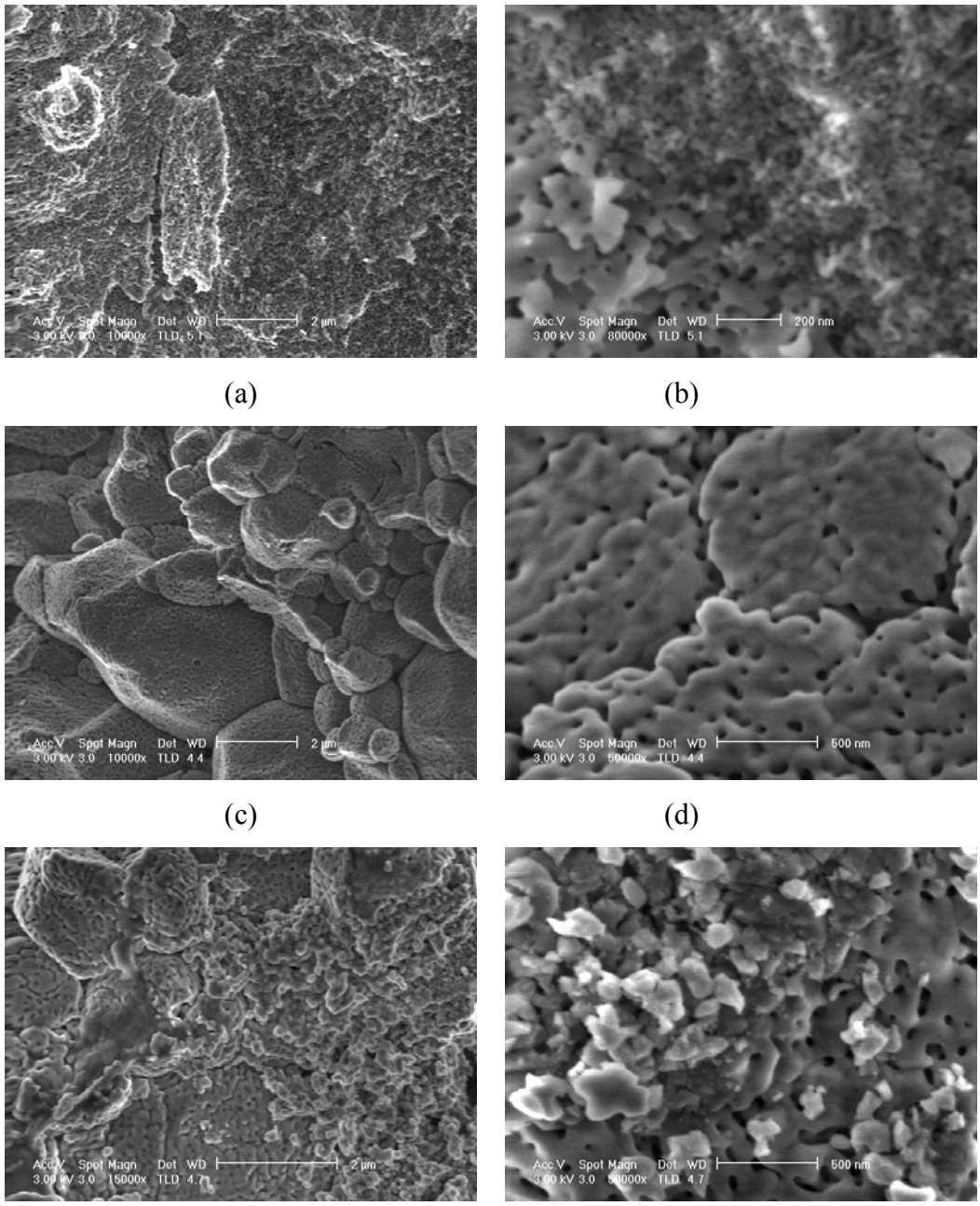

Fig.6.14. SEM micrographs of B, A1 and A2 compacts sintered at 1150ºC. (a,b) appearance of α-alumina crystallites surrounded by θ-phase which is still dominating in B samples, (c,d) coalescence behavior of α-alumina crystallites as the uniform microstructure of A1 samples, (e,f) two types of microstructures; vermicular and faceted α-alumina crystallites, caused by seeding in A2 samples.

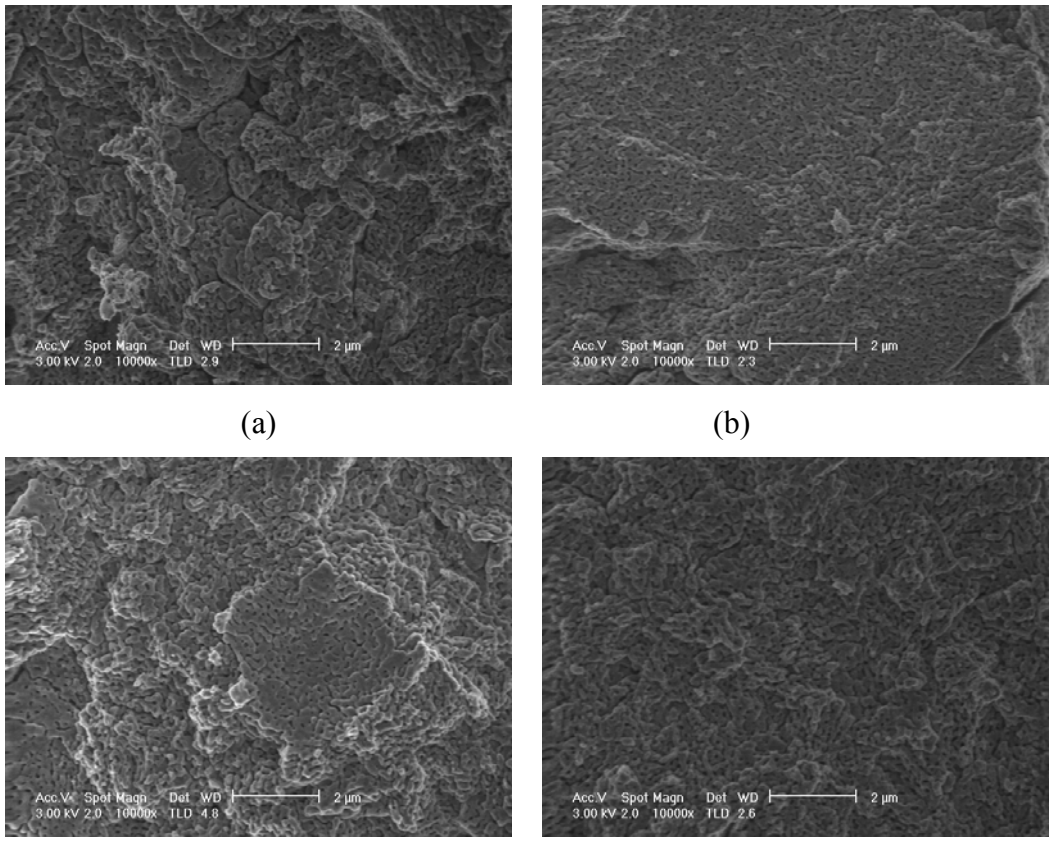

Fig.6.15. SEM micrographs of A1 and A2 compacts sintered at 1200ºC (a,b) A1 compacted at 120 MPa and 600MPa and (c,d) A2 compacted at 120 MPa and 600MPa respectively.

As mentioned before, even little content of α-alumina reduced θ→α phase transformation temperature down to below 1100ºC. At 1100ºC θ-phase was still visible in A2 samples but the dominating phase was α. The crystallite sizes were less than 100 nm, but the porosity due to vermicular structure couldn't be eliminated at even higher sintering temperatures.

The phase transformation route of seeded samples are illustrated in Fig.6.16. As shown in micrograph (b), seeding partially prevented vermicular structure at 1150ºC. But the illustrated structure didn't have a uniform distribution through the sample and disappeared with further heating.

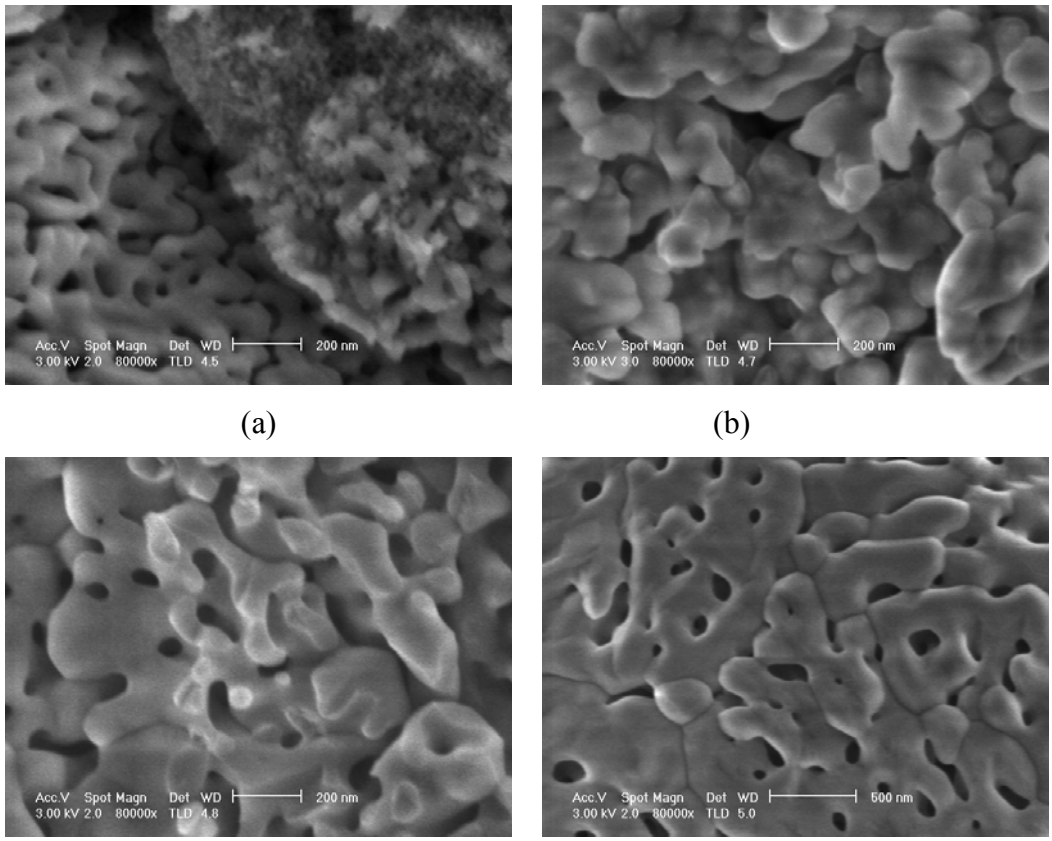

Fig.6.16. SEM micrographs illustrating phase transformation behavior of seeded boehmite samples (A2) sintered at (a) 1100ºC, (b) 1150ºC, (c) 1200ºC (d) 1300ºC.

The crystallite structure of seeded samples didn't change much after 1200ºC. In general the microstructure didn't show noticable differences from unseeded samples at higher temperatures and exhibited much more homogeneous microstructure compared to untreated samples. But local observations exhibited exceptional cases which may help understanding the evolutions in phase transformations of seeded alumina samples. The comparison of seeded sample (A2) with boehmite powder compacted and sintered as received showed the great distinction between alpha structures. The fusion of grain boundaries might rarely cause abnormal grain growth, yielding sections with grain sizes measured in micrometers (Fig.6.17.b). In order to fully understand the effect of seeding, samples with higher seed contents have to be investigated.

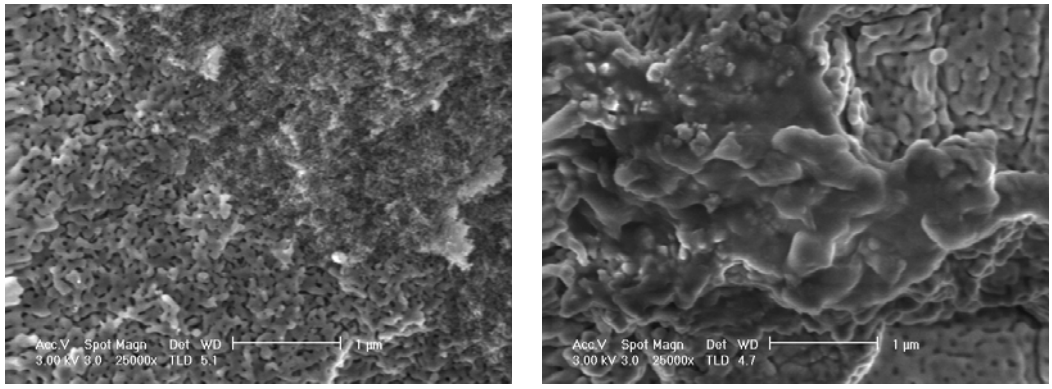

(a) (b)

Fig.6.17. SEM micrographs of (a)B and (b)A2 sintered at 1150ºC.

The effect of ultrasonic treatment and spray drying is mainly depending on crystallite size and particle size reduction. The effect of treatment on phase transformation and microstructure during transition may explain the improvement in densification behavior of the sintered bodies at reduced sintering temperatures.

The following SEM investigations were comparison of microstructures of A1 sintered compacts with B. Comparison of Fig.6.18 and Fig.6.19 show that the microstructures of the two samples were very similar in submicron scale. But the homogeneity of A1 at larger scale that was kept through since compaction yielded slightly higher densities.

Sample B exhibited the characteristics of a delayed transition path compared to A1. Hence, it was not surprising to see coalescence of alpha particles at 1200ºC growing into bigger grains which was observed for A1 samples at 1150ºC where densification rate considerably decreased as observed in Fig.6.12. The differences in microstructures were obvious in Fig.6.20 which compares treated A1 sample with B sintered at 1200ºC. The grain growth due to coalescence of α-phase varied in size and form because of untended agglomeration (Fig.6.20.b). Another irregular structure within B sample is shown in Fig.6.21.c. The exhibited orientation and pore structure was unexpected. It is interesting that similar occurances existed in A1 compacts sintered at 1250ºC but rarely and were much smaller in size (Fig.6.21.d).

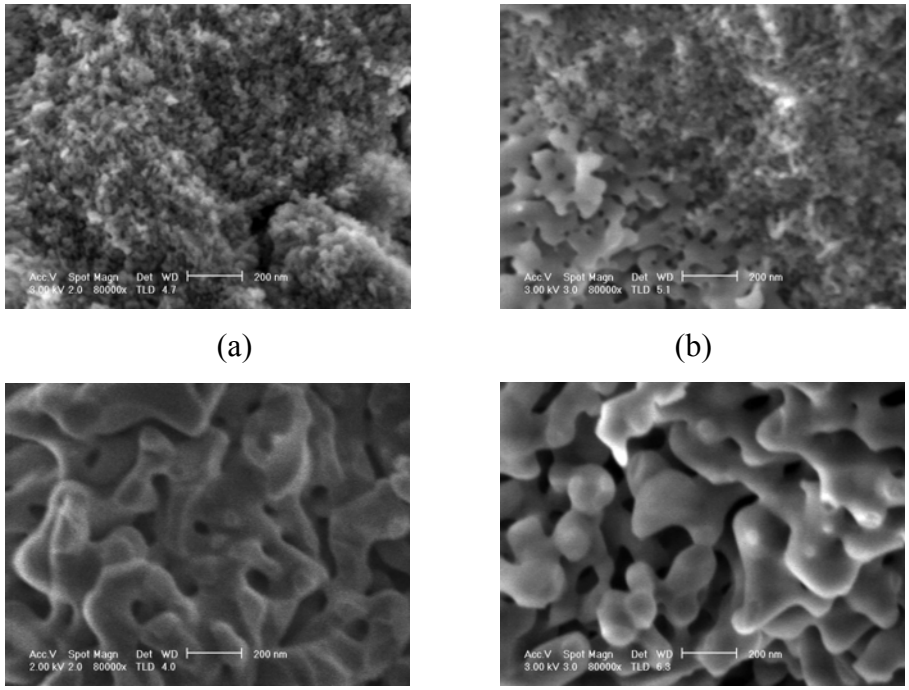

Fig.6.18. SEM micrographs illustrating phase transformation behavior of untreated boehmite samples 'B' sintered at (a) 1100ºC, (b) 1150ºC, (c) 1200ºC (d) 1250ºC.

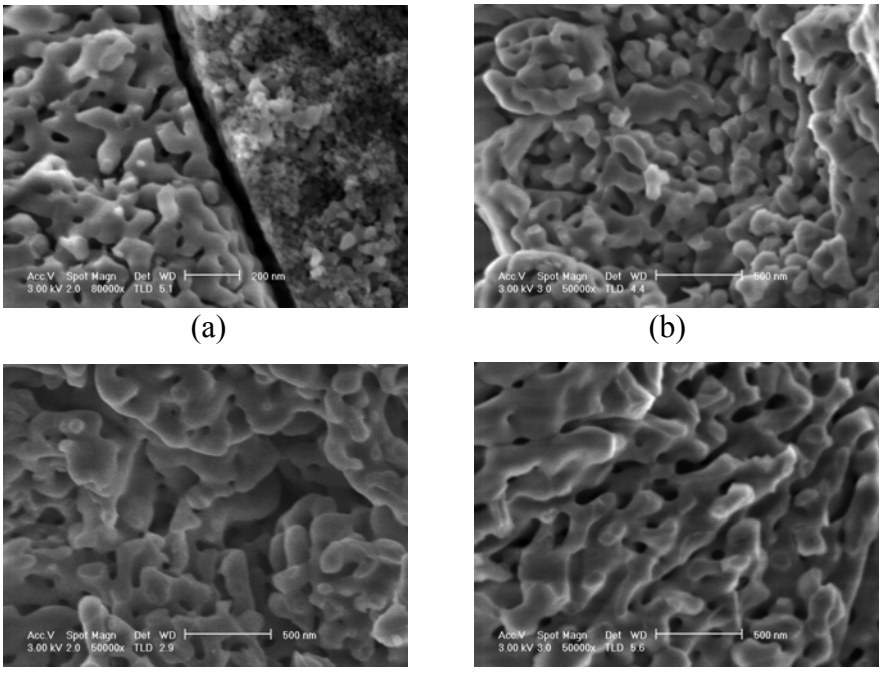

Fig.6.19. SEM micrographs illustrating phase transformation behavior of ultrasonically treated and spray-dried boehmite samples 'A1' sintered at (a) 1100ºC, (b) 1150ºC, (c) 1200ºC (d) 1250ºC.

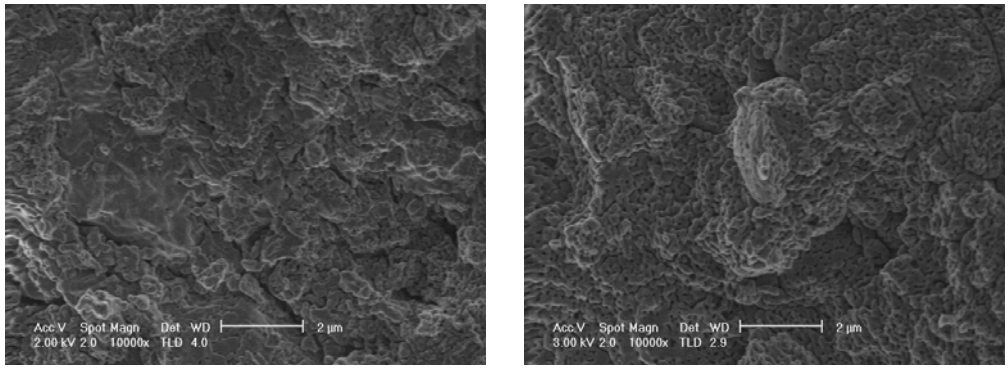

(a) (b)

Fig.6.20. SEM micrographs of untreated and treated boehmite samples; (a)B and (b)A1 sintered at 1200ºC.

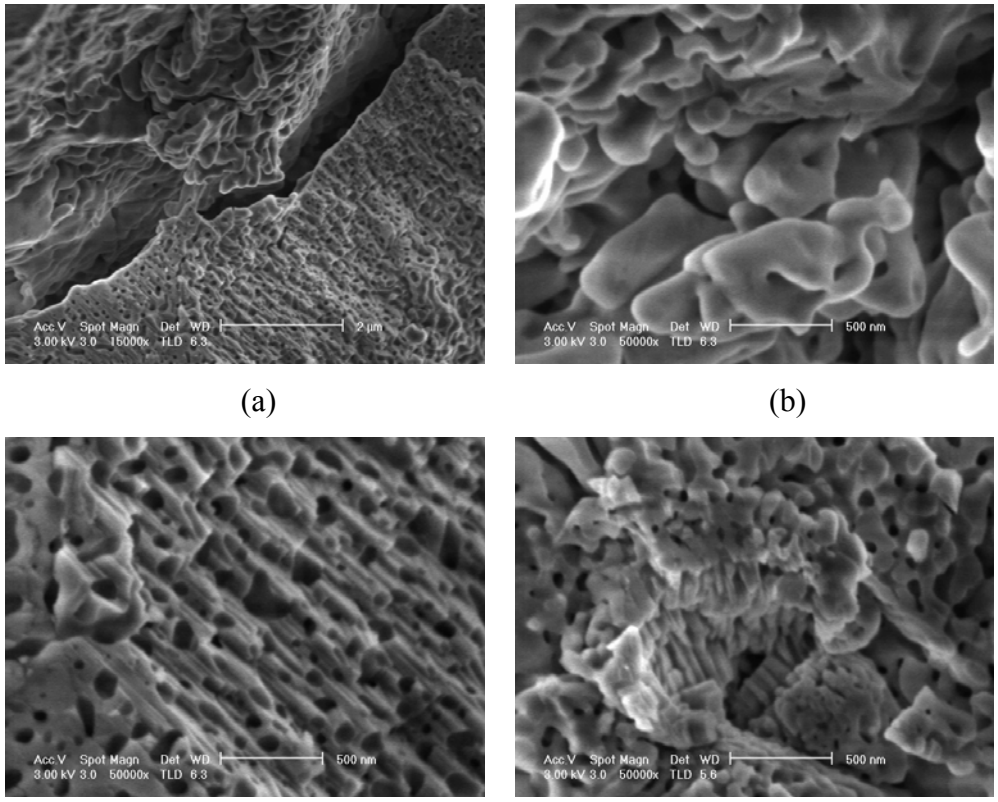

(a) (b)

(c) (d)

Fig.6.21. SEM micrographs of (a) B with a magnification of 15000x, (b,c) details from '(a)' with 50000x magnification and (d) A1 samples, sintered at 1250ºC.

The densities of the green bodies were 1.60-1.70 g/cm^3 (40-42% of the theoretical density) as mentioned in the previous section. The sintered density values given in Table 6.8 and illustrated in Fig.6.12 state that there has not already been a significant increase in densities of the samples at 1050ºC. The irregular microstructures due to uncontrolled agglomeration in untreated samples explains the decrease in densities at sintering temperatures over 1200ºC. And the slight increase in density of seeded and treated samples resulted from grain growth after completion of alpha formation. But seeded samples still did not yield higher densities than the ones that were only exposed to ultrasonic treatment and spray drying. The effect of the regular microstructure -led by the pretreatment- on densification which depended on phase transformation temperature and duration was investigated by XRD analysis of sintered compacts in the critical range of 1100-1200ºC.

X-Ray Diffraction diagrams of sintered compacts of A1 and B powders showed remarkable differences within the temperature range of 1100-1150ºC which was also the interval of change in densification characteristics of the two boehmite powders. The steepest section of density curve of A1 existed in 1110-1140ºC that corresponded to faster formation of alpha phase (Fig.6.12.b). In treated samples of A1, nucleation of α-phase had almost completed within the 20ºC interval between 1110-1130ºC (Fig.6.22) while this stage of phase transformation of B started at 1120ºC and densification increased until 1200ºC with a lower rate compared to the fast densification of A1.

Densification rate decreased at 1150-1200ºC interval and seemed to seize at about 1220ºC. No considerable microstructural changes were observed between 1200-1300ºC. The constant density value that A1 samples converged was detected to be 2.60 g/cm^3 reached at 1220ºC and is about 65.5 % of the theoretical density (Fig.6.12). This is a superior density when compared to previous investigations on sintering behaviors of transitional aluminas which report densities below 2.00 g/cm^3 with the same sintering conditions [56].

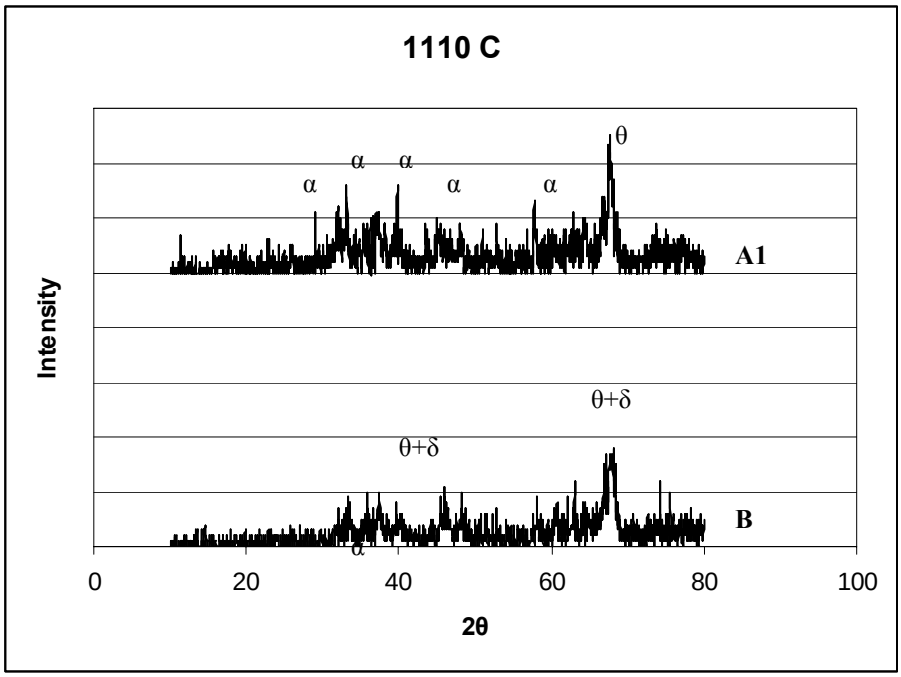

(a)

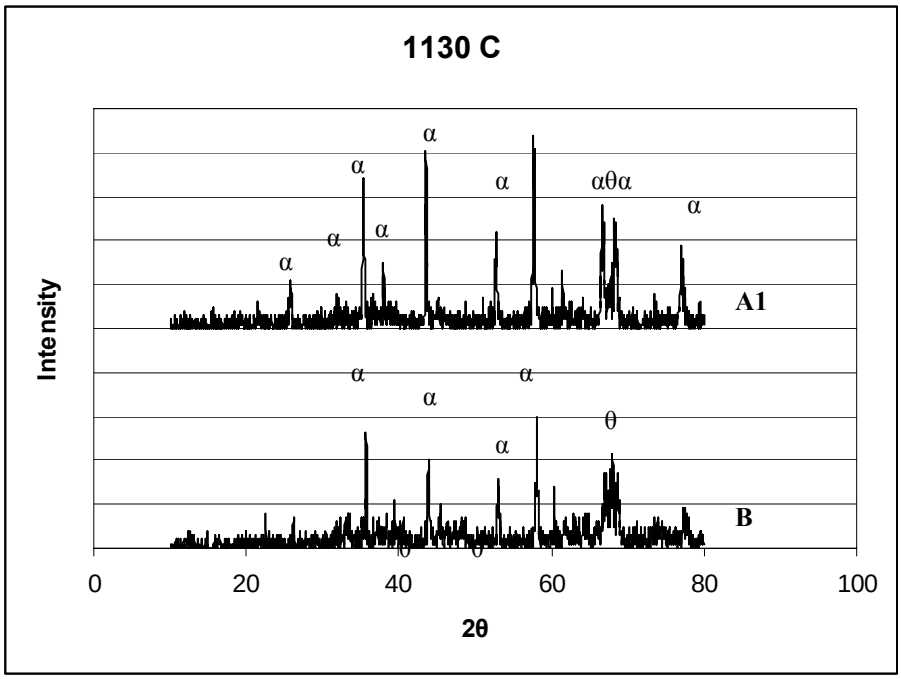

(b)

Fig.6.22. Comparison of X-RD diagrams of sintered pellets A1 and B at (a) 1110ºC and (b) 1130ºC. (App.D)

Chapter 7

CONCLUSIONS AND RECOMMENDATIONS

Particle size reduction by ultrasonic treatment of boehmite slurries and granulation by spray drying yielded higher density and more uniform microstructure of the final α-alumina product when compared to untreated and slightly seeded compacts.

The characteristics of slurry required optimization for an efficient particle size reduction, drying and compaction. Slurries having pH=4.0 and 30 wt% solid load, prepared by 120 min of ultrasonic treatment by the aid of glass-ball milling yielded low viscosities of 10.3 mPa.s with full dispersing efficiencies without using a dispersing agent. 2.5 % PVA added on dry basis aided compaction of spray-dried slurries. PVA addition did not cause a handling difficulty since a dispersant didn't have to be used.

Spray drying yielded a particle size distribution of powder granules between 0.1-10 μ. The particles are solid spheres covered by a thin layer of PVA which aided adhesion during compaction. The powders are compacted at 120 MPa yielded green bodies with density 40-42 % of the theoretical density. When compaction stress is increased to 600 MPa, the green densities increased to 64-66% but then no densification took place during sintering.

α-alumina used as seeding material is produced by combustion synthesis yielding 28 nm crystallite size while grain sizes exceeded 1μ as synthesized. Ultrasonic treatment with vibrational ball milling could disintegrate the grains into crystallites with an efficiency of 7%. Seeding with an α-alumina content less than 0.5wt% lowered the α-phase transformation temperature down to 1100ºC from 1200ºC but couldn't yield remarkably higher densities than the samples of untreated boehmite compacts.

The homogeneous microstructure led by particle size reduction and controlled granulation by spray-drying remained all through consolidation processes. Compacts had a more homogeneous pore distribution and phase transformations occurred more orderly. Phase transformation temperature to final α-phase has been reduced to 1150ºC by just the physical pretreatment of ultrasonic dispersion and spray-drying of boehmite slurries. These characteristics yielded significantly higher densities than seeded boehmite samples as well as untreated boehmite samples and treated transitional

alumina samples. The relative density reached 64.55 % of the theoretical density when sintered at 1200ºC while untreated samples had a relative density of 60.27 % and seeded samples had even lower densities at that sintering temperature. The densities could not be improved by further heating because of vermicular structure which essentially requires an extra treatment of doping or seeding with much higher α-Al_2O_3 contents.

The primary densification of treated samples is observed in the temperature range of 1100-1150ºC. This also corresponds to the range that treated samples show a distinct phase transformation behavior compared to untreated samples as confirmed by XRD diagrams. So it has been approved that densification primarily occurs in phase transformation stage rather than grain growth due to coalescence of α-Al_2O_3 grains and homogeneity of the microstructure has influence on the densification rate. The treated samples exhibited a comparatively faster densification within a narrower temperature range as a result of uniform microstructure in nanoscale, having influence on phase transformation behavior.

A more detailed investigation on sintering conditions including heating rate, sintering intervals and preheating treatments are required for completion of the study. As boehmite and alumina dispersions with comparatively high solid contents and low viscosities could be achieved, wet processing techniques are suggested for further studies, too. Pressure filtration, slip-casting or tape-casting may yield better results in terms of density of alumina bodies derived from boehmite.

Higher levels of seeding is another recommended subject. In this study the seeding material was pure alumina with an initial grain size of 1 μ. A seeding material with metal oxide impurities would provide a nanocrystalline material. Composites of Al_2O_3, with zirconia, magnesia and ferric oxide are reccomended for further seeding studies.

REFERENCES

1. Mayo. M.J., "Processing of nanocrystalline ceramics from ultrafine particles", *International Materials Rewievs,* Vol. 41, No.3 (1996) 85-116
2. Mayo. M.J., "Synthesis and applications of nanocrystalline ceramics", *Materials and Design,* Vol. 14, No.6 (1993) 323-329
3. Mayo. M.J., Ciftcioglu. M., "Issues in the processing of bulk nanocrystalline ceramics for structural applications", *Material Research Society Symposium Proceedings* (1991) 206
4. Mayo. M.J., "Superplasticity of nanostructured ceramics", Proceedings of a NATO-ASI Mechanical Properties and Deformation Behavior of Materials Having Ultrafine Microstructures (1993) 361-380
5. Langdon T.G., Watanabe T., Wadsworth J., Mayo M.J., Nutt S.R., Kassner M.E., "Future research directions for interface engineering in high temperature plasticity", *Materials Science and Engineering,* A166 (1993) 237-241
6. Kim B-N., Hiraga K., Morita K., Sakka Y., "Superplasticity in alumina by co-dispersion of 10% zirconia and 10 % spinel particles", *Acta Materialia,* 49 (2001) 887-895
7. Sakka Y., Hiraga K, "Preparation Methods and Superplastic Properties of Fine-Grained Zirconia and Alumina Based Ceramics", *National Research Institute for Metals*, 1-2-1, Sengen, Tsukuba-shi 305-0047, Japan
8. Zhang Q., Gao L., Guo J., "Effect of hydrolysis conditions on morphology and crystallization of nanosized TiO_2 powder", *Journal of European Ceramic Society,* 20 (2000) 2153-2158
9. Hare'l G., Ravi B.G., Chaim R, "Effects of solvent and agitation on microstructural characteristics of sol-gel derived nanocrystalline Y-TZP powders", *Materials Letters*, 39 (1999) 63-68
10. Suresh C, Biju V., Mukundan P., Warriar K.G.K., "Anatase to rutile transformation in sol-gel titania by modification of precursor", *Polyhedron*, 17 (1998) 3131-3135
11. Brodsky C.J., Ko E.I., "Effect of supercritical drying temperature on the properties of zirconia, niobia and titania-silica aerogels", *Journal of Non-Crystalline Solids,* 186 (1995) 88-95
12. Georgi U., Schlottig F., Graebner H., Steensel L., Wolf G., Roewer G., "Influence

of additives on properties of sol-gel layers", *Journal of Non-Crystalline Solids,* 277 (2000) 173-181

13. Li G.L., Wang G.H., "Synthesis of nanometer-sized TiO_2 particles by a microemulsion method", *Nanostructured Materials*, 11 (1999) 663-668
14. Christy R.V., Zhang Z.J., "Normal micelle synthesis and characterization of $MgAl_2O_4$ spinel nanoparticles", *Journal of Solid State Chemistry,* 175 (2003) 59-62
15. Aruna S.T., Rajam K.S., "Mixture of fuels approach for the solution combustion synthesis of Al_2O_3-ZrO_2 nanocomposite", *Materials Research Bulletin,* 2376 (2003) 1-11
16. Bhaduri S., Bhaduri S.B., "Enhanced low temperature toughness of Al_2O_3-ZrO_2 nano/nano composites", *NanoStructured Materials,* 8 (1997) 755-763
17. Bowen P., Carry C., "From powders to sintered pieces: forming, transformations and sintering of nanostructured ceramic oxides", *Powder Technology*, 128 (2002) 248-255
18. Hague D.C., Mayo M.J., "Sinter-forging of nanocrystalline zirconia: 1, Experimental", *Journal of American Ceramic Society,* 80 (1997) 149-156
19. Liao S.C., Chen J., Kear B.H., Mayo W.E., "High pressure low temperature sintering of nanocrystalline alumina", *NanoStructured Materials,* 10 (1998) 1063-1079
20. Chen D-J., Mayo M.J., "Rapid rate sintering of nanocrystalline ZrO_2- 3 mol% Y_2O_3", *Journal of American Ceramic Society,* 79 (1996) 906-912
21. Ramakrishnan K.N., "Powder particle size relationship in microwave sythesized ceramic powders", *Materials Science and Engineering,* A259 (1999) 120-125
22. Mayo M.J., "High and low temperature superplasticity in nanocrystalline materials", *NanoStructured Materials,* 9 (1997) 717-726
23. Voytovych. R, MacLaren I., Gülgün M.A., Cannon R.M., Rühle M., "The effect of ytrrium on densification and grain growth in alumina", *Acta Materialia,* 50 (2002) 3453-3463
24. Rossignol S. , Kappenstein C., "Effect of doping elements on the thermal stability of transition alumina", *International Journal of Inorganic Materials*, 3 (2001) 51–58
25. Bloch B., Ravi B.G., Chaim R., "Stabilization of transition alumina and grain growth inhibition in ultrafine Al O –5 wt.% SrO alloy", *Materials Letters*, 42 (2000) 61–65

26. Sathiyakumar M., Gnanam D., “Influence of additives on density, microstructure and mechanical properties of alumina”, *Journal of Materials Processing Technology*, 133 (2003) 282-286
27. Sathiyakumar M., Gnanam D., “Role of wollastonite additive on density, microstructure and mechanical properties of alumina”, *Ceramics International*, 29 (2003) 869-873
28. Nair J., Nair P., Mizukami F., Oosawa Y., Okubo T., “Microstructure and phase transformation behavior of doped nanostructured titania”, *Materials Research Bulletin*, 34 (1999) 1275-1290
29. Sakka Y., Ishii T., Suzuki T.S., Morita K., Hiraga K., “Fabrication of high strain rate superplastic yttria doped zirconia polycrystals by adding manganese and aluminum oxides”, *Journal of European Ceramic Society*, 24 (2004) 449-453
30. Chaim R. , Basat G., Kats-Demyanets A., “Effect of oxide additives on grain growth during sintering of nanocrystalline zirconia alloys”, *Materials Letters*, 35 (1998) 245–250
31. Wu Y., Zhang Y., Pezotti G., Guo J., “Influence of AlF_3 and ZnF_3 on the phase transformation of gamma to alpha alumina”, *Materials Letters,* 52 (2002) 366-369
32. Seidensticker J.R., Mayo M.J., “Superplasticity in 3Y-TZP doped with small amounts of copper oxide”, *Scripta Metallurgica et Materialia,* 31 (1994) 1749-1754
33. Seidensticker J.R., Mayo M.J., “Thermal analysis of 3mol%-yttria-stabilized tetragonal zirconia powder doped with copper oxide”, *Journal of American Ceramic Society*, 79 (1996) 401-406
34. IkuharaY., Yoshida H., Sakuma T., “Impurity effects on grain boundary strength in structural ceramics”, *Materials Science and Engineering*, A319–321 (2001) 24–30
35. Chaim R., Ramamoorthy R., Goldstein A., Eldror I., Gurman A.G., “Uniaxial plastic deformation in the zirconia-based nanocrystalline ceramics containing a silicate glass”, *Journal of European Ceramic Society*, 23 (2003) 647-657
36. Li G.-J., Huang X.-X., Guo J.-K., “Fabrication, microstructure and mechanical properties of Al_2O_3/Ni nanocomposites by a chemical method”, *Materials Research Bulletin,* 38 (2003) 1591-1600
37. Wang T.C., Chen R.Z., Tuan W.H., “Oxidation resistance of Ni-toughened Al_2O_3”, *Journal of European Ceramic Society*, 23 (2003) 927-934
38. Chevalier J., Olagnon C., Fantozzi G., Gros H., “Creep behaviour of alumina,

zirconia and zirconia-toughened alumina", *Journal of European Ceramic Society*, 17 (1997) 859-864

39. Boutz M.M.R., Minden C., Janssen R., Claussen N., "Deformation processing of reaction bonded alumina ceramics", *Materials Science and Engineering*, A233 (1997) 155-166
40. Anklekar R.M., Borkar S.A., Bhattacharjee S., Page C.H., Chatterjee A.K., "Rheology of concentrated alumina suspension to improve the milling output in production of high purity alumina powder", *Colloids and Surfaces A*, 133 (1998) 41-47
41. Tsetsekou A., Agrafiotis C., Milias A., "Optimization of the rheological properties of alumina slurries for ceramic processing applications Part I: Slip-casting", *Journal of the European Ceramic Society,* 21 (2001) 363-373
42. Tsetsekou A., Agrafiotis C., Leon I., Milias A., "Optimization of the rheological properties of alumina slurries for ceramic processing applications Part II: Spray-drying", *Journal of the European Ceramic Society,* 21 (2001) 493-506
43. Okuyama K., Lenggoro I.W., "Preparation of nanoparticles via spray route", *Chemical Engineering Science*, 58 (2003) 537-547
44. Bertrand G., Filiatre C., Mahdjoub H., Foissy A., Coddet C., "Influence of slurry characteristics on the morphology of spray-dried alumina powders", *Journal of the European Ceramic Society*, 23 (2003) 263-271
45. Santhiya D., Subramanian S., Natarajan K.A., Malghan S.G., "Surface chemical Studies on the competitive adsorption of poly(acrylic acid) and poly(vinyl alcohol) onto alumina", *Journal of Colloid and Interface Science*, 216 (1999) 143-153
46. Romdhane M.R.B., Baklouti S., Bouaziz J., Chartier T., Baumard J.-F., "Dispersion of Al_2O_3 concentrated suspensions with new molecules able to act as binder", *Journal of European Ceramic Society,…*
47. Romdhane M.R.B., Baklouti S., Bouaziz J., Chartier T., Baumard J.-F., "Dispersion of Al_2O_3 suspension with acrylic copolymers bearing carboxylic groups", *Colloids and Surfaces A: Physicochemical Engineering Aspects,* 212 (2003) 271-283
48. Baklouti S., Romdhane M.R.B., Boufi S., Pagnoux C., Chartier T., Baumard J.-F., "Effect of copolymer dispersant structure on the properties of alumina suspensions", *Journal of European Ceramic Society,* 23 (2003) 905-911

49. Baklouti S., Bouaziz J, Chartier T., Baumard J.-F., “Binder burnout and evolution of the mechanical strength of dry-pressed ceramics containing poly vinyl alcohol”, *Journal of European Ceramic Society,* 21 (2001) 1087-1092
50. Baklouti S., Chartier T., Baumard J.-F., “Binder distribution in Spray-Dried alumina agglomerates”, *Journal of European Ceramic Society,* 18 (1998) 2117-2121
51. Mandanas M.M:, Messing G.L., “Thermogravimetric analysis of organic binder segregation during drying of particulate suspensions”, *Thermochimica Acta*, 363 (2000) 37-45
52. Carneim R.D., Messing G.L., “Response of granular powders to uniaxial loading and unloading”, *Powder Technology*, 115 (2001) 131-138
53. Baklouti S., Chartier T., Gault C., Baumard J.-F., “Young’s modulus of dry-pressed ceramics: The effect of binder”, *Journal of European Ceramic Society,* 19 (1999) 1569-1574
54. Briscoe B.J., Özkan N., “Compaction behavior of agglomerated alumina powders”, *Powder Technology*, 90 (1997) 195-203
55. Özkan N., Briscoe B.J., “Overall shape of sintered alumina compacts”, *Ceramics International*, 23 (1997) 521-536
56. Legros C., Carry C., Bowen P., Hofman H., “Sintering of a transition alumina: Effects of phase transformation, powder characteristics and thermal cycle” , *Journal of the European Ceramic Society,* 19 (1999) 1967-1978
57. Ahn J.-P., Park J.-K., Lee H.-W., “Effect of compact structures on the phase transition, subsequent densification and microstructure evolution during sintering of ultrafine gamma alumina powder”, *NanoStructured Materials,* 11 (1999) 133-140
58. Ferkel H., Hellmig R.J., “Effect of nanopowder deagglomeration on the densities of nanocrystalline ceramic green bodies and their sintering behaviour”, *Nanostructured Materials,* 11 (1999) 617-622
59. Chen I.W., Wang X.H., “Sintering dense nanocrystalline ceramics without final stage grain growth”, *Nature*, 404 (2000) 168-171
60. Lim L.C., Wong P.M., Jan M., “Microstructural evolution during sintering of near-monosized agglomerate-free submicron alumina powder compacts”, *Acta Materialia,* 48 (2000) 2263-2275

61. Ma J., Lim L.C., “Effect of particle size distribution on sintering of agglomerate-free submicron alumina powder compacts”, *Journal of the European Ceramic Society,* 22 (2002) 2197-2208
62. Lance D., Valdivieso F., Goeuriot P., “Corellation between densification rate and microstructural evolution for pure alpha alumina”, *Journal of the European Ceramic Society,* -
63. Nettleship I., McAfee R., “Microstructural pathways for the densification of slip cast alumina”, *Materials Science and Engineering,* A352 (2003) 287-293
64. Bokhimi X., Toledo-Antonio J.A., Guzman-Castillo M.L., Mar-Mar B., Hernandez-Beltran F., Navarette J., “Dependence of boehmite thermal evolution on its atom bond lengths and crystallite size,” *Journal of Solid State Chemistry*, 161 (2001) 319-326
65. Wen H-L., Yen F-S., “Growth characteristics of boehmite-derived ultrafine theta and alpha-alumina particles during phase transformation”, *Journal of Crystal Growth*, 208 (2000) 696-708
66. Shelleman R.A., Messing G.L., Kumagai M., “Alpha alumina transformation in seeded boehmite gels”, *Journal of Non-Crystalline Solids*, 82 (1986) 277-285
67. Nordahl C.S., Messing G.L., “Sintering of α-Al_2O_3-seeded nanocrystalline γ-Al_2O_3 powders”, *Journal of the European Ceramic Society,* 22 (2002) 415-422
68. Yoshizawa Y., Hirao K., Kanzaki S., “Fabrication of low cost fine-grained alumina powders by seeding for high performance sintered bodies”, *Journal of the European Ceramic Society,* 24 (2004) 325-330
69. Shiau, F-S., Fang T-T., “Low temperature synthesis of α-alumina using citrate process with α-alumina seeding”, *Materials Chemistry and Physics,* 60 (1999)91-94
70. Youn H-J., Jang J.W., Kim I-T., Hong K.S., “Low-temperature formation of α-alumina by doping of an alumina-sol”, *Journal of Colloid and Interface Science*, 211 (1999) 110-113
71. Boccaccini A.R., Kaya C., “Alumina ceramics based on seeded boehmite and electrophoretic deposition”, *Ceramics International,* 28 (2002) 893-897
72. Tartaj J., Messing G.L., “Anisotropic grain growth in α-Fe_2O_3-doped alumina”, *Journal of European Ceramic Society,* 17 (1997) 719-725

APPENDIX A

Product Information Data Sheet of DISPERAL/Condea

A1. Product Information

DISPERAL®

Acid dispersible boehmite alumina systems

Typical chemical and physical properties		DISPERAL
Al_2O_3	[%]	77
Na_2O	[%]	0.002
Loose bulk density	[g/l]	400-600
Particle size (d_{50})*	[µm]	25
Surface area (BET)**	[m^2/g]	180
Pore volume**	[ml/g]	0.5
Crystallite size [120]	[nm]	10
Dispersed particle size***	[nm]	80
Dispersibility (10% Al_2O_3/1.2 % HNO_3)	[%]	98
Dispersibility (30% Al_2O_3/0.1 % HNO_3)	[%]	-

Chemical purity:C:0.25%, SiO_2:0.01-0.015 %, Fe_2O_3: 0.005-0.015 %, TiO_2: 0.01-0.15 %

***Particle size as measured on the powder.**

****After activation at 550°C for 3 hours.**

*****10 wt% Al_2O_3 in 0.4 wt% HNO_3. Dispersions of acid dispersible products may be formed by dispersing in dilute aqueous monovalent acids (typically 1 wt% acid) such as nitric, hydrocloric, formic, lactic or acetic acid.**

A2. Product Information Data Sheet

DISPERAL

Product information data sheet

DISPERAL **is an alumina hydrate which may be readily dispersed in diluted mono-valent** acids (e.g. nitric acid, acetic acid etc.). Stable dispersions are obtained up to 30 wt-% alumina concentration. The dispersion is viscosity stable for several months.

Typical Data

Chemical Composition:		AlO(OH)
Crystal Structure:		boehmite
crystallite size [021]-reflex:		9-12 nm
Chemical Data:		
Al_2O_3	%	> 72
Physical Properties:		
loose bulk density	g/ml	0.40 – 0.60
pore volume	ml/g	0.50
Surface Area (3h/550°C)	m^2/g	> 160
Dispersibility in acid	%	> 97 %
Zeta potential (at pH 2.1)	mV	+ 43

A3. Product Information – Particle Size

DISPERAL

Product information data sheet

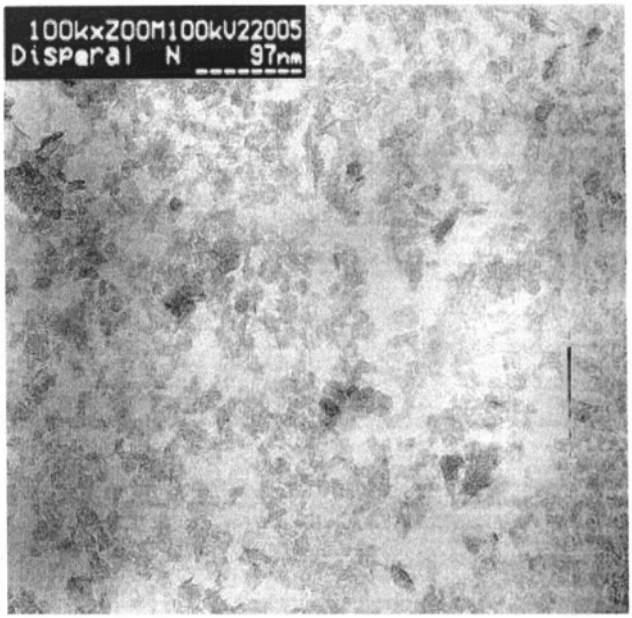

1. TEM-picture of DISPERAL, 100 KV (Max-Planck-Institut für Kohlenforschung, Mülheim)

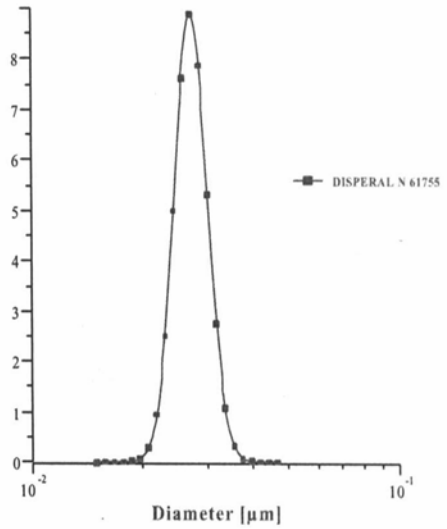

2. Particle size distribution of DISPERAL measured by elektroacoustic attenuation (DT1200 by Dispersion Technology). The median particle size lies at 27 nm.

A4. Product Information – IR Spectrum and DTA/TG

DISPERAL

Product information data sheet

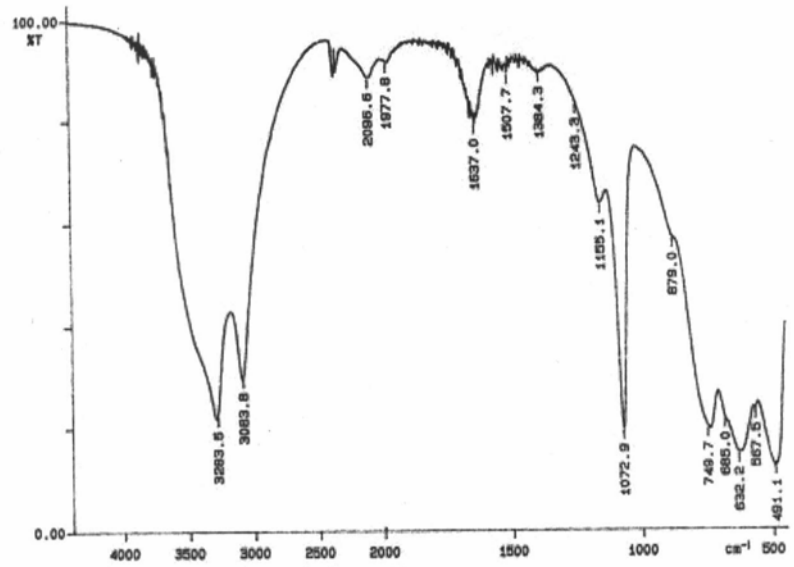

1. IR spectrum of DISPERAL

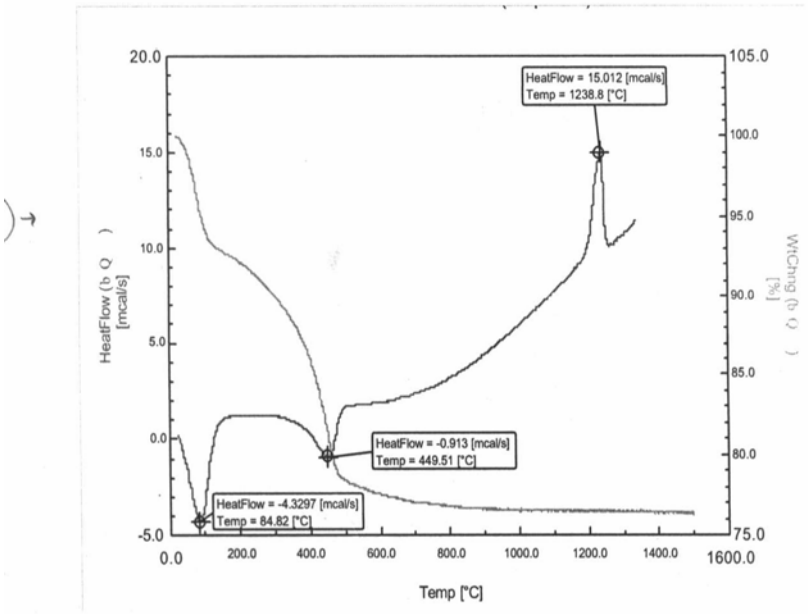

2. DTA / TG of DISPERAL

A5. Product Information – X-Ray Diffraction Diagram and Pore Radii Distribution

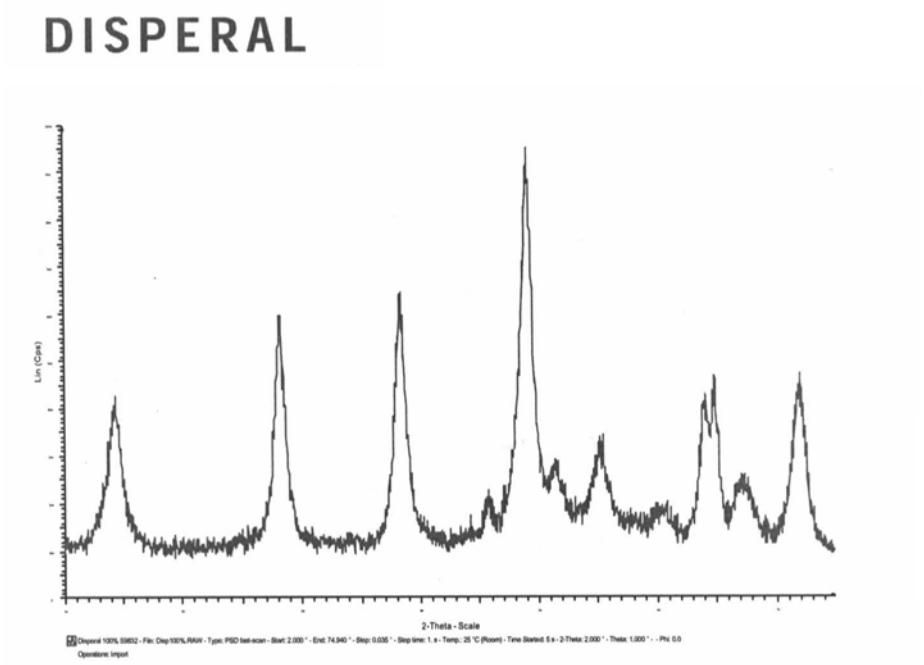

1. XRD of DISPERAL

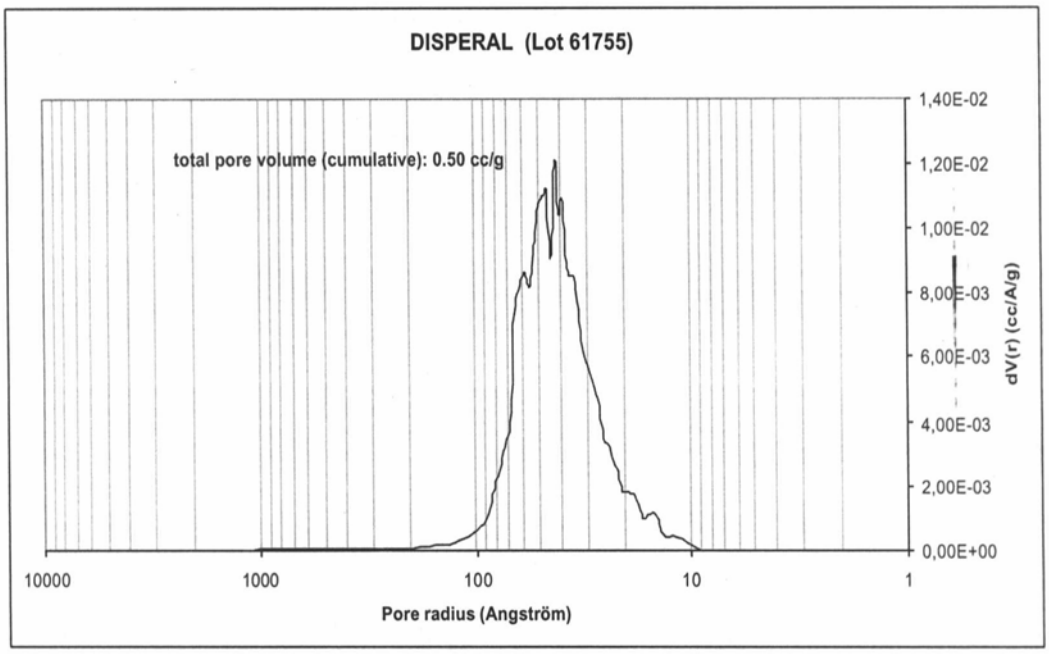

2. Pore radii distribution (N_2) of DISPERAL

A6. Product Information – Preparation of a DISPERAL Dispersion

DISPERAL

Dispersing Procedure

Please check first the Al_2O_3-content (X) which is given in the certificate of analyses.
In order to prepare an alumina sol of 10 (30) wt.% Al_2O_3 content, pour 10:X*100 (=Y) (30:X*100) (=Y') g of DISPERAL powder under intensive stirring into 100-Y (100-Y') g of 0.31-0.32 (0.94 - 1.25)% HNO_3. After stirring for 30 min. the sol is ready for use.
The viscosity of this sol is below 10 (500) mPas.
Under aforesaid conditions DISPERAL offers a dispersibility (20 min at 2400 rpm) of min. 97 % at a pH of 3.0- 4.0. The dispersion can be diluted with water afterwards if necessary.

Viscosity

The dynamic viscosity and viscosity stability of a boehmite dispersion is an important feature in many applications. Boehmite dispersions may become thixotropic after a certain time of storage. This means mechanical energy (shaking, stirring) results in a decrease of viscosity. The viscosity can also be adjusted by dilution with distilled water. Viscosity behaviour of a boehmite dispersion depends strongly on alumina-content, acid concentration, acid type (HNO_3 or other) and additives like salts etc. Generally, addition of salts, especially 2- and more valent salts, tend to increase viscosity.The use of tapwater should, therefore, be avoided when preparing a dispersion.

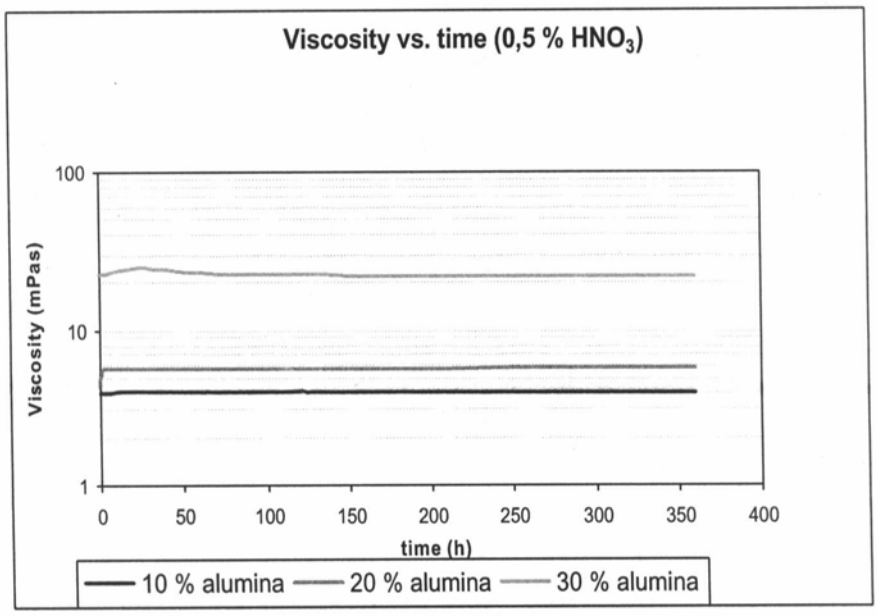

Dynamic viscosity was measured using a Brookfield viscosimeter at room temperature.

A7. Product Information – Dispersibility, pH, Particle Size and Transmission

DISPERAL

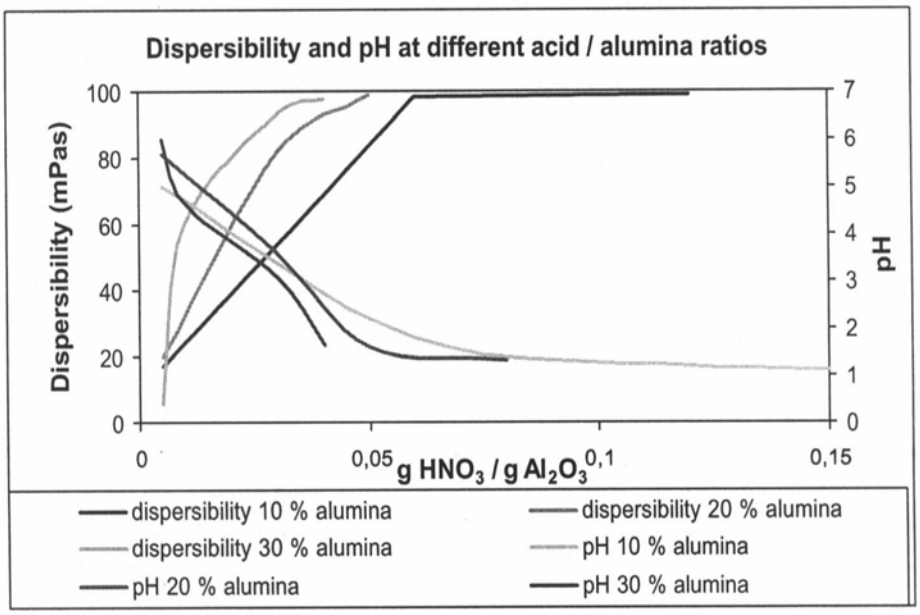

1. The dispersibility of DISPERAL varies strongly dependent of acid concentrations. A ratio of 0.1 g HNO_3 / g Al_2O_3 should not be exceeded. Dispersibility is determined after centrifugation of a 10 % Al_2O_3 dispersion at 2400 upm (10 min). When acid concentration is varied, the pH is strongly influenced depending on the alumina concentration of the dispersion. The optimum pH value for a stable DISPERAL dispersion is 3-4. An excess of acid leads to increased gelation velocity whereas a lack of acid results in incomplete dispersion.

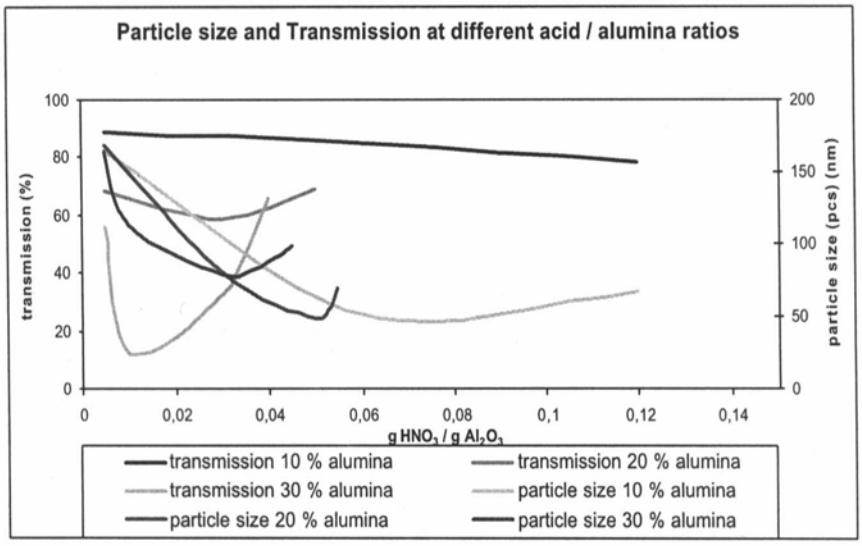

2. The transmission of a dispersion increases with decreasing particle size and increasing dispersibility. Transmission was measured at 450 nm at 10 % Al_2O_3 concentration. Particle size is measured using a Malvern Zetamaster PCS instrument.

APPENDIX B

Crystallite Sizes by Scherrer Formula

B1. Crystallite size of Boehmite Precursor

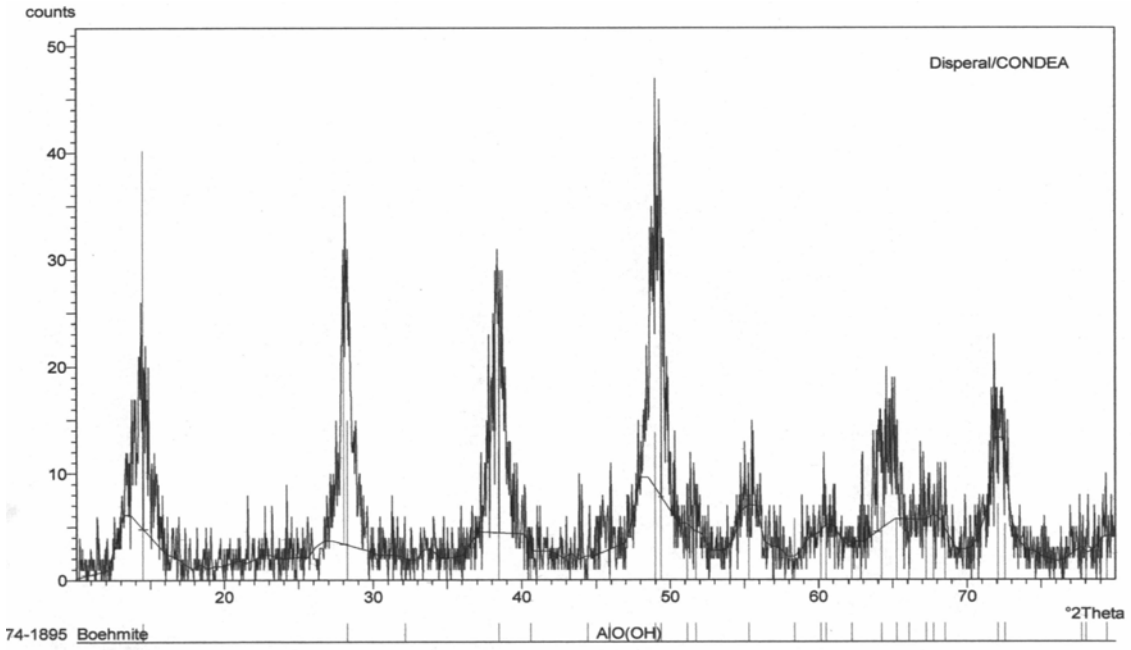

BOEHMITE Crystal Size

No.	B Size[°2Th]		B Strain[°2Th]		Peak pos.[°2Th]	Cryst.size[Å]		Latt.strain[%]	
1	1.630	1.000	0.630	1.287	14.509	127		4.412	
2	1.551	1.000	0.551	1.186	28.009		149		2.074
3	1.787	1.000	0.787	1.481	38.469	107		1.852	
4	1.384	1.000	0.384	0.957	49.394	228		0.908	

B2. Crystallite size of α-Alumina Seed

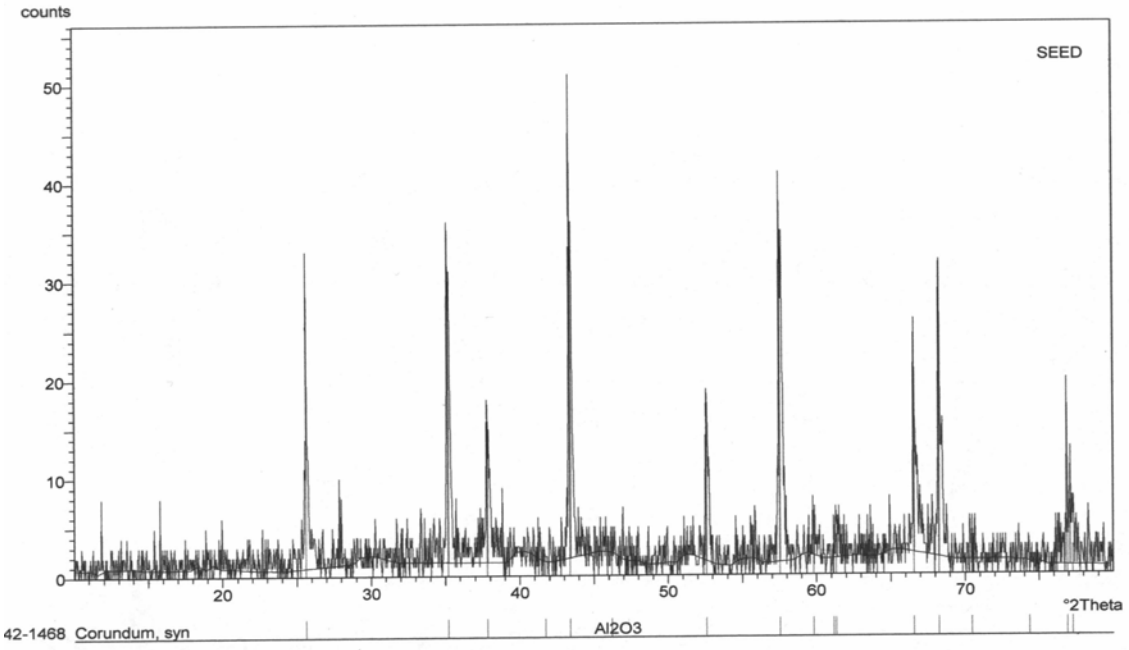

SEED Crystal Size

No.	B Size[°2Th]		B Strain[°2Th]		Peak pos.[°2Th]	Cryst.size[Å]	Latt.strain[%]
1	1.157	1.000	0.157	0.582	25.592	519	1.118
2*	1.236	1.000	0.236	0.726	35.182	353	1.000
3	1.197	1.000	0.197	0.658	37.815	426	0.838
4*	1.197	1.000	0.197	0.658	43.412	434	0.721
5	1.118	1.000	0.118	0.500	52.570	751	0.442
6*	1.157	1.000	0.157	0.582	57.528	577	0.463
7	1.144	1.000	0.144	0.556	66.548	660	0.369
8	1.144	1.000	0.144	0.556	68.239	666	0.358
9	1.384	1.000	0.384	0.957	77.072	264	0.524

APPENDIX C

X-Ray Powder Diffraction Patterns

C1. XRD Diagram of Alumina Powders Calcined at 350ºC

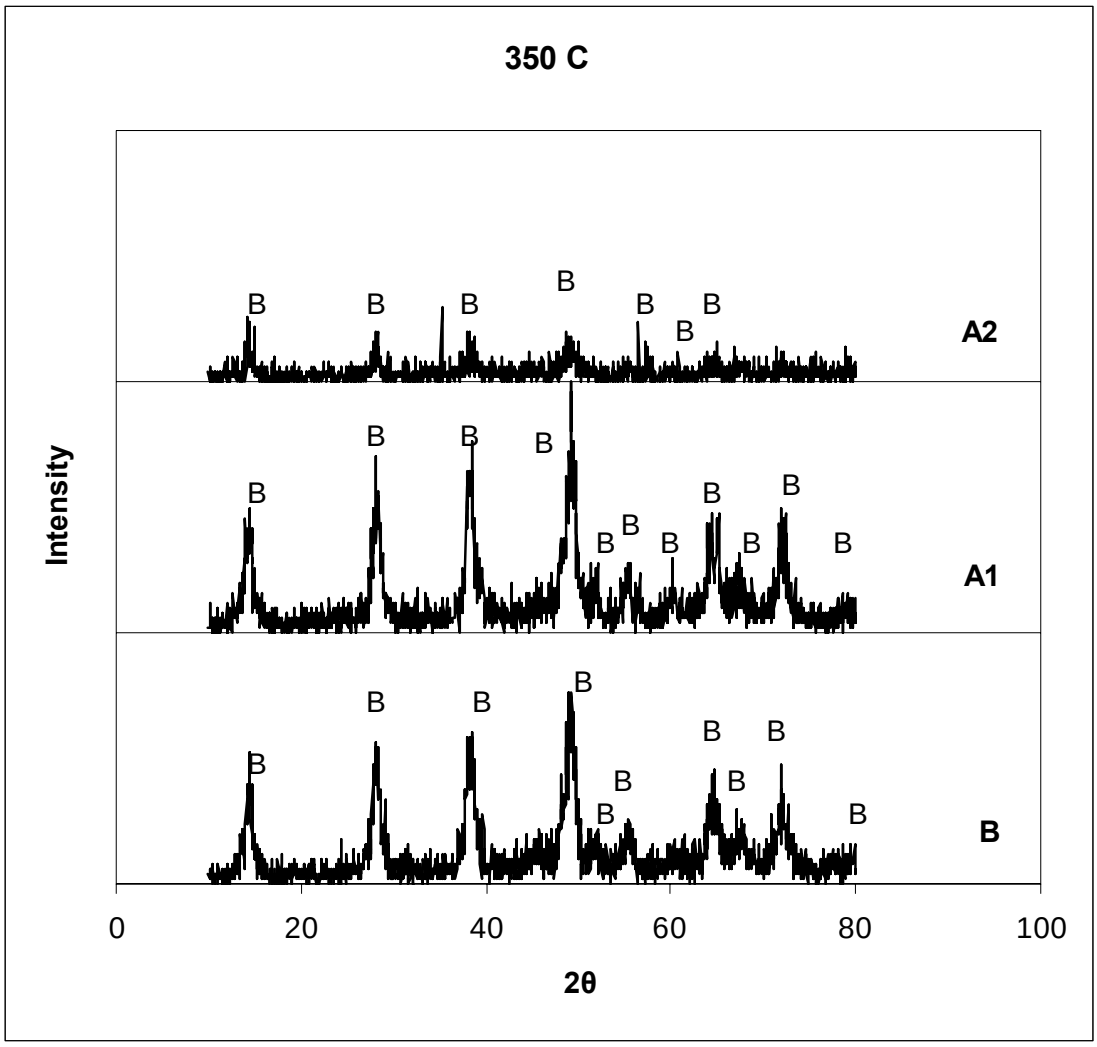

Fig. C1. XRD patterns of B, A1 and A2 Powders Calcined at 350ºC

C2. XRD Diagram of Alumina Powders Calcined at 400ºC

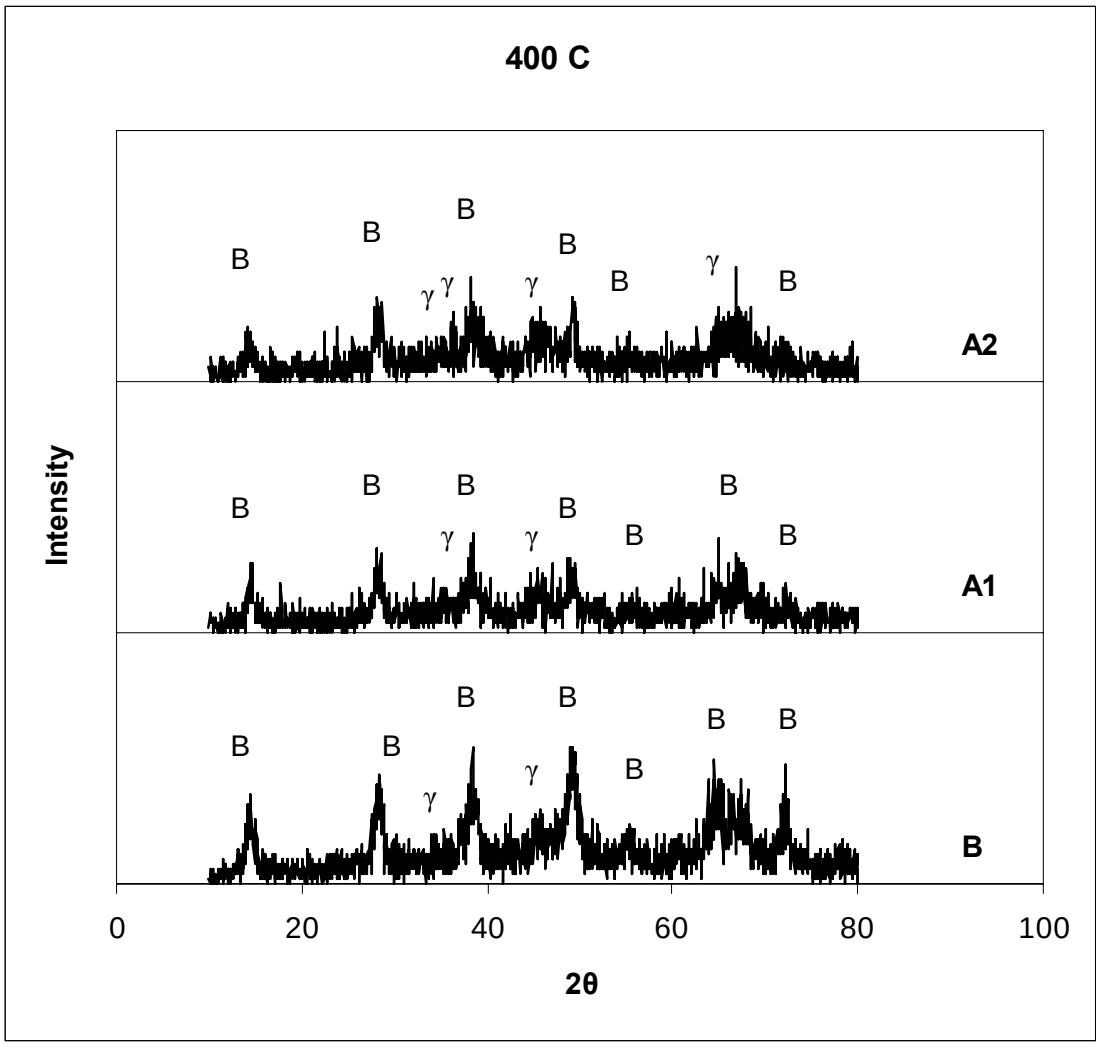

Fig. C2. XRD patterns of B, A1 and A2 powders calcined at 400ºC

C3. XRD Diagram of Alumina Powders Calcined at 500ºC

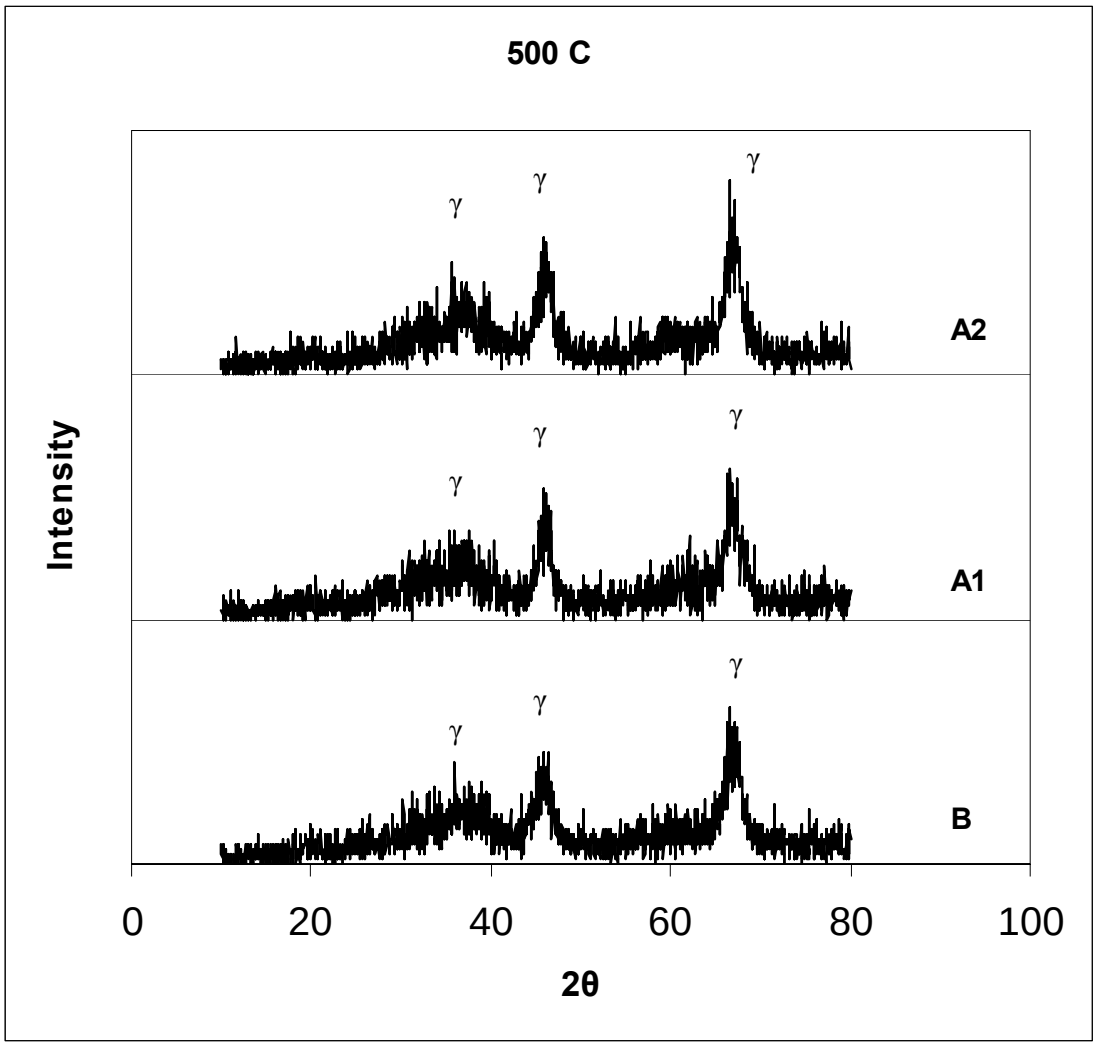

Fig. C3. XRD patterns of B, A1 and A2 powders calcined at 500ºC

C4. XRD Diagram of Alumina Powders Calcined at 600ºC

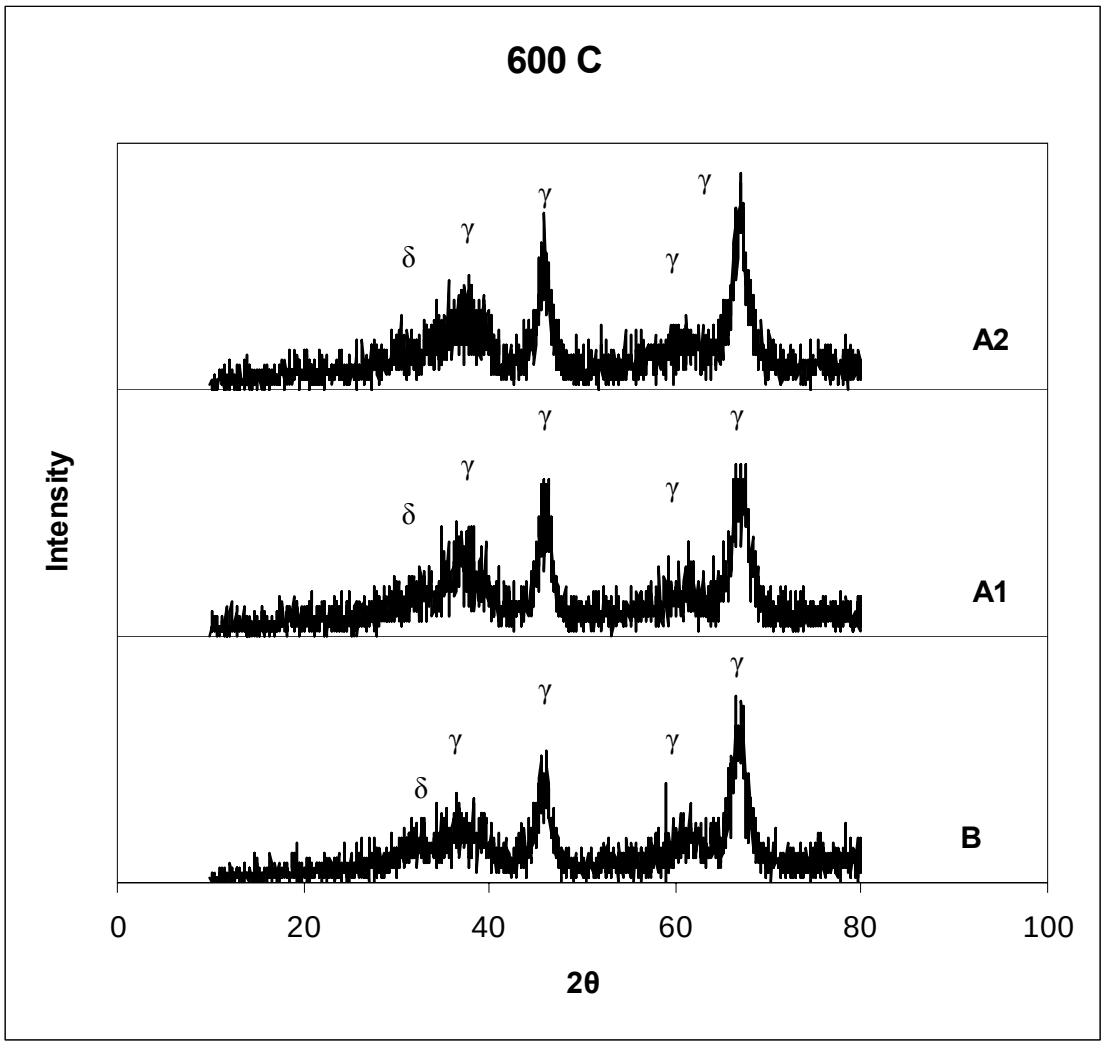

Fig. C4. XRD patterns of B, A1 and A2 powders calcined at 600ºC

C5. XRD Diagram of Alumina Powders Calcined at 700ºC

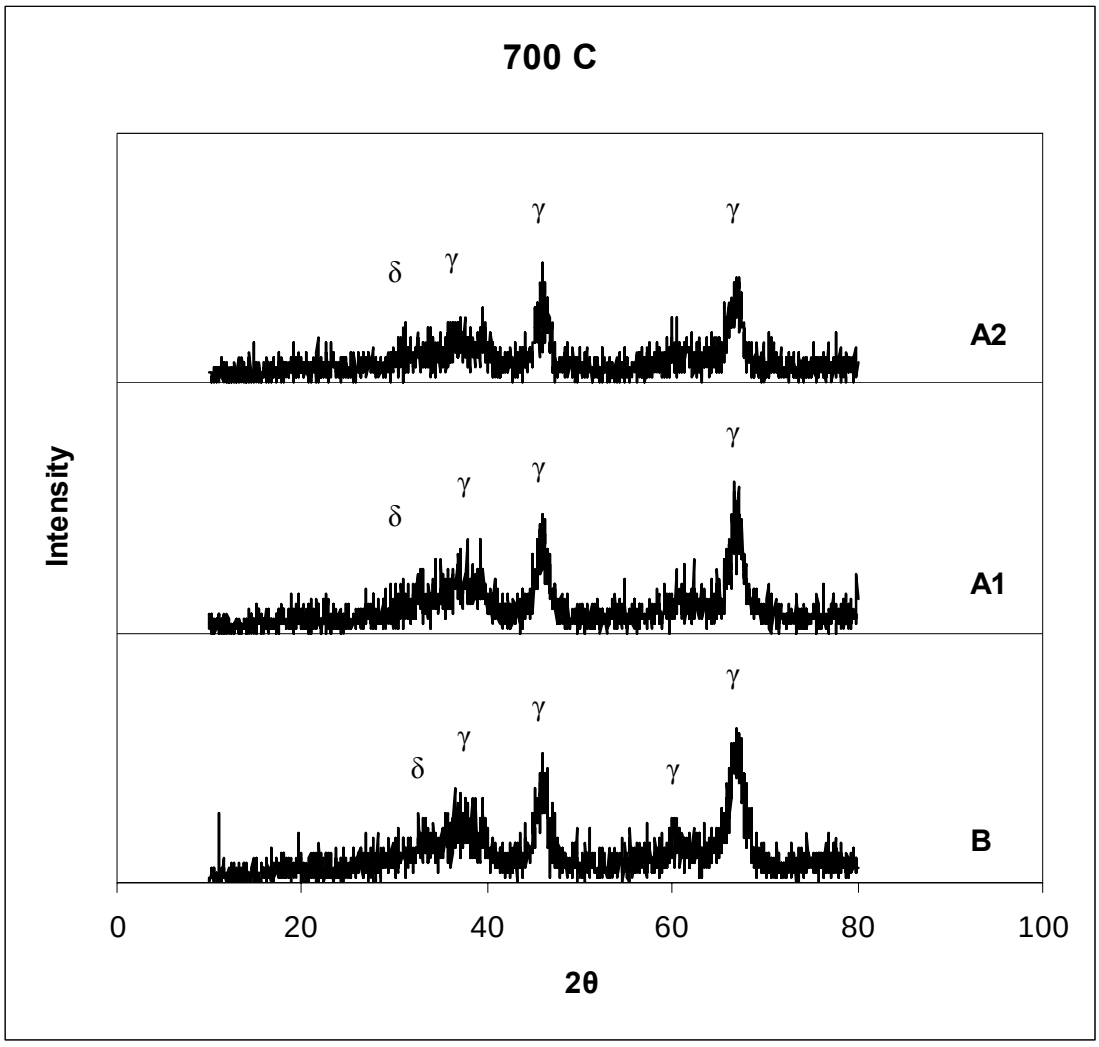

Fig. C5. XRD patterns of B, A1 and A2 powders calcined at 700ºC

C6. XRD Diagram of Alumina Powders Calcined at 800ºC

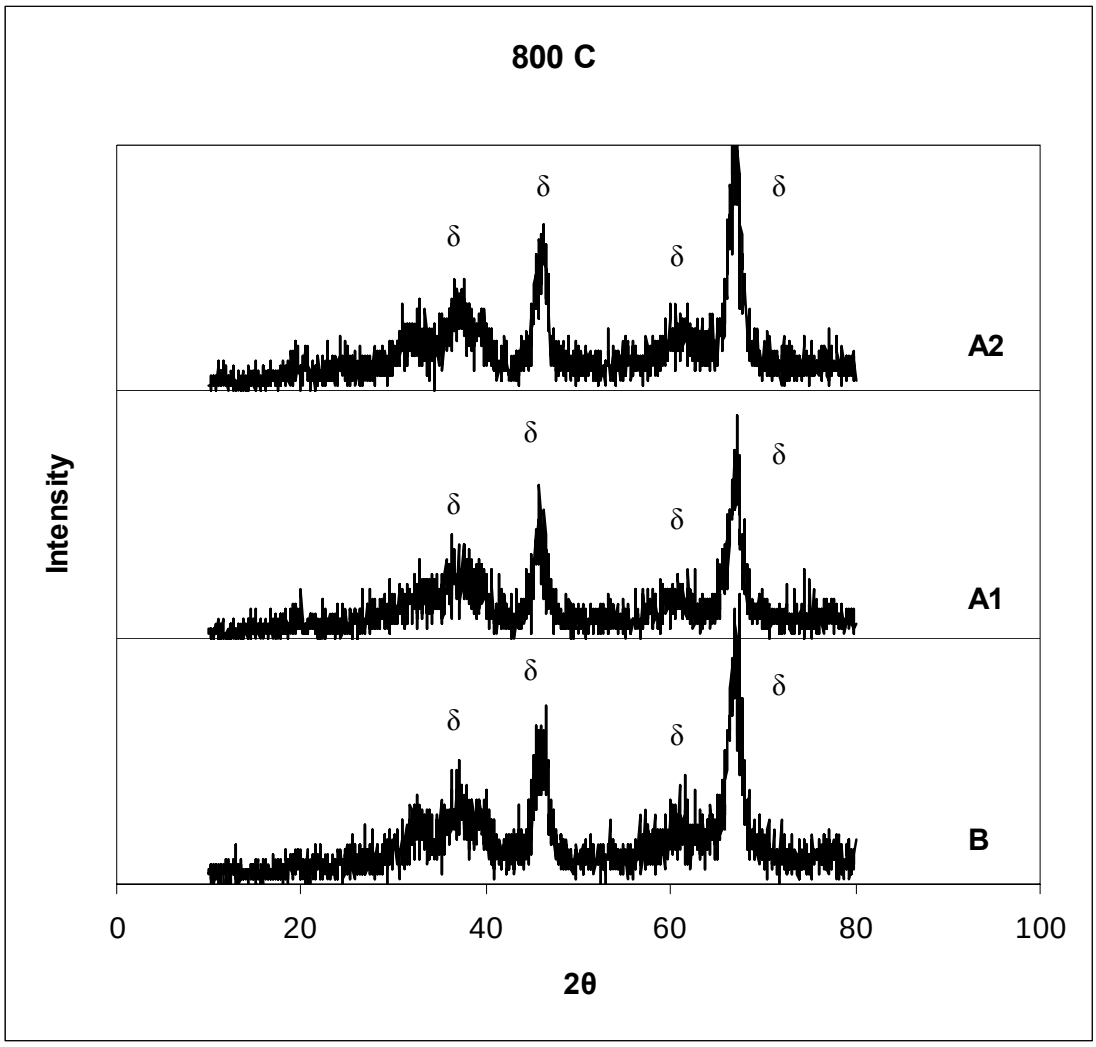

Fig. C6. XRD patterns of B, A1 and A2 powders calcined at 800ºC

C7. XRD Diagram of Alumina Powders Calcined at 900ºC

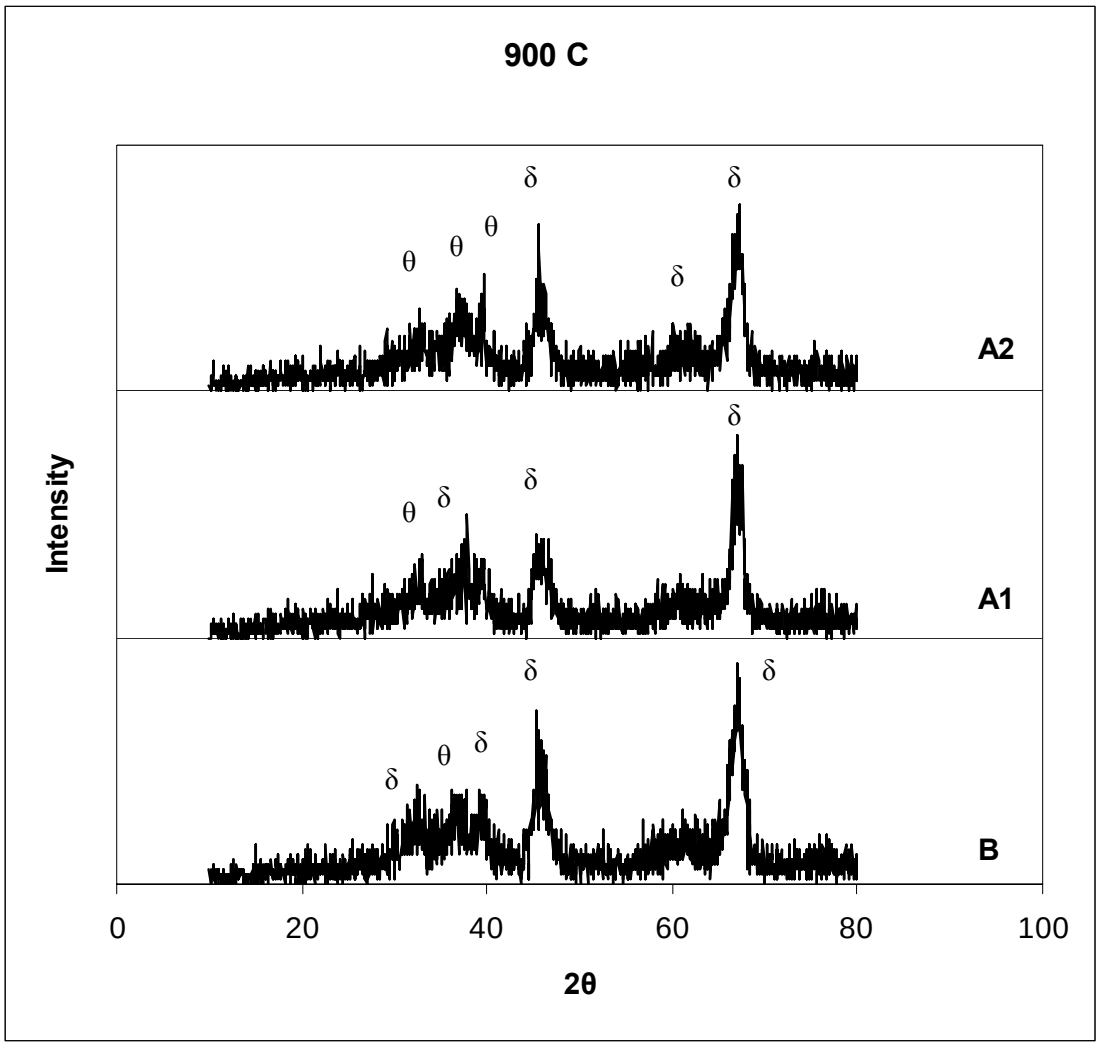

Fig. C7. XRD patterns of B, A1 and A2 powders calcined at 900ºC

C8. XRD Diagram of Alumina Powders Calcined at 1000ºC

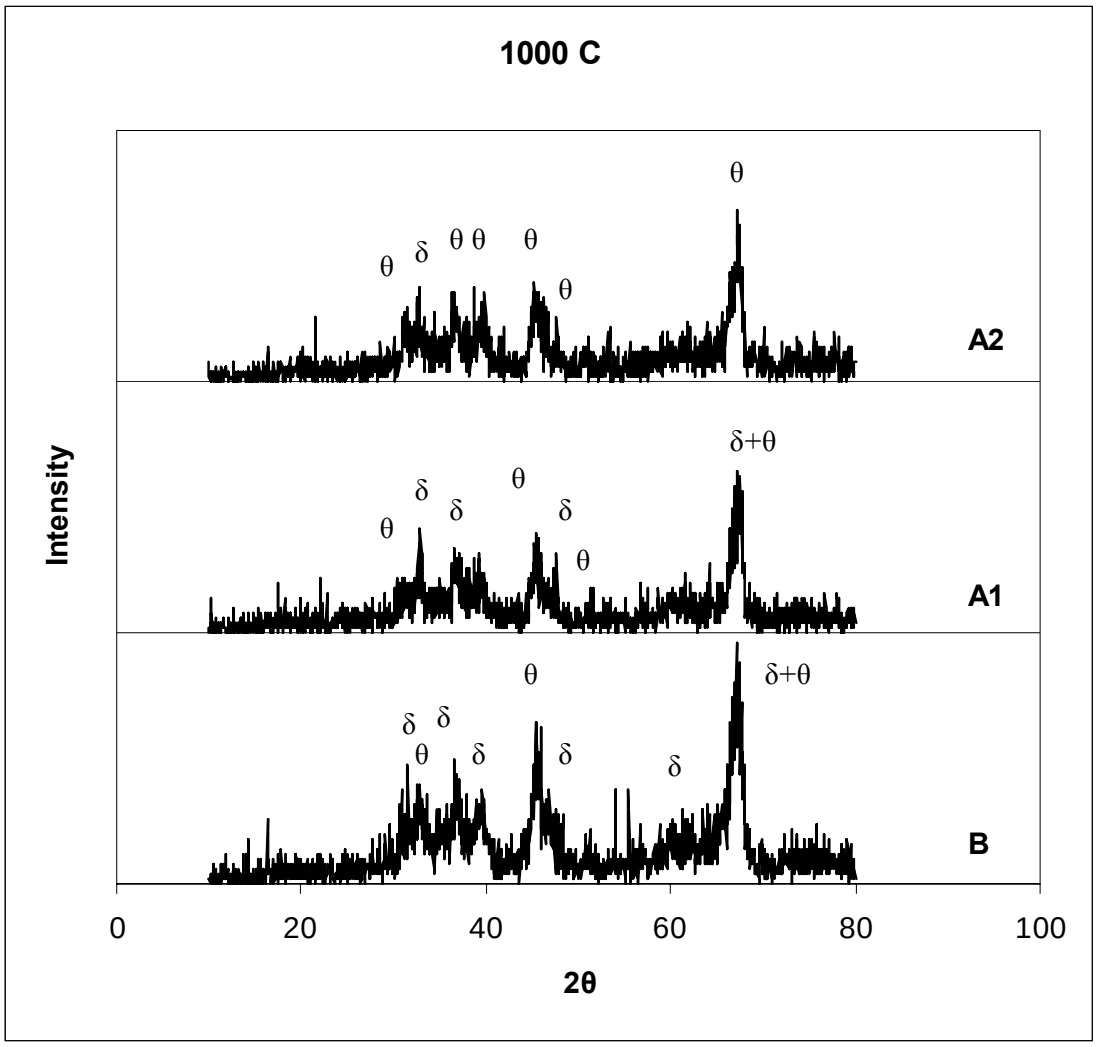

Fig. C8. XRD patterns of B, A1 and A2 powders calcined at 1000ºC

C9. XRD Diagram of Alumina Powders Calcined at 1050ºC

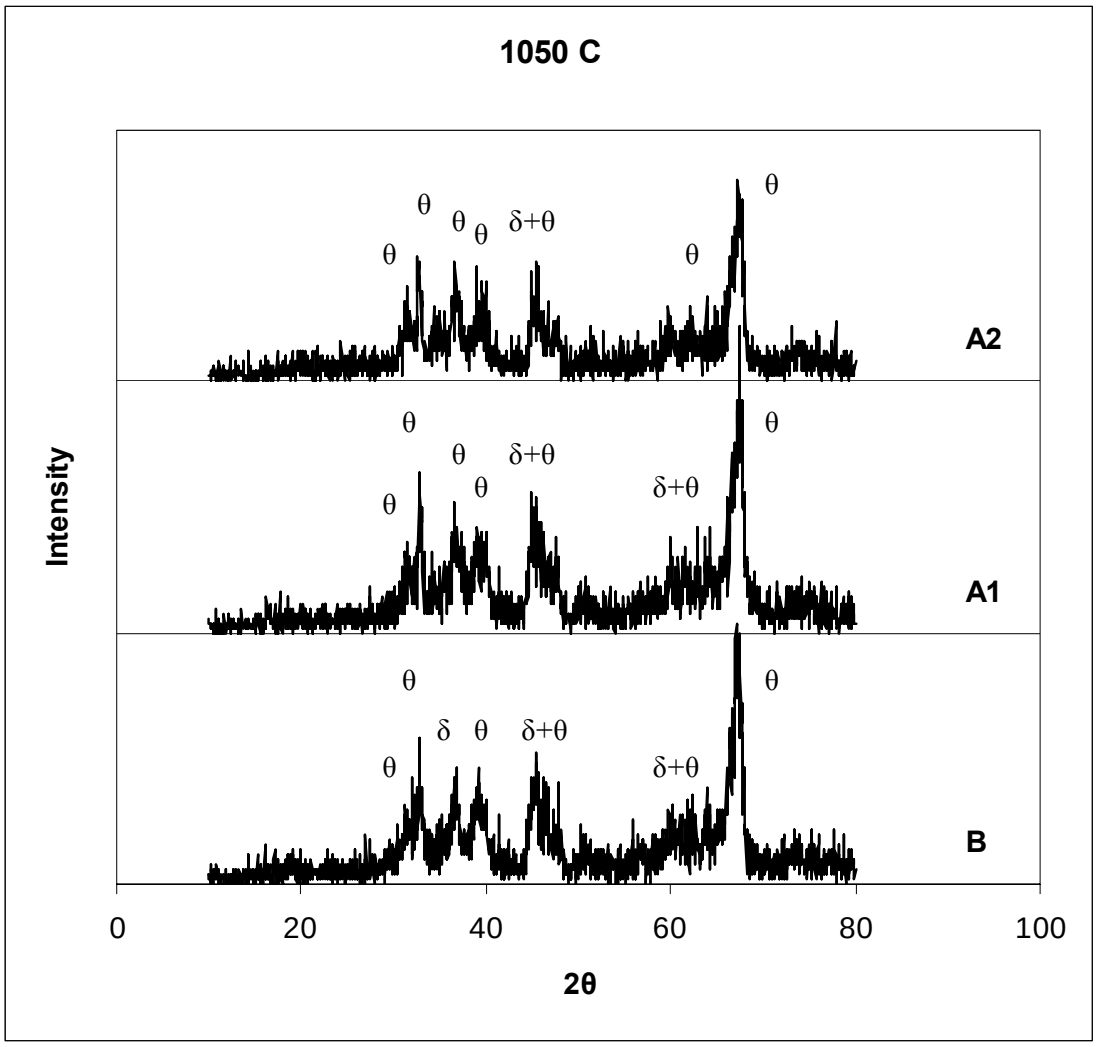

Fig. C9. XRD patterns of B, A1 and A2 powders calcined at 1050ºC

C10. XRD Diagram of Alumina Powders Calcined at 1100ºC

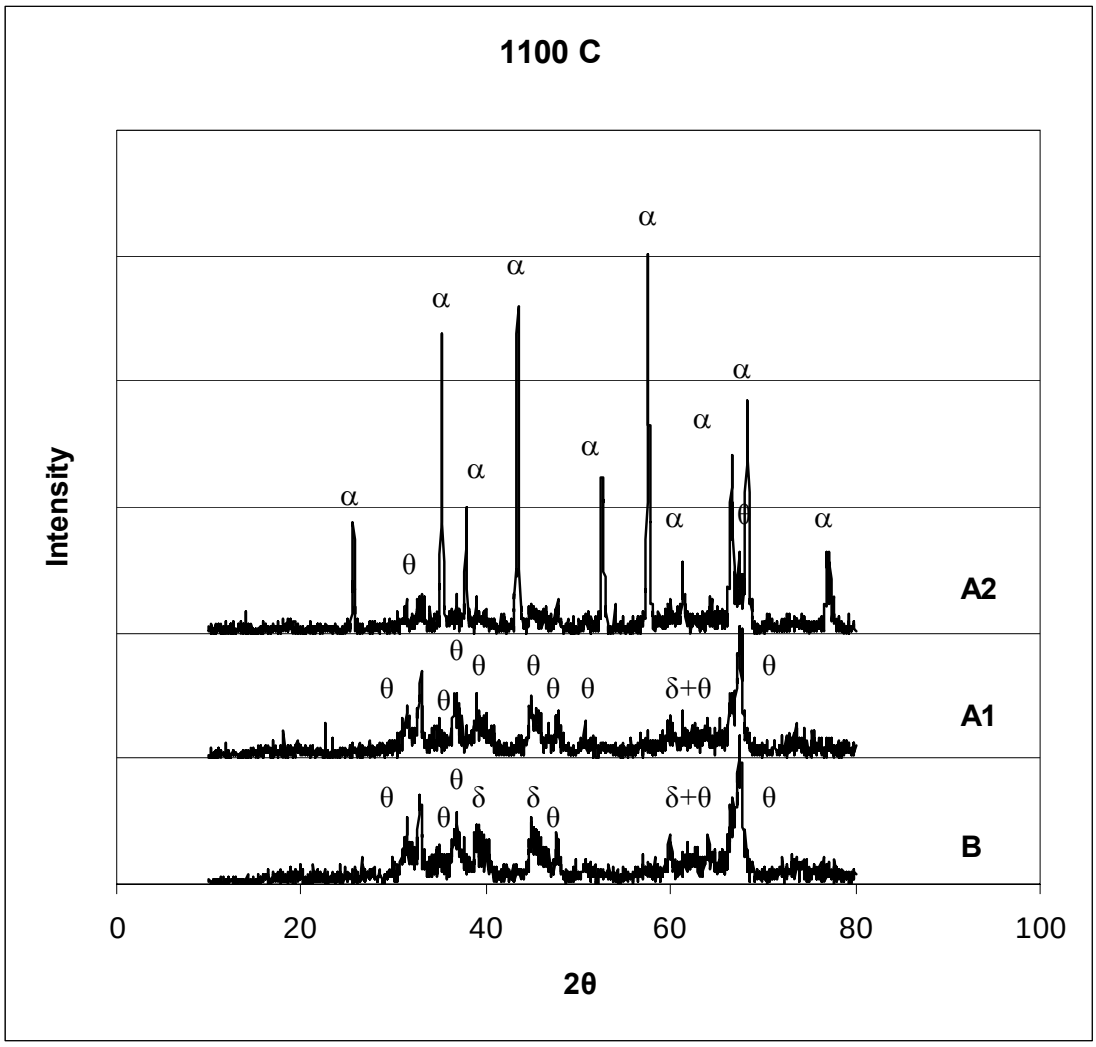

Fig. C10. XRD patterns of B, A1 and A2 powders calcined at 1100ºC

C11. XRD Diagram of Alumina Powders Calcined at 1150ºC

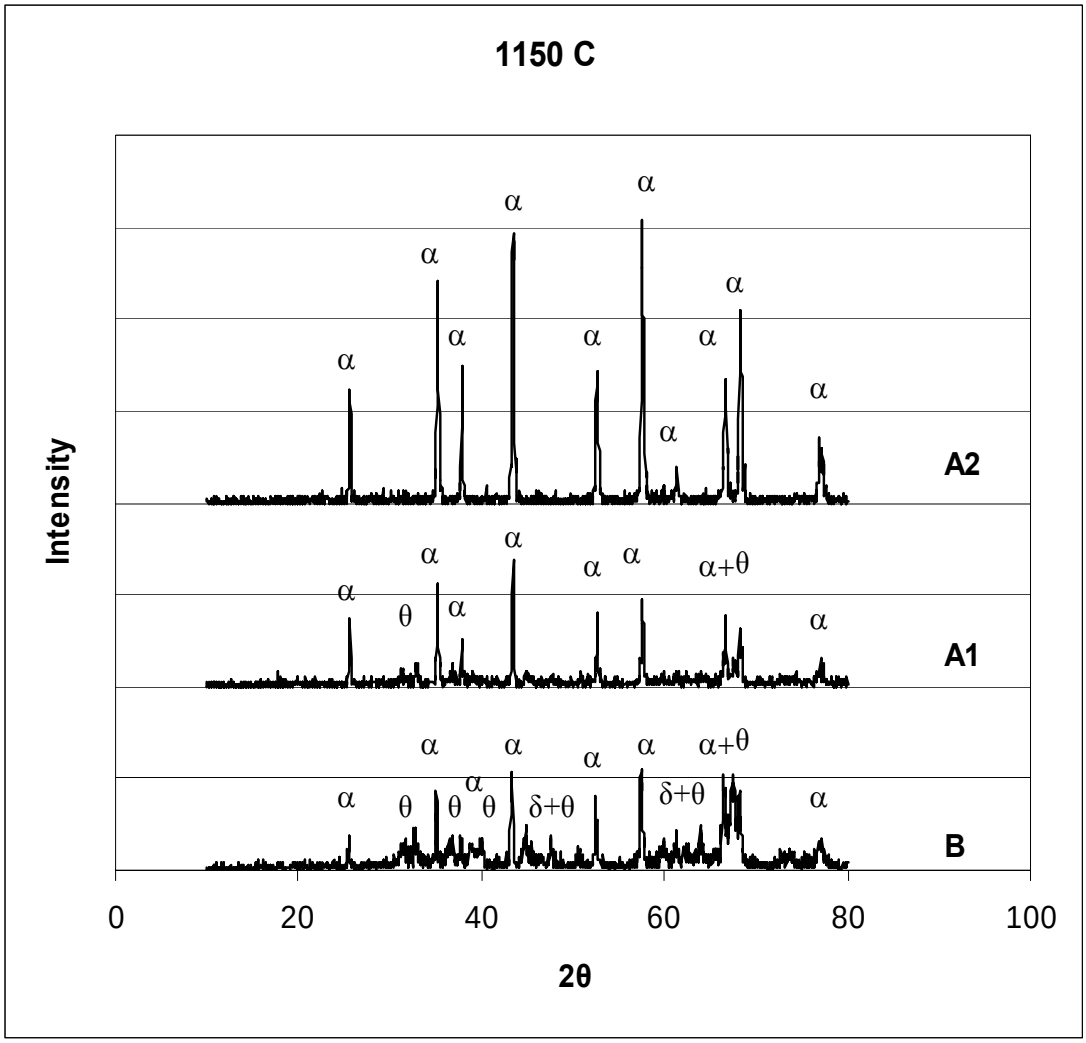

Fig. C11. XRD patterns of B, A1 and A2 powders calcined at 1150ºC

C12. XRD Diagram of Alumina Powders Calcined at 1200ºC

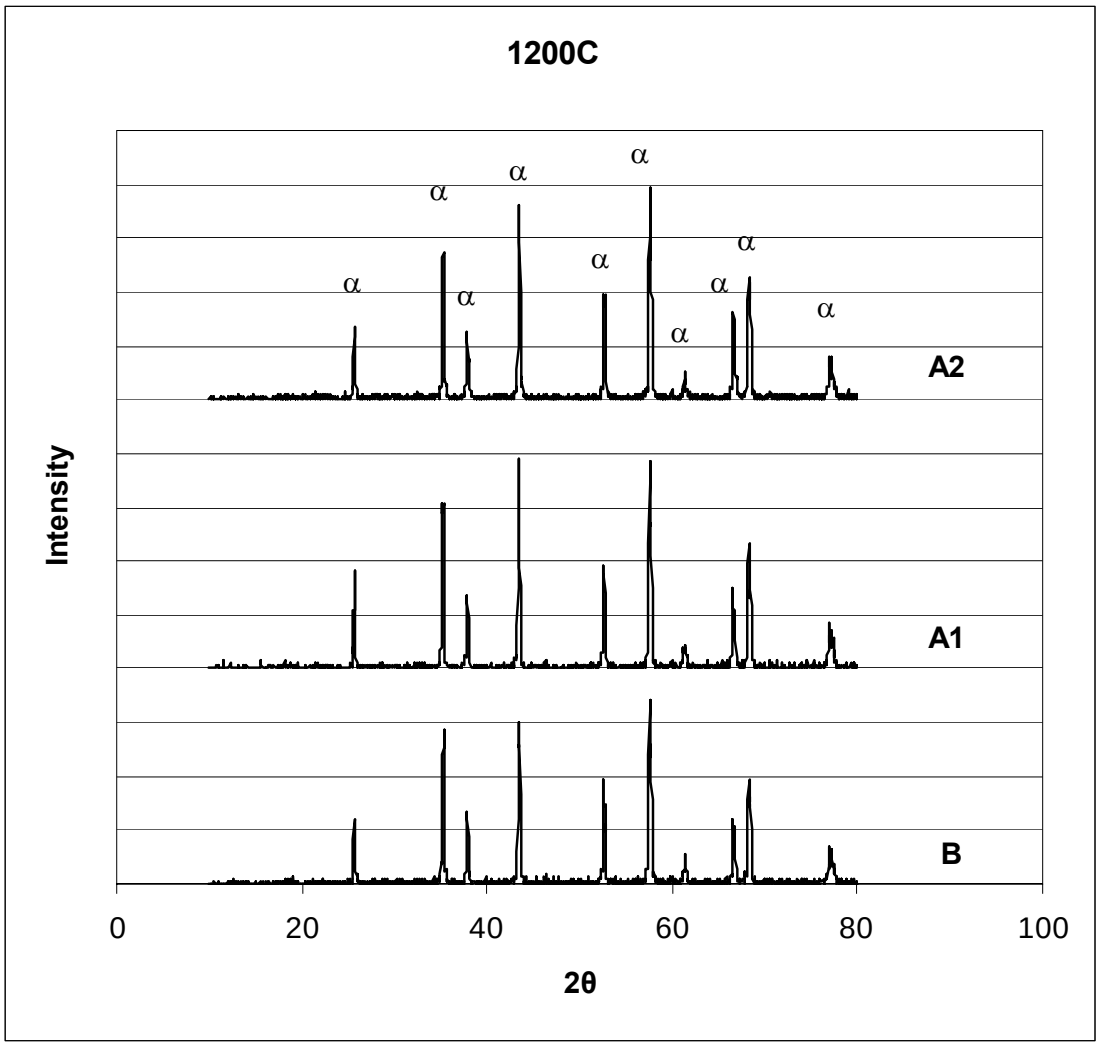

Fig. C12. XRD patterns of B, A1 and A2 powders calcined at 1200ºC

APPENDIX D

X-Ray Diffraction Patterns of Sintered Compacts

D1. XRD Diagrams of Alumina Pellets Sintered at 1100ºC &1110ºC

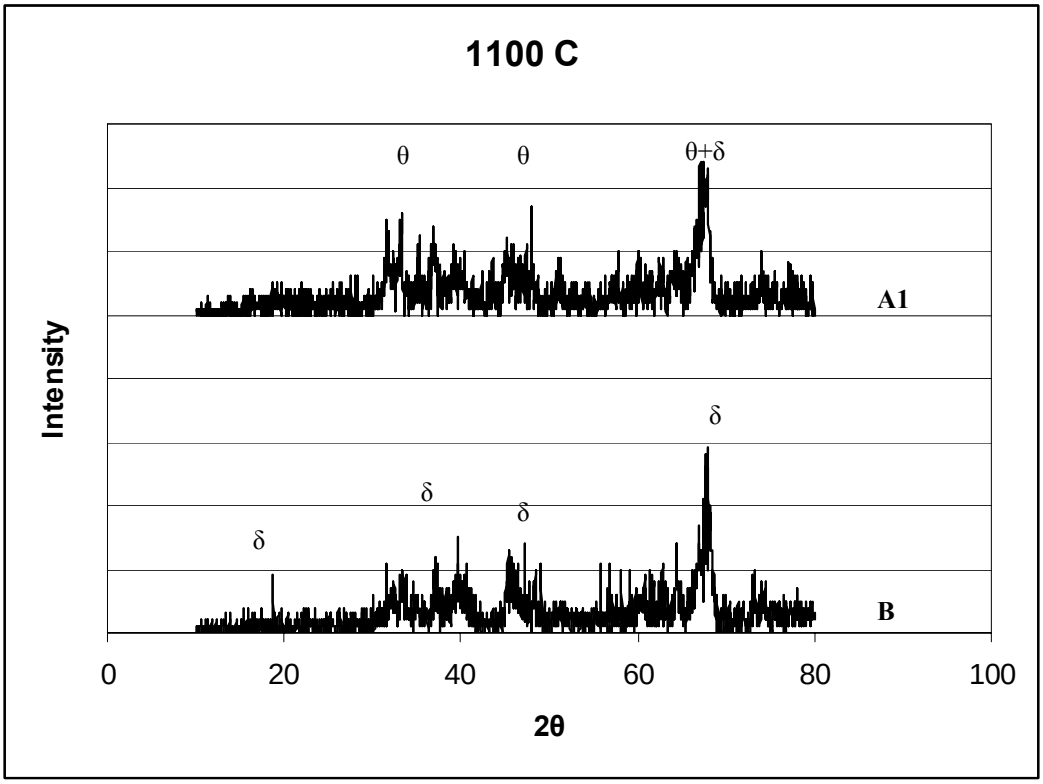

Fig. D1. XRD Patterns of A1 and B compacts sintered at 1100ºC.

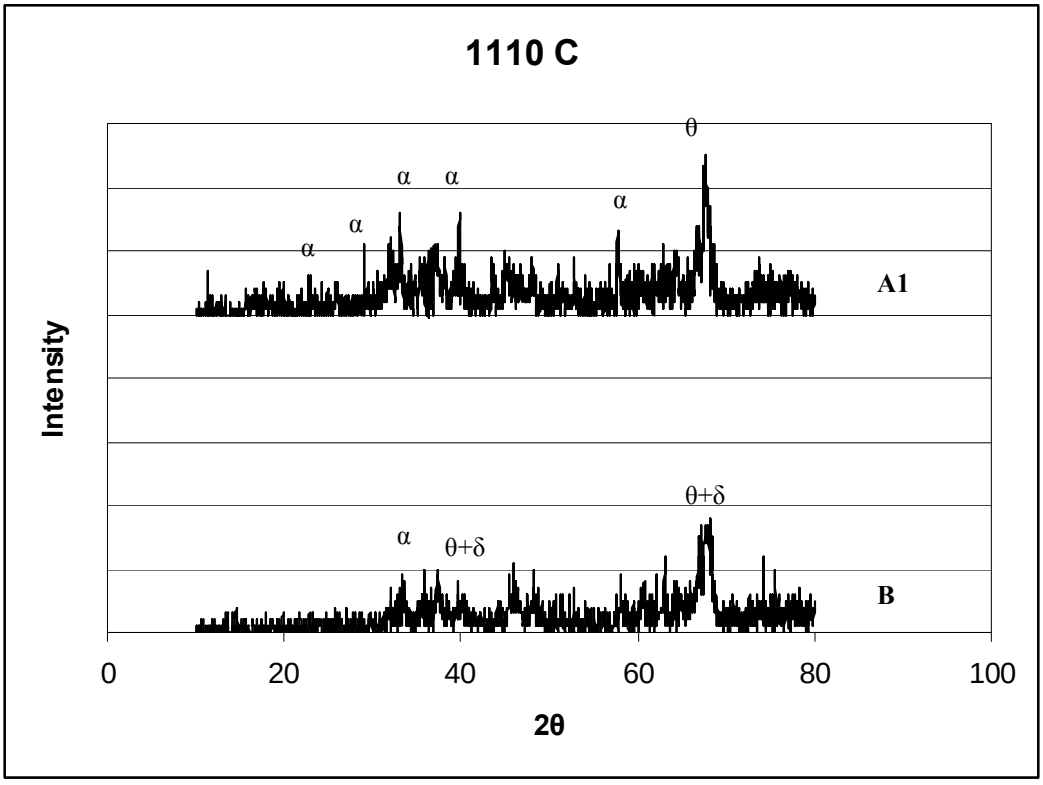

Fig. D2. XRD Patterns of A1 and B compacts sintered at 1110ºC.

D2. XRD Diagrams of Alumina Pellets Sintered at 1120ºC &1130ºC

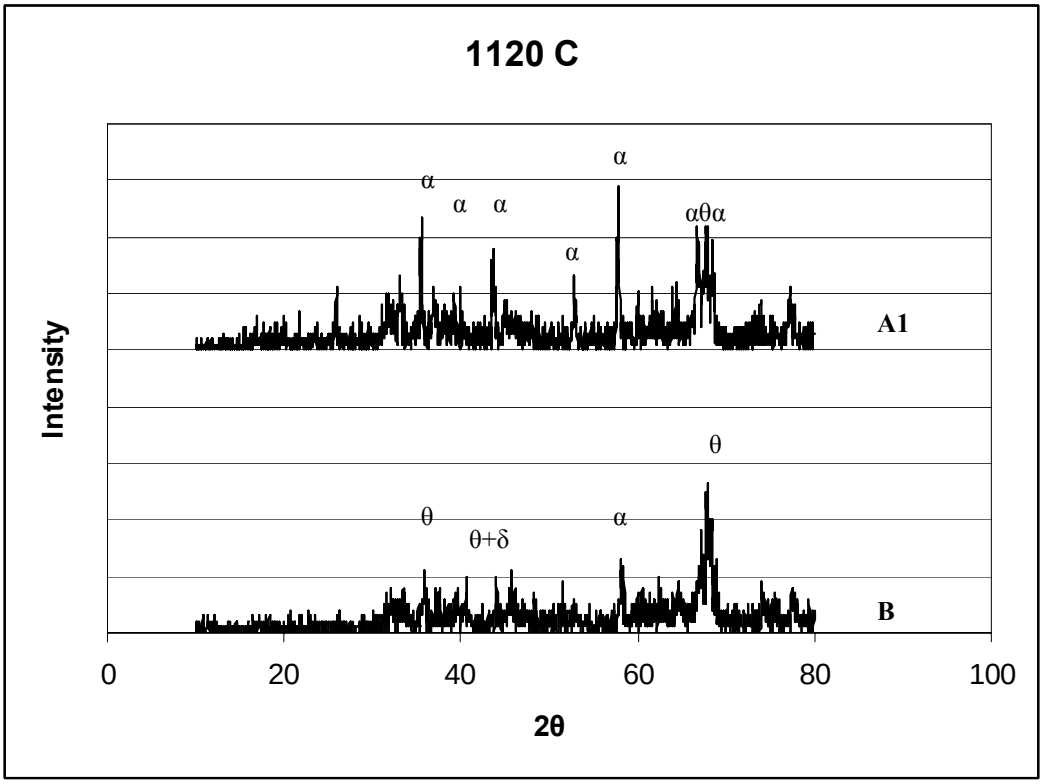

Fig. D3. XRD Patterns of A1 and B compacts sintered at 1120ºC.

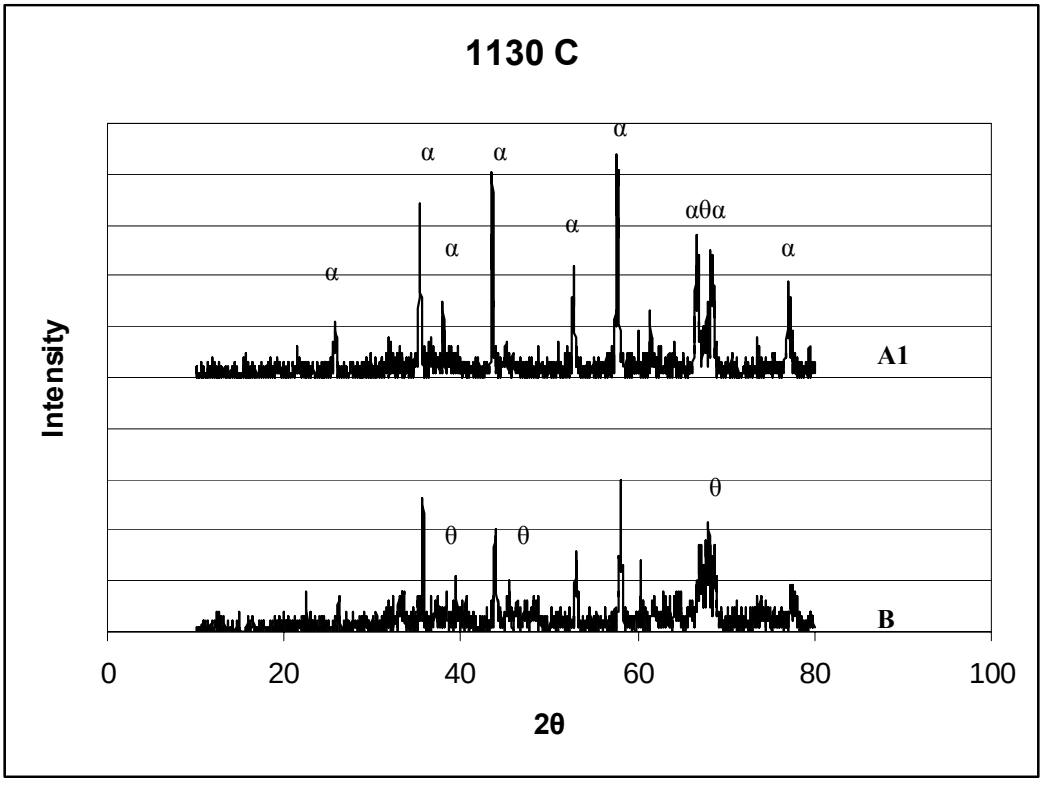

Fig. D4. XRD Patterns of A1 and B compacts sintered at 1130ºC.

D3. XRD Diagrams of Alumina Pellets Sintered at 1140ºC &1150ºC

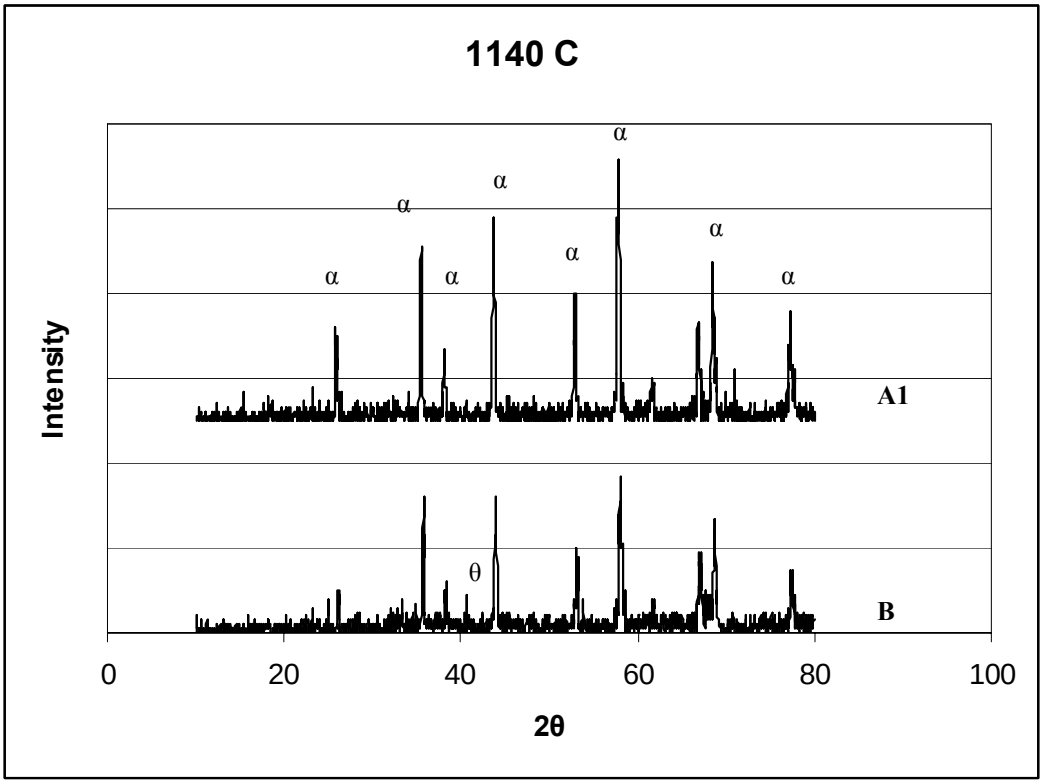

Fig. D5. XRD Patterns of A1 and B compacts sintered at 1140ºC.

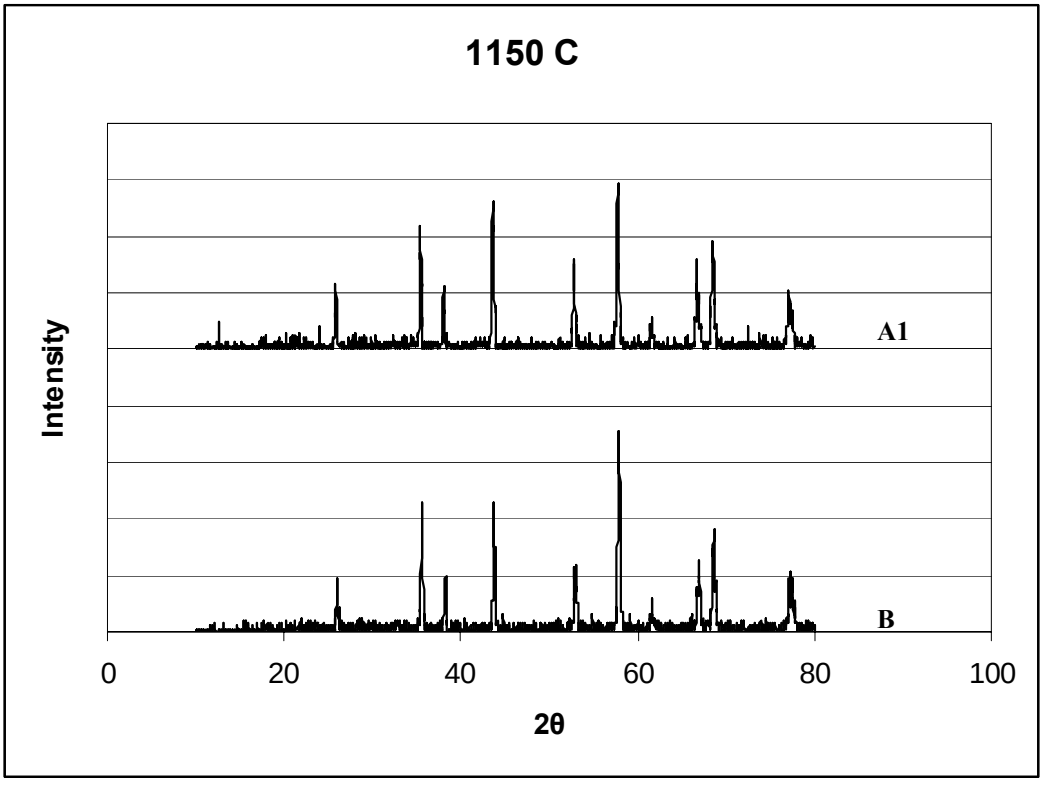

Fig. D6. XRD Patterns of A1 and B compacts sintered at 1150ºC.

D4. XRD Diagrams of Alumina Pellets Sintered at 1160ºC &1170ºC

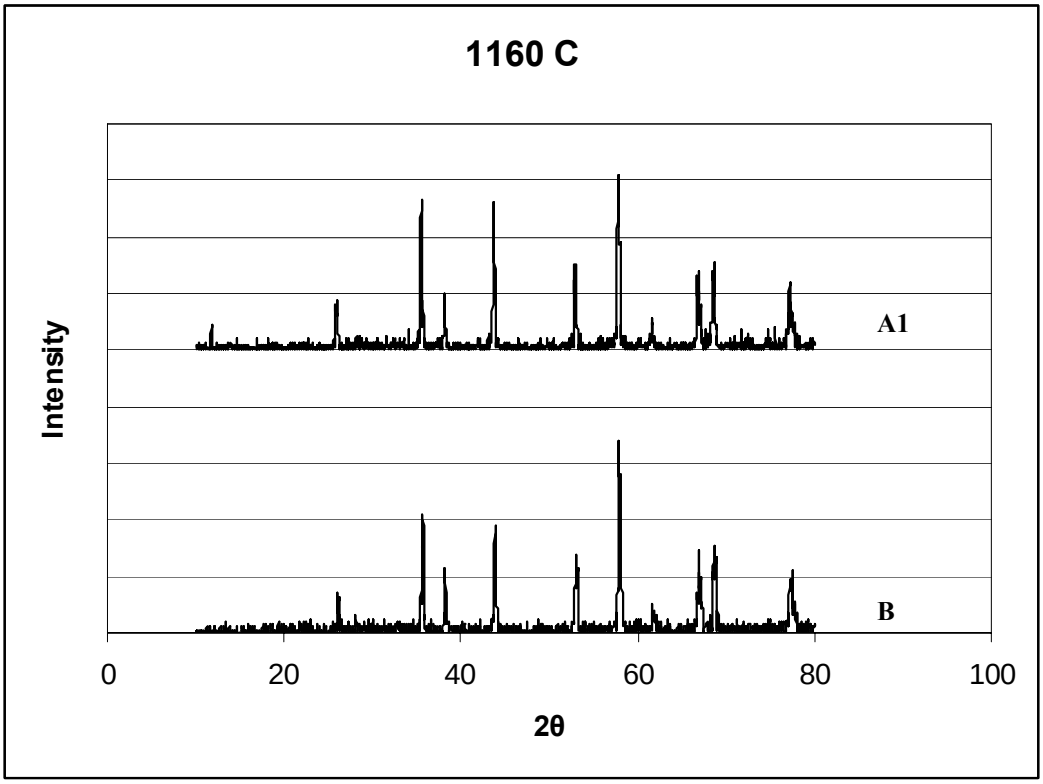

Fig. D7. XRD Patterns of A1 and B compacts sintered at 1160ºC.

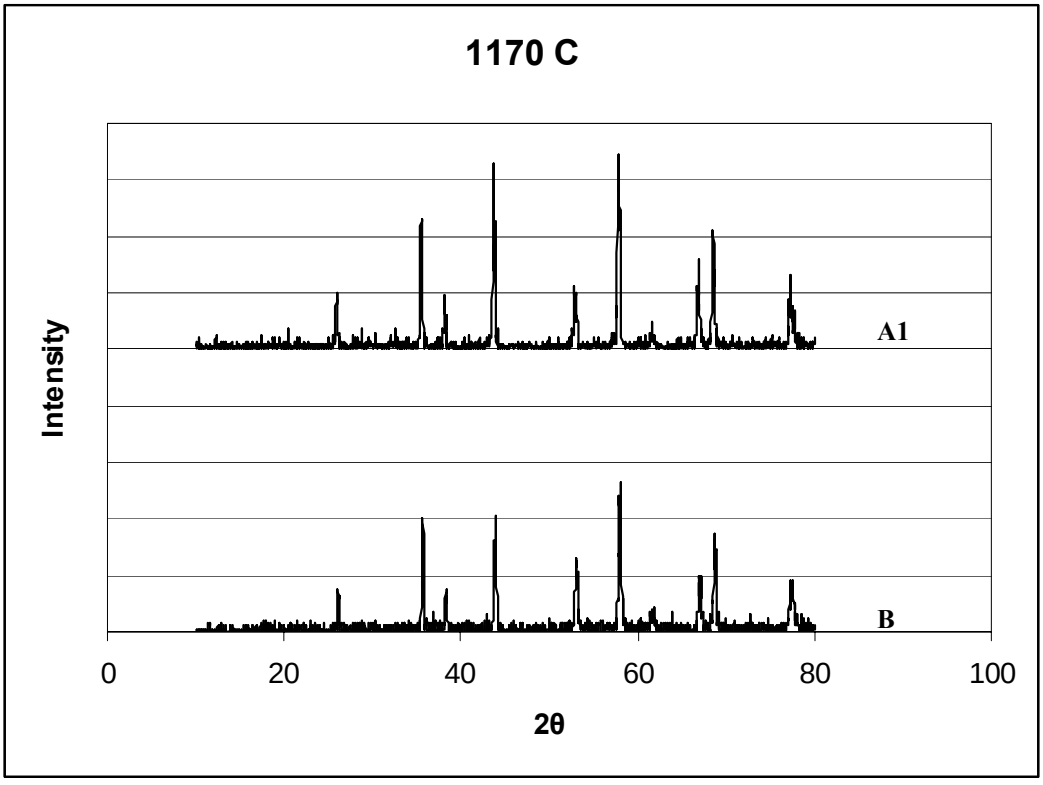

Fig. D8. XRD Patterns of A1 and B compacts sintered at 1170ºC.

D5. XRD Diagrams of Alumina Pellets Sintered at 1180ºC &1200ºC

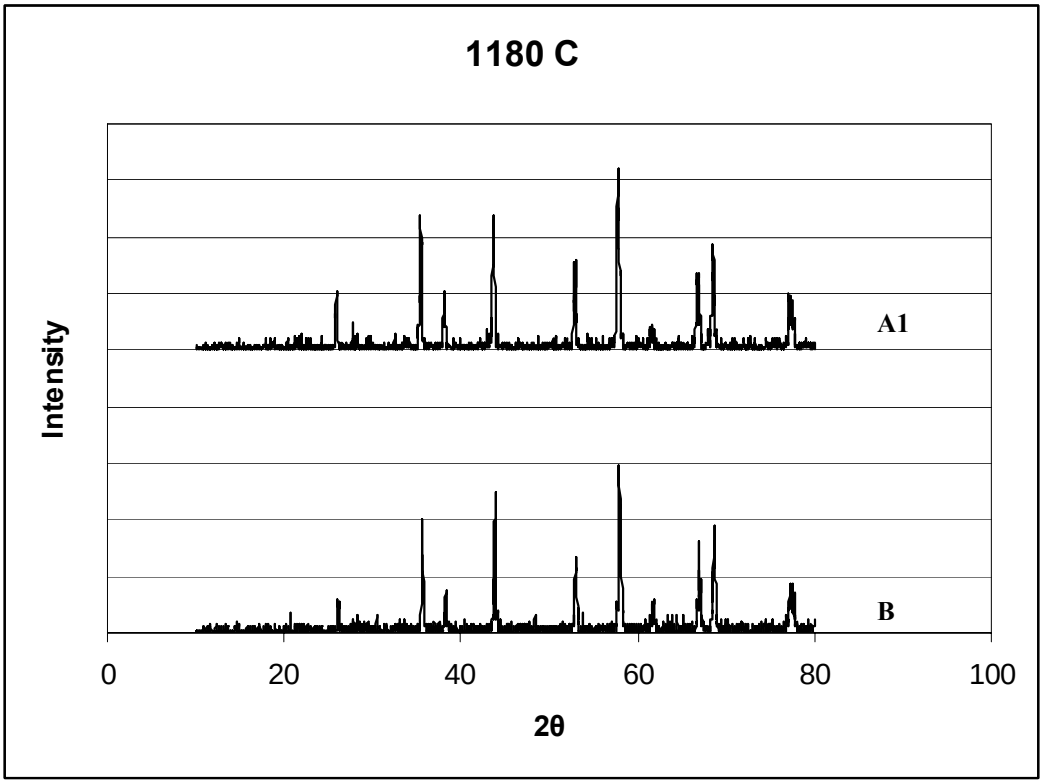

Fig. D9. XRD Patterns of A1 and B compacts sintered at 1180ºC.

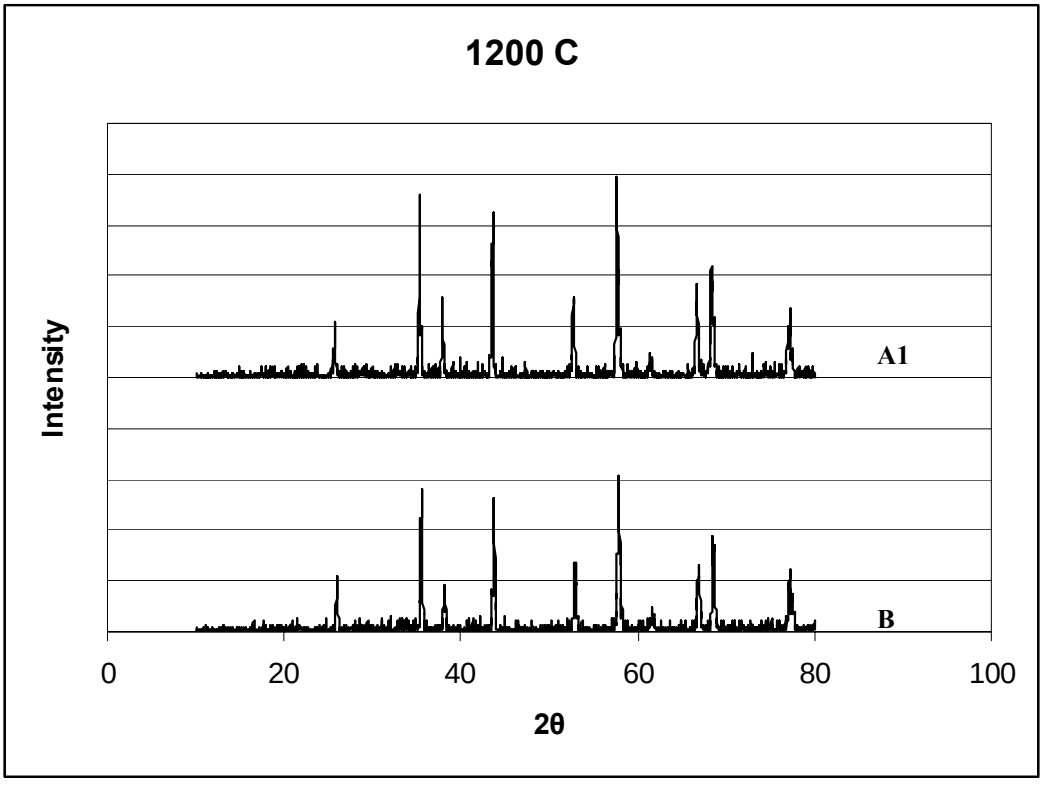

Fig. D10. XRD Patterns of A1 and B compacts sintered at 1200ºC.